THE UNIVERSITY OF CHICAGO

NEW METHODS AND MATERIALS FOR DIRECTED SELF-ASSEMBLY OF BLOCK COPOLYMERS

A DISSERTATION SUBMITTED TO

THE FACULTY OF THE PRITZKER SCHOOL OF MOLECULAR ENGINEERING

IN CANDIDACY FOR THE DEGREE OF

DOCTOR OF PHILOSOPHY

BY

MOSHE DOLEJSI

CHICAGO, ILLINOIS

AUGUST 2019

Contents

List of Tables

List of Figures

Acknowledgements

I remember growing up outside of town in Texas, with no air conditioning, where something was always broken. I am so incredibly grateful to all the people that helped me get where I am today. I have to thank Mrs. Marshall for getting me interesting in science, Mrs. Melton for getting me into debate (and getting into debates with me over whether or not Metallica was just too old to be so angry). Then at NCSU how could I possibly forget the terrible twosome of Dr. Efimenko and Dr. Genzer, who showed me how much fun not just science but lab work could be.

Once at UChicago, Robert and Lance taught me all I needed to know about DSA. I always remember being blown away by how Lance could A: juggle, B: ride a unicycle, and C: recall the exact right reference for every fact he knew. Chun and Jiaxing helped me out at the start with all my experimental work, and taught me how to first do DSA, and I continued to look to them for help with process development throughout my PhD. In addition to the other members of the Nealey group, I also need to thank Zach, Alec, Emre, Arin, Jeff, Ryan, Grant and Cody for keeping me sane. Of course Alec, Emre and Cody were also incredibly helpful collaborators and were often willing to run any quick simulations that would put my mind at ease.

I've also recently come to enjoy the distraction of Julia and Jon from the Siebener Group, I'm always surprised how such a similar group can have such a different breadth of knowledge. My other collaborators, Priya Moni, Alice Chang, Dan Sunday, and Hongbo Feng all helped immensely. I'm glad I got the opportunity to work with so many interesting people on so many really cool projects. Without them many of my chapters would have just stayed dreamy scribbles on paper passed between Dr. Nealey and myself during our meetings. Lastly I have to thank Dr. Nealey for all of his help and advice throughout my Ph.D. I'm always blown away by how patient he is with each and every one of us, especially when I'm sure we drive him crazy. If it weren't for

the opportunities he gave me to interact with funding agencies and interact with industry I likely wouldn't have the job lined up that I do now. Somehow he figured out what I needed and then he figured out a way to get me to want it. I can barely recognize the researcher I was when I joined the group in comparison to now.

Finally I have to thank my wife, Victoria, who has always been there for me. Even when we're both stressed I know we can get through anything. You give me the courage I need to go on and finish this thesis, finish my papers, even when I'd really rather not. I also have to thank her mom Regina, and grandmother, Brenda for all they've done for me. I really don't know where I would be without any of you, but I'd likely not have made it through undergrad. Your support has been immeasurable, and I'm so glad to be a part of the family.

Abstract

Directed Self-Assembly (DSA) is a promising strategy for quickly and cheaply manufacturing nanoscale features. DSA leverages the natural nanoscale phase separation of materials, which are guided by lithographically defined precise chemical cues. Polystyrene block polymethylmethacrylate (PS-*b*-PMMA) is ubiquitous for DSA, as the blocks possess equal surface free energy, and a random copolymer brush of the two blocks presents a balanced substrate surface both of which are a necessary prerequisite for achieving through film structures. In a standard process, PS guide stripes at pitches of 70-90 nm, are backfilled with a brush to direct PS-*b*-PMMA to form features down to ~24 nm pitch (3x density multiplication). In chapter 2, we show how metal – polymer interactions can be used in place of polymer – polymer interactions to provide the necessary chemical cues for DSA. This enables a new kind of self-aligned process in which a patterning layer is thermodynamically driven to align precisely not with a lithographically defined guide or mandrel, but instead with an existing metal – dielectric pattern on an underlying layer. Next in chapter 3, we turn to the DSA hole shrink process, where great effort has been expended to use various wet processes to selectively modify the sidewall and bottoms of lithographically defined template holes to provide the proper chemical cues. Here we demonstrate that ultraconformal initiated chemical vapor deposition (iCVD) can be used as a drop in replacement to conventional wet processes. Finally we turn towards the material itself. The repulsion between PS and PMMA, quantified by the Flory Huggins parameter χ, is too low to achieve sub 24 nm pitch features. Increasing the χ often goes hand in hand with increasing differences in surface free energy, which can be ameliorated only by additional complex processing involving top coats or solvent atmospheres. A further complication is that if the product of χ and the polymer size, N, is too high, defects become trapped. Thus for each pitch desired, there exists a range of acceptable χ.

One method to sidestep these limitations is by engineering the polymer microstructure such that these fundamental relationships might be changed. Chapter 4, studies the fundamental physics underlying graft polymer architecture in thin film confinement. Here we discovered substrate interactions can shift materials from perfectly symmetric lamella to cylindrical morphologies. A second method is the use of A-b-(B-r-C) architectures. Chapter 5, outlines a high throughput process to use click chemistry to modify a common platform polystyrene block polybutadiene, to rapidly achieve multiple materials with differing χ, each of which has equal surface energies and is fully compatible with DSA flows. Second we expand to a new platform polystyrene block polyglyicdyl methacrylate which we demonstrate is suitable not just for DSA of 16 nm full pitch features, but can also serve as its own non-preferential brush enabling new self-brushing DSA processes, and can even be modified with etch resistance through the incorporation of silicon. As a result DSA is no longer material limited, and is now enabled for a near infinite diversity of chemistry, providing the potential for further optimization.

Chapter 1: Introduction

1.1 Interest is ever turning towards smaller and smaller features

As technology marches ever onwards, the demand for more powerful computers, with larger storage than ever before is driving an ever increasing demand for smaller feature sizes in semiconductor manufacturing. Up until about the mid 2000s, these smaller sizes were achieved by successively shrinking the wavelength of light used for photolithography while at the same time increasing the numerical aperture to capture more light, as well as using methods like source mask optimization to more effectively fight back diffraction (Figure 1). While 13.5 nm EUV light was originally planned for insertion in 2004, EUV is long overdue to issues increasing source power, creating protective pellicles, understanding stochastics present at high energies, and a whole host of over problems.[1-5] Nonetheless it is now arriving thought at a great cost of well over 150 million dollars per tool.

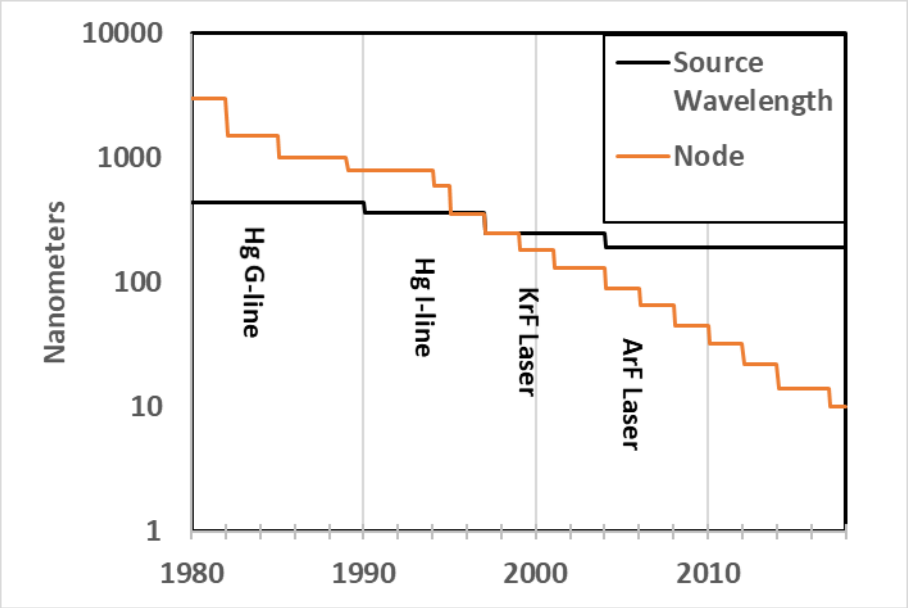

Figure 1. Source wavelength as well as high volume manufacturing node size over the last forty years. Labels are the light source in use. Note: While node once corresponded approximately to half pitch of the smallest features, it now represents approximately one third pitch.

Yet even with EUV overdue, manufacturers moved towards other density multiplication techniques such as litho etch litho etch (LELE or LE^2) or Self-Aligned Multiple Patterning (SAMP) each of which has their own advantages and drawbacks (Table 1). Directed Self-Assembly (DSA) is one incredibly intriguing approach for many processes because it exists within the family of self-aligned processes, is cheap, and is an equilibrium process. That is to say that at infinite times, DSA will achieve a target size plus or minus some variation entirely based on the material properties of the block copolymer, which is useful to achieve well defined electrical properties in advanced chips.[6-8]

Table 1. Comparison of approaches to continue shrinking feature sizes. Process scaling gives the number of steps of a given type required to achieve N factor density multiplication i.e. N = 4 = 4X density multiplication equivalent to SAQP.

Process	Pros	Cons	Process Scaling
EUV Lithography	Minimal Extra Steps	Cost	Litho : 1-2 Dep : 1 Etch : 1
Self-Aligned Multiple Patterning (SADP, SAQP, SAOP)	Self-Aligned	Pitch Walking Mainly 1D layout	Litho : 1 + (cuts) Dep : $\propto \sqrt{N}$ Etch : $\propto \sqrt{N}$
Litho-Etch **Litho-Etch** **(LELE, LE2, LELELE…)**	2D layout	Overlay is Tricky	Litho : $\propto$N Dep : $\propto$N Etch : $\propto$N
Directed Self-Assembly	Self-Aligned, Minimal Steps, Cheap, Thermodynamically Guaranteed CD/Pitch	Defects (~0.5/cm^2) CD/Pitch is Material Specific	Litho : 1 + (cuts) Dep : 1 Etch : 1

1.2 Self-Assembly of Block Copolymers

To understand the DSA process we first have to understand the natural driving force for block copolymer phase separation. A block copolymer is a molecule consisting of two chemically dissimilar polymer blocks which are covalently bound together. Whether or not a block-copolymer microphase separates depends on the free energy associated with mixing which has both an entropic and an enthalpic term.[9-14] The entropic term specifically captures the number of conformations available to each block when it is mixed versus separated. As the size of the molecule represented by N, the number of unit volumes occupied, increases, the difference in the number of accessible conformations for mixed and separated morphology shrinks decreasing the entropic term. On the other hand, the enthalpic term solely involves the number of contacts

between the two blocks as well as their interaction energy, which we call the Flory-Huggins parameter, χ. These interactions are thus maximized for symmetric block copolymers where the blocks are most likely to find each other and least likely to find themselves. Finding the point at which entropic and enthalpic terms balance gives the classic block copolymer phase diagram a characteristic U shape. Where increasing χ or decreasing N is required to phase separate as you move towards asymmetric block sizes due to a decreasing number of enthalpic contacts. Because it is this balance that determines phase separation it is common to think of phase separation in terms of the product of χ and N, with $\chi N = 10.4$ widely considered the cut off microphase separation for perfectly symmetric materials.[12] Here it is important to note that, by tuning the block size from symmetric to asymmetric the resulting morphology of the block copolymer can be changed from lamellar to cylindrical to sphere forming, though in this work we specifically investigate mostly symmetric lamella forming materials.

While phase separation might be governed by χN, both self-consistent field theory,[10] and strong segregation theory have shown that the lamellar period (L_0) is instead governed by the dynamics of a slightly expanded Gaussian coils which is only weakly a function of χ but strongly a function of N ($L_0 \propto \chi^{1/6} N^{2/3}$).[14] Thus when smaller feature sizes are desired, the approach is often to increase χ which directly encourages phase separation but only weakly effects feature size, and then decrease N inversely proportional to the increase in χ to maintain a given χN while drastically decrease the L_0. This approach works well, but often causes issues once the effects of the thin film on the self-assembly process is considered.

1.3 Controlling self-assembly in thin films

To direct the self-assembly first the block copolymer must be induced to form perpendicular through film structures which are of industry for patterning. These features necessarily require each block to equally wet the free interface as well as the substrate. This is only possible when the penalty of the substrate with each block is precisely balanced as well as the Surface Free Energy (SFE) of each block.[15-16] In the case of imbalanced penalties at one or both interfaces that interface will pin the lower energy material, which often results in propagating a parallel assembly throughout the film. If the same block is pinned at both interfaces we call that condition symmetric wetting, and we expect the block copolymer to naturally desire to phase separate into film thickness which are integer multiples of the lamellar period ($N \cdot L_0$). That way the same block can wet both interfaces fulfilling the commensurability condition. On the other hand if a different block is pinned at each interface we call that condition asymmetric wetting and we expect instead integer plus a half multiples of the lamellar period ($(N + 0.5) \cdot L_0$). By carefully spincoating at varying thicknesses that span the commensurability conditions from symmetric to asymmetric we can simply look for the presence of topography indicating the film is incommensurate. If the film is incommensurate we then immediately know if the wetting is symmetric or asymmetric. If we can then make a reasonably assumption about the wetting of one of the interfaces we can use this approach to precisely probe the other interface. This is called the hole-island test, because we can spin at a single incommensurate thickness and simply examine whether holes or island forms to immediately determine the wetting (Figure 2).

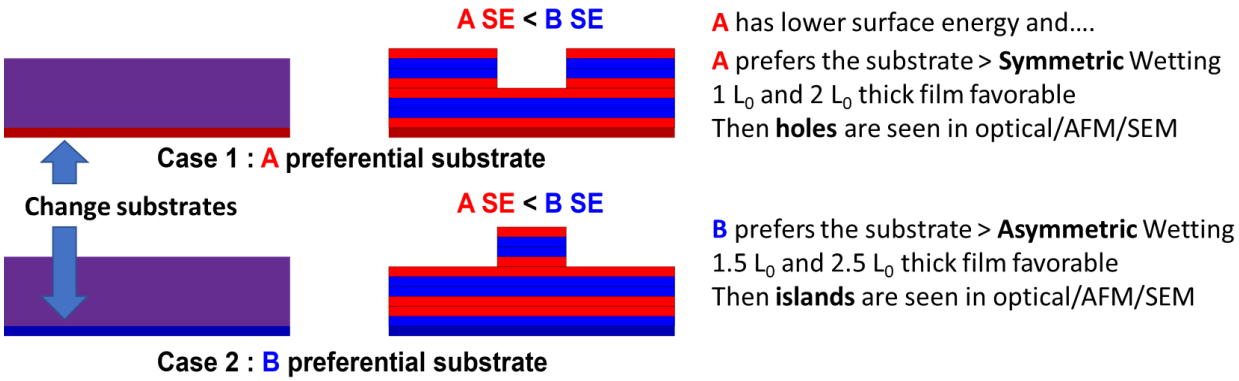

Figure 2. Example of the hole-island test where a film is spuncoat to a thickness of 1.75 L0. If we know the surface energy of the 'A' block is lower we can use the presence of holes or islands to determine qualitatively the substrates preference.

Using this test, extensive work has been conducted to understand how to properly control both the surface free energy (SFE) as well as the interfacial energy to achieve the desired through film structures. Polystyrene-*block*-polymethylmethacrylate (PS-*b*-PMMA) has longed served as benchmark block copolymer, because the relative SFE of the blocks can be tuned simply with temperature. Below 170°C PS has a lower SFE, while above 270°C PMMA has a lower SFE, with a goldilocks zone of equal surface energy in the middle.[17-18] Using this platform it was found that random copolymers grafted to the surface could be used to create non-preferential substrates,[19-23] although now many other materials have been found.[16, 24-25]

Once through film assembly could be reliably achieved, the breakthrough for DSA came when these non-preferential substrates were patterned with preferential features at or close to an integer multiple of the lamellar period. These guide stripes act like fence posts to organize the so called fingerprint assembly into uniform features. In general these guide stripes are separated into one of two categories, either graphoepitaxial or chemoepitaxial. In graphoepitaxy the guiding force is entirely given by a topographic guiding pattern, while in chemoepitaxy the pattern may be

topographic but also consists of a chemical pattern. Graphoepitaxial templates have been used for numerous applications from contact-holes for the semiconductor industry, through polymer dynamics studies, and even for ionic conductivity[26-31]. Most DSA conducted by our group though, especially for lamella forming BCP utilizes the well-studied chemoepitaxial Liu-Nealey (LiNe) flow as shown in Figure 3. In this flow the pitch is finally controlled by the lithography use to create the original pattern, either e-beam lithography in academia or 193i lithography at imec.[32-33] The width of the guide pattern can then be controlled through a subsequent trim-etch step with very high precision, before finally a non-preferential brush is grafted onto the silicon and DSA is performed. Traditionally the preferential surface consists of a crosslinked polystyrene mat,[34] although crosslinked PMMA mats have also been tried.[35]

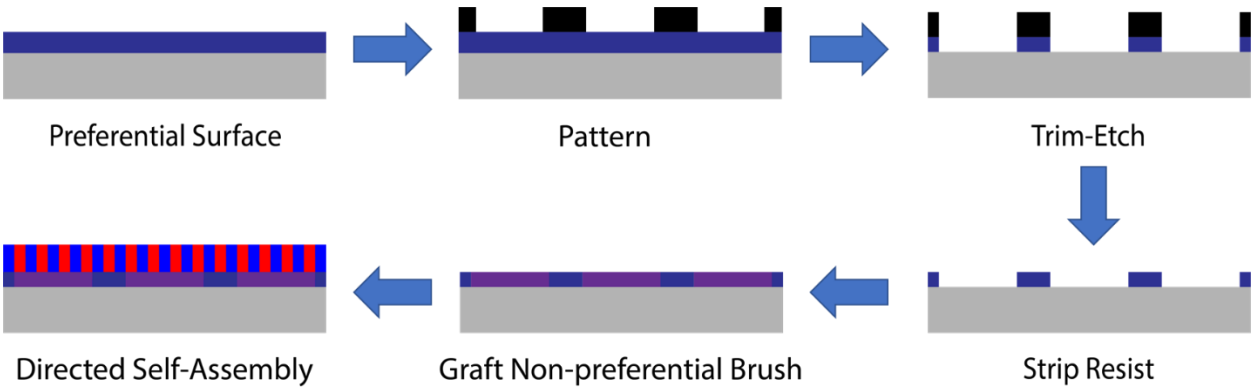

Figure 3. Scheme outlining the process steps for LiNe Flow.

As the guide stripe is PS preferential the non-preferential brush must be shifted to be slightly PMMA preferential in order to balance the overall interactions.[34] The spacing of the guide stripes (L_s) must be within approximately 10% of an integer multiple of the bulk lamellar spacing in order for good assembly to be observed, otherwise the entropic penalties associated with chain re-arrangement under compression or expansion are too high for the polymer.[36-37] Similarly the guide stripe width should be approximately 0.7 L_0 or 1.5 L_0 in order to just slightly hold one guided domain, or two guided and one non-guided domain.[37-38] Studies have also shown that the optimum

LiNe flow should incorporate 0.5 L_0 topography between the brush and the preferential guide stripe, in order to prohibit the formation of long lived stitch defects.[39-40]

1.4 Objectives for DSA development

Our first objective was to add new functionality into the DSA LiNe flow. One particular problem faced by industry is that increasingly more and more exposures must be conducted in order to create finer and finer features. These exposures must all overlay with few nanometer precision in order to insure a functioning device is made. While previously the industry has investigated mis-alignment tolerant processes such as self-aligned contacts.[41] It would be particularly ideal if a process could be created which intrinsically aligned one layer with the last. DSA as a bottom up, thermodynamic approach was uniquely suited for such a process. In chapter 2 we investigate how metal or metal oxide and dielectric patterns, which mimic the layers of a functioning device, can be used to guide a true Self-Aligned DSA process.

After having successfully showed the possibility of metals and metal oxides as chemoepitaxial materials, in Chapter 3, we turn towards a collaboration with MIT focused around initiated chemical vapor deposition (iCVD). iCVD is an all organic ultra-conformal deposition technique with good control over substrate surface energy, and critically it is an all vapor or dry process. This is important because the current state of the art graphoepitaxial DSA hole shrink process involves depositing and rinsing multiple brushes into high aspect ratio holes, where it might be hard to truly rinse out the brush. We show how this tricky process can be replaced by a single clean iCVD deposition using both qualitative, and quantitative methods as well as the pairing of simulation and experiment.

Next we sought to examine the benchmark material for DSA. PS-*b*-PMMA, while easy to process is fundamentally limited by its low χ to only form features above 20 nm,[42] and due to chain dynamics it is very slow at 100 nm + feature sizes. In order to address both these concerns we began a materials collaboration with the Grubb group and NIST seeking to understand how the new polymer microarchitecture of graft polymers behaved under thin film conditions. These first steps towards graft polymer DSA are presented in chapter 4. We identified for the first time that in the absence of solvent effects, substrates can have strong morphological effects on these graft polymers.

Finally we sought to develop a new high throughput approach for the synthesis of families of polymers as suitable for DSA as PS-*b*-PMMA, but with the freedom to choose functional chemistry or χ as desired. While usually increasing χ requires increasing chemical differences and thus creating large differences in SFE; here we targeted the A-*b*-(B-*r*-C) architecture which decouples χ from surface free energy. This is because in these architectures SFE is shown to be a linear combination of B and C whereas χ is shown to be a harmonic mean of χ_{AC}, χ_{AB}, and χ_{BC}.[43] Using this approach two families of materials were developed using reactive block copolymer and click chemistry. The first PS-*b*-polybutadiene (PS-*b*-PB) family, detailed in chapter 5, proved the concept though the materials were synthetically challenging to make and possessed limited χ. We then improved upon these materials with the new PS-*b*-polyglycidylmethacrylate (PS-*b*-PGMA) family detailed in chapter 6. Here we also set a goal to incorporate new chemistry allowing for better processing in terms of both overall DSA flow and etch contrast.

1.5 References

1. Bakshi, V., *EUV Lithography, Second Edition*. 2018; Vol. 2.

2. Bisschop, P. D.; Hendrickx, E., *Stochastic effects in EUV lithography*. SPIE: 2018; Vol. 10583.

3. Bisschop, P. D.; Hendrickx, E., *Stochastic printing failures in EUV lithography*. SPIE: 2019; Vol. 10957.

4. Erdmann, A.; Evanschitzky, P.; Bottiglieri, G.; Setten, E. v.; Fliervoet, T., *3D mask effects in high NA EUV imaging*. SPIE: 2019; Vol. 10957.

5. Goldfarb, D. L.; Bloomfield, M. O.; Colburn, M., *Thermomechanical behavior of EUV pellicle under dynamic exposure conditions*. SPIE: 2016; Vol. 9776.

6. Hohle, C. K.; Gronheid, R.; Chi, C.; Liu, C.-C.; Meli, L.; Guo, J.; Parnell, D.; Mignot, Y.; Schmidt, K.; Sanchez, M.; Farrell, R.; Singh, L.; Furukawa, T.; Lai, K.; Xu, Y.; Sanders, D.; Hetzer, D.; Metz, A.; Burns, S.; Felix, N.; Arnold, J.; Corliss, D., Electrical study of DSA shrink process and CD rectification effect at sub-60nm using EUV test vehicle. **2017,** *10146*, 101460Q.

7. Doise, J.; Bekaert, J.; Chan, B. T.; Hori, M.; Gronheid, R., Via patterning in the 7-nm node using immersion lithography and graphoepitaxy directed self-assembly. *Journal of Micro/Nanolithography, MEMS, and MOEMS* **2017,** *16* (2).

8. Liu, C.-C.; Franke, E.; Mignot, Y.; Xie, R.; Yeung, C. W.; Zhang, J.; Chi, C.; Zhang, C.; Farrell, R.; Lai, K.; Tsai, H.; Felix, N.; Corliss, D., Directed self-assembly of block copolymers for 7 nanometre FinFET technology and beyond. *Nature Electronics* **2018,** *1* (10), 562-569.

9. Bates, F. S.; Fredrickson, G. H., Block Copolymers—Designer Soft Materials. *Physics Today* **1999,** *52* (2), 32.

10. Matsen, M. W.; Bates, F. S., Unifying Weak- and Strong-Segregation Block Copolymer Theories. *Macromolecules* **1996,** *29* (4), 1091-1098.

11. Khandpur, A. K.; Foerster, S.; Bates, F. S.; Hamley, I. W.; Ryan, A. J.; Bras, W.; Almdal, K.; Mortensen, K., Polyisoprene-Polystyrene Diblock Copolymer Phase Diagram near the Order-Disorder Transition. *Macromolecules* **1995,** *28* (26), 8796-8806.

12. Bates, F. S.; Fredrickson, G. H., Block copolymer thermodynamics: theory and experiment. *Annual review of physical chemistry* **1990,** *41*, 525-57.

13. Matsen, M. W., Phase Behavior of Block Copolymer/Homopolymer Blends. *Macromolecules* **1995,** *28* (17), 5765-5773.

14. Semenov, A. N., Theory of block copolymer interfaces in the strong segregation limit. *Macromolecules* **1993,** *26* (24), 6617-6621.

15. Maher, M. J.; Self, J. L.; Stasiak, P.; Blachut, G.; Ellison, C. J.; Matsen, M. W.; Bates, C. M.; Willson, C. G., Structure, Stability, and Reorganization of 0.5 L0 Topography in Block Copolymer Thin Films. *ACS nano* **2016**.

16. Suh, H. S.; Kang, H.; Nealey, P. F.; Char, K., Thickness Dependence of Neutral Parameter Windows for Perpendicularly Oriented Block Copolymer Thin Films. *Macromolecules* **2010,** *43* (10), 4744-4751.

17. Russell, T. P.; Menelle, A.; Anastasiadis, S. H.; Satija, S. K.; Majkrzak, C. F., Unconventional Morphologies of Symmetric, Diblock Copolymers Due to Film Thickness Constraints. *Macromolecules* **1991,** *24*, 6263-6269.

18. Wu, S., *Polymer Interface and Adhesion*. 2017.

19. Ji, S.; Liu, C.-C.; Son, J. G.; Gotrik, K.; Craig, G. S. W.; Gopalan, P.; Himpsel, F. J.; Char, K.; Nealey, P. F., Generalization of the Use of Random Copolymers To Control the Wetting Behavior of Block Copolymer Films. *Macromolecules (Washington, DC, U. S.)* **2008,** *41* (23), 9098-9103.

20. Ji, S.; Nealey, P. F.; Gopalan, P., Self-assembly of poly(styrene-b-2-vinylpyridine) on neutral substrates. *Polym. Prepr. (Am. Chem. Soc., Div. Polym. Chem.)* **2007,** *48* (2), 434-435.

21. In, I.; La, Y.-H.; Park, S.-M.; Nealey, P. F.; Gopalan, P., Side-chain grafted random copolymer brushes as neutral surfaces for controlling the orientation of block copolymer microdomains in thin films. *Polym. Prepr. (Am. Chem. Soc., Div. Polym. Chem.)* **2006,** *47* (2), 442-443.

22. Mansky, P., Controlling Polymer-Surface Interactions with Random Copolymer Brushes. *Science* **1997,** *275* (5305), 1458-1460.

23. Han, E.; Gopalan, P., Cross-linked random copolymer mats as ultrathin nonpreferential layers for block copolymer self-assembly. *Langmuir : the ACS journal of surfaces and colloids* **2010,** *26* (2), 1311-5.

24. Chang, T.-H.; Xiong, S.; Jacobberger, R. M.; Mikael, S.; Suh, H. S.; Liu, C.-C.; Geng, D.; Wang, X.; Arnold, M. S.; Ma, Z.; Nealey, P. F., Directed self-assembly of block copolymer films on atomically-thin graphene chemical patterns. *Sci. Rep.* **2016,** *6*, 31407.

25. Moni, P.; Suh, H. S.; Dolejsi, M.; Kim, D. H.; Mohr, A. C.; Nealey, P. F.; Gleason, K. K., Ultrathin and Conformal Initiated Chemical-Vapor-Deposited Layers of Systematically Varied Surface Energy for Controlling the Directed Self-Assembly of Block CoPolymers. *Langmuir : the ACS journal of surfaces and colloids* **2018,** *34* (15), 4494-4502.

26. Gronheid, R.; Hori, M.; Chan, B. T.; Doise, J., Dual brush process for selective surface modification in graphoepitaxy directed self-assembly. *Journal of Micro/Nanolithography, MEMS, and MOEMS* **2017,** *16* (03).

27. Han, E.; Kang, H.; Liu, C.-C.; Nealey, P. F.; Gopalan, P., Graphoepitaxial Assembly of Symmetric Block Copolymers on Weakly Preferential Substrates. *Adv. Mater. (Weinheim, Ger.)* **2010,** *22* (38), 4325-4329.

28. Xiao, S.; Yang, X.; Edwards, E. W.; La, Y.-H.; Nealey, P. F., Graphoepitaxy of cylinder-forming block copolymers for use as templates to pattern magnetic metal dot arrays. *Nanotechnology* **2005,** *16* (7), 324-329.

29. Tong, Q.; Sibener, S. J., Visualization of Individual Defect Mobility and Annihilation within Cylinder-Forming Diblock Copolymer Thin Films on Nanopatterned Substrates. *Macromolecules* **2013,** *46* (21), 8538-8544.

30. Sundrani, D.; Sibener, S. J., Spontaneous Spatial Alignment of Polymer Cylindrical Nanodomains on Silicon Nitride Gratings. *Macromolecules* **2002,** *35* (22), 8531-8539.

31. Kambe, Y.; Arges, C. G.; Czaplewski, D. A.; Dolejsi, M.; Krishnan, S.; Stoykovich, M. P.; de Pablo, J. J.; Nealey, P. F., Role of Defects in Ion Transport in Block Copolymer Electrolytes. *Nano letters* **2019**.

32. Rincon-Delgadillo, P.; Craig, G.; Gronheid, R.; Nealey, P. F., Scale-up of a chemo-epitaxy flow for feature multiplication using directed self-assembly of block-copolymers. *J. Photopolym. Sci. Technol.* **2013,** *26* (6), 831-839.

33. Rincon Delgadillo, P. A.; Gronheid, R.; Thode, C. J.; Wu, H.; Cao, Y.; Somervell, M.; Nafus, K.; Nealey, P. F., All track directed self-assembly of block copolymers: process flow and origin of defects. *Proc. SPIE* **2012,** *8323* (Alternative Lithographic Technologies IV), 83230D/1-83230D/9.

34. Liu, C.-C.; Ramírez-Hernández, A.; Han, E.; Craig, G. S. W.; Tada, Y.; Yoshida, H.; Kang, H.; Ji, S.; Gopalan, P.; de Pablo, J. J.; Nealey, P. F., Chemical Patterns for Directed Self-Assembly of Lamellae-Forming Block Copolymers with Density Multiplication of Features. *Macromolecules* **2013,** *46* (4), 1415-1424.

35. Seidel, R.; Delgadillo, P. R.; Ramirez-Hernandez, A.; Wu, H.; Her, Y.; Yin, J.; Nealey, P.; de Pablo, J.; Gronheid, R., Investigation of cross-linking poly(methyl methacrylate) as a guiding material in block copolymer directed self-assembly. *Proc. SPIE* **2014,** *9051* (Advances in Patterning Materials and Processes XXXI), 90510K/1-90510K/10.

36. Suh, H. S.; Nair, A.; Delgadillo, P. R.; Doise, J.; Lorusso, G.; Nealey, P.; Monreal, V.; Baskaran, D.; Cao, Y.; Padmanaban, M.; Li, J.; Kato, T.; Sutani, T.; Ishimoto, T.; Ikota, M.; Koshihara, S. In *Impact of annealing temperature on DSA process: toward faster assembly kinetics (Conference Presentation)*, SPIE Advanced Lithography, SPIE: 2018.

37. Garner, G. P.; Rincon Delgadillo, P.; Gronheid, R.; Nealey, P. F.; de Pablo, J. J., Design of surface patterns with optimized thermodynamic driving forces for the directed self-assembly of block copolymers in lithographic applications. *Mol. Syst. Des. Eng.* **2017**.

38. Williamson, L. D.; Seidel, R. N.; Chen, X.; Suh, H. S.; Rincon Delgadillo, P.; Gronheid, R.; Nealey, P. F., Three-Tone Chemical Patterns for Block Copolymer Directed Self-Assembly. *ACS applied materials & interfaces* **2016,** *8* (4), 2704-12.

39. Ren, J.; Zhou, C.; Chen, X.; Dolejsi, M.; Craig, G. S. W.; Rincon Delgadillo, P. A.; Segal-Peretz, T.; Nealey, P. F., Engineering the Kinetics of Directed Self-Assembly of Block Copolymers toward Fast and Defect-Free Assembly. *ACS applied materials & interfaces* **2018,** *10* (27), 23414-23423.

40. Raybin, J.; Ren, J.; Chen, X.; Gronheid, R.; Nealey, P. F.; Sibener, S. J., Real-Time Atomic Force Microscopy Imaging of Block Copolymer Directed Self Assembly. *Nano letters* **2017,** *17* (12), 7717-7723.

41. Ghani.;, M. T. B. T. Self-Aligned Contacts. USOO8436404B2.

42. Wan, L.; Ruiz, R.; Gao, H.; Patel, K. C.; Albrecht, T. R.; Yin, J.; Kim, J.; Cao, Y.; Lin, G., The Limits of Lamellae-Forming PS-b-PMMA Block Copolymers for Lithography. *ACS nano* **2015,** *9* (7), 7506-14.

43. Kim, S.; Nealey, P. F.; Bates, F. S., Decoupling Bulk Thermodynamics and Wetting Characteristics of Block Copolymer Thin Films. *ACS Macro Lett.* **2012,** *1* (1), 11-14.

Chapter 2: Utilization of metal-polymer interactions for self-aligned directed self-assembly of device relevant features

2.1 Abstract

Self-aligned strategies are required because today's feature sizes are beyond the resolution limit of the exposure tools. One self-aligned strategy is Directed Self-Assembly (DSA), where block copolymers (BCP) are thermodynamically driven to self-align with a lithographically defined template with chemical contrast and/or topography. It would be particularly advantageous to also encode existing structures into thermodynamic information, then thermodynamics would cause BCP to self-align to these existing structures rectifying placement error. These existing features could be cut masks which are required in order to fabricate devices from line and space arrays, or it could be interconnects. Here we show a new technique, by which metal – polymer interactions can be used in place of polymer – polymer interactions. These metal – polymer interactions, which cannot be adequately described by conventional surface energy comparisons, allow for a true self-aligned process. We begin by classifying process relevant metals including gold, aluminum, copper, tungsten and cobalt based upon their thermodynamic interactions with PS-*b*-MMA. We then created guide patterns using metal and dielectric line space arrays. These patterns when combined with DSA allow for lines and space patterns to be self-aligned to any exposed metal features and reduce process constraints on exposure tools. Our process can also be used to align line and space patterns to metal layers during back end of the line processing. A similar process could also be used to guide contact hole shrink to correct for placement error in the initial lithographic template.

2.2 Introduction

Directed self-assembly (DSA) of block copolymers (BCP) is a density multiplication technique with high throughput and low fabrication cost[1-4]. Unlike conventional lithographic techniques, the ideal DSA process creates nanoscale structures that represent the thermodynamic equilibrium morphology. It is thus the only technique in which critical dimension uniformity is thermodynamically guaranteed, a fact which has been looked at for rectification of CDU in EUV processes[5]. The thermodynamic landscape is controlled by both the topography of the substrate and its chemical functionality. It has been customary to refer to topographic controlled DSA as graphoepitaxy and chemistry controlled DSA as chemoepitaxy, but most modern approaches are more correctly termed hybrid DSA as they incorporate both cues[6-7]. Integration of these cues into the contact hole-shrink process has already been well explored[5, 8-9]. Similarly, work has been done to create and integrate DSA for line space array patterns[2, 7, 10-14]. While both integration strategies make use of patterns containing chemical and topographical cues, in both cases these patterns rely on an initial lithographic template to define the pattern. Thus, misalignment between the lithographic template and other device critical layers can result in catastrophic defects. If the device critical layers can be used as the template this misalignment can be prevented.

In this work, we first investigate the chemical preference of metals for PS and PMMA utilizing hole island tests. We then show the thermodynamic landscape formed by a metal/dielectric pattern, analogous to those found in devices, can present a natural pattern for hybrid DSA. Without performing any additional lithography to define a new layer, this pattern can be used to self-align BCP for DSA. This could be used to reduce the number of exposures necessary in a given process, or because metals are natural etch masks, could be implemented to create sparse arrays of lines and spaces. We use e-beam lithography to create patterns consisting of line space arrays of

alternating metal dielectrics as a simulated active surface. Finally, these simulated active surfaces are used to guide the self-aligned DSA of PS-*b*-PMMA.

2.3 Methodology

2.3.1 Preparation of Substrates

Silicon wafers were purchased from WRS materials. Wafers were hot piranha cleaned (DANGER!) utilizing 70:30 Sulfuric Acid:Hydrogen Peroxide (30%) at 130°C. The wafers were placed into the piranha bath for a minimum five minutes before being cleaned with house DI for several minutes to create a pristine ultra-hydrophilic surface. Wafers were used within days of cleaning to prevent reabsorption of organic material. Metal substrates were deposited at a rate of one angstrom per second onto cleaned wafers using the following methodologies: Copper substrates were prepared by thermal evaporation utilizing an Angstrom Nexdep at a base pressure of at least 3e-6 Torr. Gold substrates were prepared by e-beam evaporating a 10 nm chromium adhesion layer and subsequently at least 20 nm of gold using an AJA ATC-Orion 8E with a base pressure of at least 10e-7 Torr. Tungsten, cobalt, and aluminum substrates were sputtered utilizing an AJA Orion 5 UHV Sputtering system with a base pressure of at least 10e-8 Torr in an argon plasma. All substrates used have whatever native oxide may be present after an hour in an air environment. When it was desired to use the underlying copper, the native oxide was stripped by a five-minute soak in a five-weight percent citric acid solution after which the sample was DI rinsed, N2 dried, and immediately used.

2.3.2 Determination of Substrate Wetting

Substrate preferentiality was determined using the hole island test on unpatterned metal substrates. The hole island test consists of spincoating a lamella forming block copolymer to a

thickness incommensurate with its natural periodicity, L0. At these incommensurate thicknesses, the block copolymer will terrace in order to form features that maximize favorable interactions at both the substrate and free interface. In the case of asymmetric wetting, both 0.5 and 1.5 L0 thicknesses maximize the favorable interactions, and thus an incommensurate thickness of 1.25 L0 will resulting in either one L0 deep holes. Similarly, in the case of symmetric wetting both 1 and 2 L0 thicknesses are favorable resulting in the formation of one L0 high islands. One can then use optical microscopy to determine the presence of bright 'holes' or darker 'islands'. Our analysis is aided by the fact that at annealing temperatures below 200°C PS prefers the free interface. This means symmetric wetting indicates that PS wets both the top and bottom interfaces, whereas asymmetric wetting indicates that PMMA wets the bottom interface with PS still at the top interface. The hole island test is therefore a definitive probe of the substrate polymer interaction.

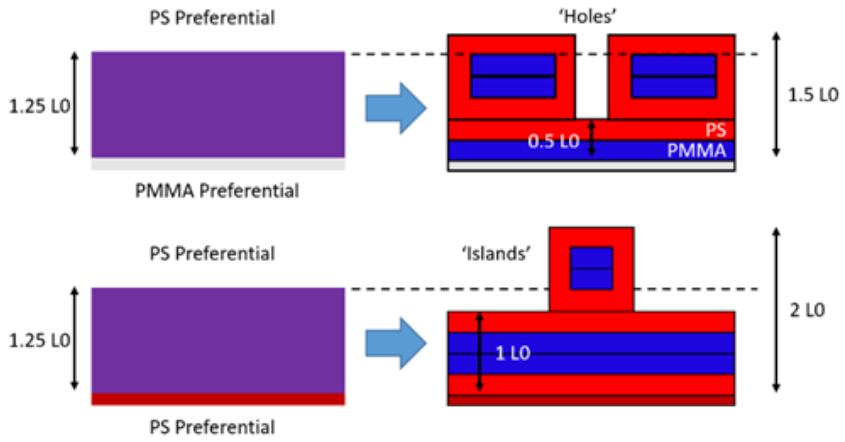

Figure 4**.** A PS-b-MMA film is spuncoat to a thickness of 1.25 L_0. After annealing at a temperature where PS prefers the free interface, the preference of the substrate can be determined by the presence of holes or islands.

Pristine substrates water contact angle was also measured using Millipore DI water in a goniometer. The angle reported was measured 100 ms after the 1 uL drop detached from syringe tip.

2.3.3 Preparation of Metal Dielectric Patterns

Gl-2000 was spun coat onto a piranha cleaned silicon wafer to a thickness of 55nm as determined by single angle ellipsometry on a J.A. Woollam Alpha SE, using a Cauchy model. The resist was softbaked at 150°C for three minutes. Patterning was performed using a JEOL 9300 at a voltage of 100 KeV and a current of 1 nA. Exposed wafers were developed for 15 seconds with gentle swirling in N-amyl acetate and then rinsed in IPA for a minimum of one minute. Metal was then deposited onto the patterns as described previously. Metal on top of the resist was then lifted off by soaking upside down in NMP at 80C for 15 minutes, after which time the sample was placed in fresh NMP and sonicated for a further 10 minutes at 80C. Metal dielectric patterns were then rinsed successively with IPA and DI water before being spun dry.

2.3.4 Self-Aligned Directed Self-Assembly

PS-*b*-MMA with a molecular weight of 22k-22k and an L0 of 25 nm was spuncoat to a thickness of 1.5 L0 as determined by single angle ellipsometry. The sample was then annealed at 250°C for 5 minutes inside a glovebox. Post annealing samples were imaged on a Zeiss Merlin through an in-lens detector with an accelerating voltage of 1 kV and a working distance of approximately 3 mm. The PMMA block is subsequently converted to alumina oxide using the sequential infiltration synthesis technique well described elsewhere[15-17]. Post SIS an oxygen plasma etch was conducted in a Plasma-Therm ICP to remove the PS block as well as any un-infiltrated PMMA. This creates a free-standing alumina oxide template which can be used for the purposes of pattern transfer.

2.4 Results

2.4.1 Hole Island Tests show metals can be non-preferential for polymers despite large differences in surface energy

Hole island tests were performed on bulk samples as described previously and optical micrographs were collected as shown in Figure 5. Piranha cleaned silicon oxide is known to be PMMA preferential and thus serves as an internal standard. PS-b-MMA was found to form holes on Chromium, Cobalt, Tungsten, Copper, and piranha cleaned silicon oxide. Copper oxide was found to be weakly PMMA preferential almost to point of non-preferentiality as subsequent SEM analysis found large areas of perpendicular assembly. Gold and aluminum had no holes or island indicating the non-preferential nature of the substrate. SEM inspection revealed extant fingerprint on the gold substrate, whereas the aluminum substrate had far poorer assembly.

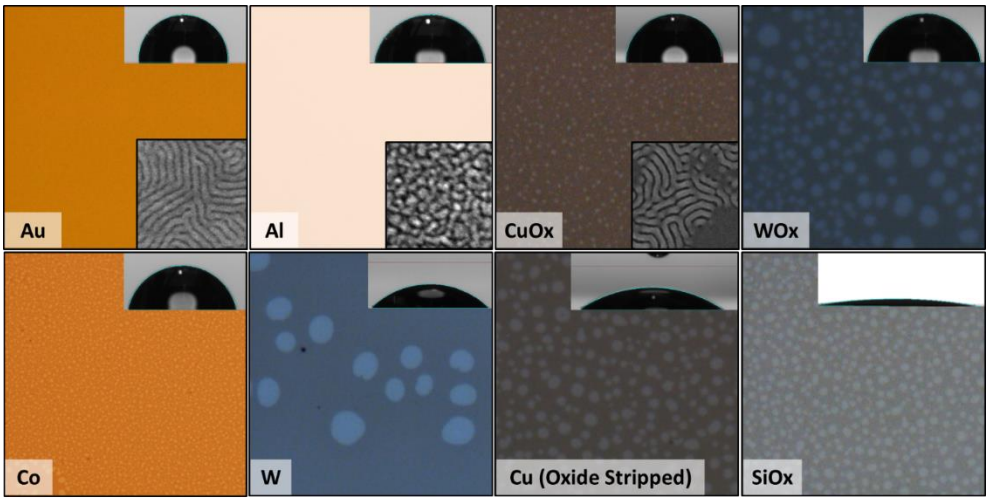

Figure 5. Optical micrographs of a 300 micron wide region captured of hole island tests conducted on substrates of interest. For Cu the native oxide was specifically stripped using citric acid. Inset shows the drop profile used to calculate water contact angle. Inset SEM image is half micron square and highlights the assembly quality.

2.4.2 Self-Aligned Directed Self-Assembly was successfully implemented on Copper Oxide/Silicon Oxide patterns

Metal dielectric lines were successfully patterned at varying pitches and width across 100 by 100 micron areas utilizing e-beam lithography, thermal evaporation, and lift off as previously described. Copper Oxide/Silicon Oxide alternating patterns were chosen because e-beam evaporation or sputtering deposition techniques alter the e-beam resist making lift off difficult at nanometer length scales. A metal line height of 10 nm was chosen as recent work within our group has shown how combining chemoepitaxy with half L0 topography to create a hybrid epitaxial flow can result in orders of magnitude speed up for the DSA process by prohibiting the formation of some defective states[18]. This patterns also differs from more pure graphoepitaxial DSA strategies as implemented elsewhere[19], in that the PS-*b*-MMA film thickness of 37.5 nm is far above that of the topography, and the bottom of the trench is preferential (silicon oxide) instead of non-preferential. These patterns were then used to implement a successful self-aligned DSA process. In this implementation a pattern with a copper oxide line width of 1.5 L0 (37.5 nm) was used to the direct the self-assembly of PS-*b*-MMA with a natural periodicity of 25 nm. The orientation of the domains relative to the substrate is confirmed via the SIS process. After infiltrating the PMMA domains with alumina and etching out the PS domains, two domains remain on top of the copper stripe. As we show schematically, the resulting structure thus consists of a PS domain centered on top of the metal stripe with two PMMA domains also on top of the stripe. The remaining free-standing alumina stripes can either be used in conjunction with the metal stripe as a hard mask to create self-aligned features or could be utilized as is.

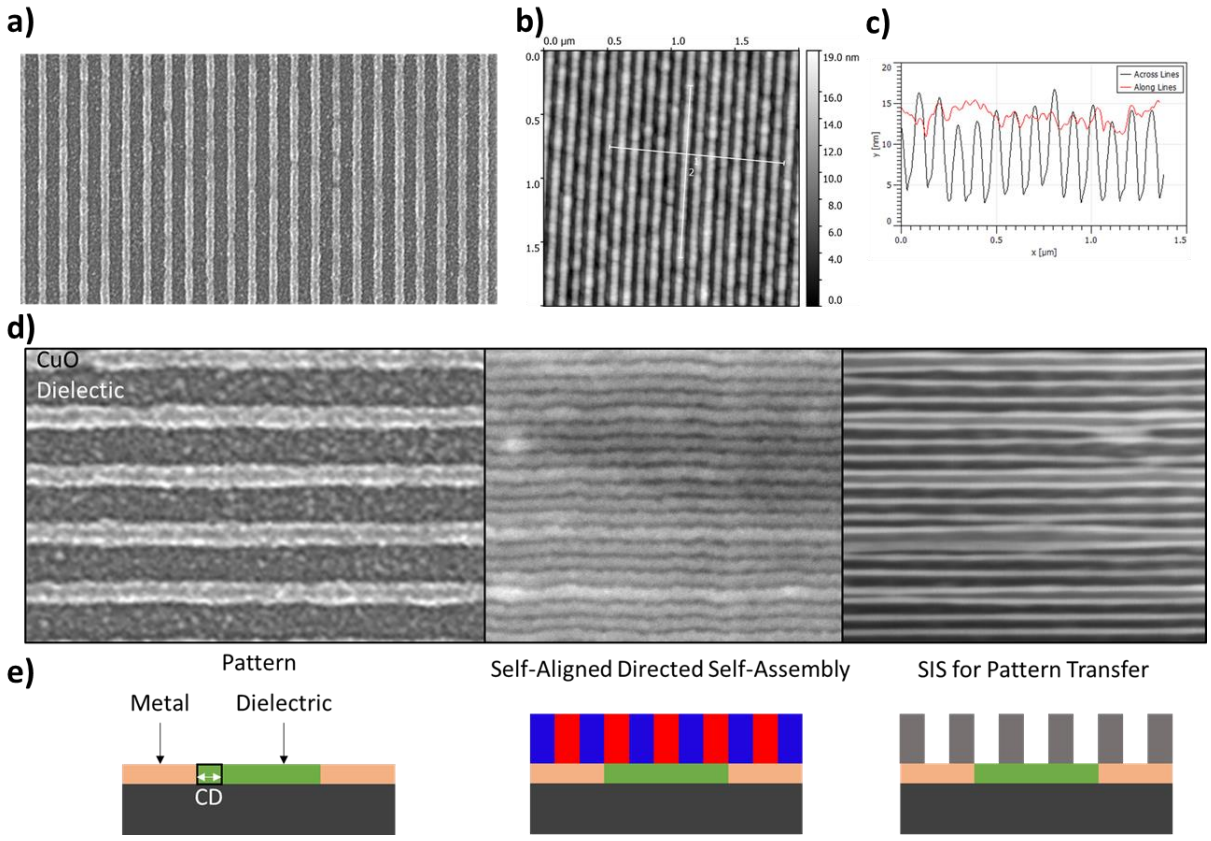

Figure 6. SEM Image (A) and AFM Height Image (B) of Metal Dielectric pattern utilized for self-aligned DSA. Extracted profiles (C) show line height and line height roughness. The self-aligned process was inspected via SEM (D) after assembly, and after the creation of alumina lines for pattern transfer. A schematic (E) showing the process at each inspection step is below for clarity. The pitch of the patterns (100 nm) serves as an internal scale bar.

2.5 Discussion

2.5.1 Metal-Polymer interactions are not explained by surface energy or water contact angle approaches

It is customary to think of substrate polymer interactions in terms of surface energies or solubility parameters[6, 20] in which substrates which interact equally with the two blocks are termed non-preferential. As a demonstration of how sensitive block copolymers are to surface free energy,

in our hole island test utilized earlier we exploit a 1% difference in surface free energy to ensure that the lower surface free energy polystyrene preferentially wets the free interface. Despite this sensitivity, non-preferential substrates can be made by creating a random copolymer of the two blocks of the block copolymer of interest and grafting it to the substrate[10, 21-22]. This random copolymer naturally has a surface energy between the two blocks and is thus non-preferential; however, it is well known that metals and their oxides have surface energies at a minimum twenty times that of many common polymers[23-24]. As a result, previous work studying metal deposition into PS-*b*-PMMA found the equilibrium metal structure formed to be metal spheres in which the metal aggregated to minimize metal polymer interactions[25]. It is thus an unexpected result that copper oxide ($\gamma \cong 1$ J/m^2) or gold ($\gamma \cong 1.6$ J/m^2)[26] would be non-preferential for PS ($\gamma \cong 40.7$ mJ/m^2) and PMMA ($\gamma \cong 41.1$ mJ/m^2)[20].

Another approach often used to analyze the preferentiality of a substrate is that of water contact angle (WCA). This technique allows for the probing of the hydrogen bonding component of the surface free energy, and trends in a roughly linear manner for random copolymers of PS-*b*-PMMA. Previously this technique was used to probe the nature of the LiNe flow chemical pattern after processing, where it was found the preferential XPS guide stripe (AZEMBLY NLD-128) and the non-preferential backfill brush (AZEMBLY NLD-127, 51% PS) had water contact angles of 83.7° and 76.0° respectively[6]. While we found that all PMMA preferential substrates had WCA below 74°, we do note that copper oxide with a WCA of 74° is close enough to non-preferential to be used in DSA. Chromium with a WCA of 78° which, by WCA, should be more PS preferential than the non-preferential backfill brush is instead PMMA preferential.

WCA and surface energy analyses only include information about dispersive, polar, and hydrogen bonding interactions, which may adequately capture the polymer - polymer interactions

as have been previously studied, but are not immediately translatable to metal – polymer interactions. As one example, the apparent non-preferentiality but poor assembly of the aluminum substrate can be understood through recent work which has demonstrated the ability of PMMA to graft strongly to aluminum through acid – base interactions[27]. These strong interactions compete with the assembly kinetics which traps a poorly assembled morphology. Still they can guide us to potential non-preferential substrates which we can confirm via the hole-island test. All three metal surfaces which were non-preferential had water contact angles above 70° and surface free energies lower than 1500 mJ/m^2.

Table 2. The preferentiality of each substrate as determined via the hole island test, as well as the pristine substrates water contact angle and surface free energy. The surface free energy of metals presented are those previously summarized by Vitos et al.[26] The water contact of piranha cleaned SiOx though 10 degrees after 100 ms, quickly approaches 0 degrees as the water drop wets the entire surface of the wafer

Material	Preferentiality	Water Contact Angle (degrees)	Surface Free Energy (mJ/m^2)
Au	Non-preferential	94	1400
Al	Non-preferential	83	1140
CuOx	Weakly PMMA	74	1300
WOx	PMMA	82	2350
Co	PMMA	73	2520
W	PMMA	45	3400
Cu	PMMA	35	1650
SiOx	PMMA	10*	

2.5.2 Self-Aligned DSA is complementary to other self-aligned strategies and can correct for placement error

Self-aligned DSA is complementary to the family of self-aligned strategies already developed by industry including self-aligned double patterning[28] and self-aligned contacts[29]. Self-aligned double patterning produces density multiplied features which are self-aligned to a lithographically defined template yielding intra-layer aligned features. Self-aligned contacts are created by covering transistor gates in an insulating cap allowing for source/drain contacts to be made without shorting to the gate. In contrast to these strategies our work utilizes self-alignment to align one device layer with lithographically defined features on the layer below it. Our work further serves as an expansion of recently published work by IBM and Tel[30]. Their work utilizes an organic planarization layer which allows for similar creation of sparse features. They also highlight the importance of DSA's thermodynamically driven CDU. Where our work differs is in the use of materials. We utilize dielectric and metal patterns without the need for brush grafting. Through the use of metal patterns, we also allow for the possibility of self-alignment of a new set of features to an existing patterned feature. With many processes now potentially requiring metal traces even below the active layer, self-aligned DSA could present a more tolerant path towards patterning transistors. These self-aligned strategies can also be utilized to create cut masks which must align to metal dielectric patterns.

2.6 Conclusions

In this work, we have successfully probed the wetting characteristics of different metals and metal oxides useful to the semiconductor industry. We have shown substrates such as metals and their oxides which have surface energies more than twenty times those of PS or PMMA can still

be non-preferential to PS-*b*-PMMA. Non-preferential substrates discovered in this work had lower surface energies and specifically lower polar surface energies as measured via water contact angle which will guide future studies. We have utilized e-beam lithography, thermal evaporation and lift off to create metal dielectric patterns which are analogous to those which might be find in a device layer. We then used the knowledge we gained about the wetting behaviors of these substrates, along with our patterns to successfully perform DSA without any brush deposition. The DSA resulted in PS-*b*-MMA lamella with PS domains self-aligned to the metal line. We further performed SIS and oxygen plasma to create a pattern of features which could be useful for either pattern transfer, or as final device features.

2.7 Acknowledgements

This research was supported in part by SRC through Nanomanufacturing Materials and Processes 2673.001. Use of the Center for Nanoscale Materials, an Office of Science user facility, was supported by the U.S. Department of Energy, Office of Science, Office of Basic Energy Sciences, under Contract No. DE-AC02-06CH11357. We acknowledge the MRSEC Shared User Facilities at the University of Chicago (NSF DMR-1420709). This work made use of the Pritzker Nanofabrication Facility of the Institute for Molecular Engineering at the University of Chicago, which receives support from Soft and Hybrid Nanotechnology Experimental (SHyNE) Resource (NSF ECCS-1542205), a node of the National Science Foundation's National Nanotechnology Coordinated Infrastructure. This work was previously presented at SPIE Advanced Lithography[31].

2.8 References

1. Ruiz, R.; Kang, H.; Detcheverry, F. A.; Dobisz, E.; Kercher, D. S.; Albrecht, T. R.; de Pablo, J. J.; Nealey, P. F., Density Multiplication and Improved Lithography by Directed Block Copolymer Assembly. *Science (Washington, DC, U. S.)* **2008,** *321* (5891), 936-939.

2. Stoykovich, M. P.; Kang, H.; Daoulas, K. C.; Liu, G.; Liu, C.-C.; de Pablo, J. J.; Mueller, M.; Nealey, P. F., Directed Self-Assembly of Block Copolymers for Nanolithography: Fabrication of Isolated Features and Essential Integrated Circuit Geometries. *ACS nano* **2007,** *1* (3), 168-175.

3. Cushen, J.; Wan, L.; Blachut, G.; Maher, M. J.; Albrecht, T. R.; Ellison, C. J.; Willson, C. G.; Ruiz, R., Double-Patterned Sidewall Directed Self-Assembly and Pattern Transfer of Sub-10 nm PTMSS-b-PMOST. *ACS applied materials & interfaces* **2015,** *7* (24), 13476-83.

4. Sanders, D. P.; Cheng, J.; Rettner, C. T.; Hinsberg, W. D.; Kim, H.-C.; Trung, H.; Fritz, A.; Harrer, S.; Holmes, S.; Colburn, M., Integration of Directed Self-Assembly with 193 nm Lithography. *Journal of Photopolymer Science and Technology* **2010,** *23* (1), 11-18.

5. Somervell, M. H.; Gronheid, R.; Singh, A.; Younkin, T. R.; Rincon Delgadillo, P.; Nealey, P.; Chan, B. T.; Nafus, K.; Romo Negreira, A.; Somervell, M., Rectification of EUV-patterned contact holes using directed self-assembly. **2013,** *8682*, 86820A.

6. Williamson, L. D.; Seidel, R. N.; Chen, X.; Suh, H. S.; Rincon Delgadillo, P.; Gronheid, R.; Nealey, P. F., Three-Tone Chemical Patterns for Block Copolymer Directed Self-Assembly. *ACS applied materials & interfaces* **2016,** *8* (4), 2704-12.

7. Blachut, G.; Sirard, S. M.; Maher, M. J.; Asano, Y.; Someya, Y.; Lane, A. P.; Durand, W. J.; Bates, C. M.; Dinhobl, A. M.; Gronheid, R.; Hymes, D.; Ellison, C. J.; Willson, C. G., A Hybrid Chemo-/Grapho-Epitaxial Alignment Strategy for Defect Reduction in Sub-10 nm Directed Self-Assembly of Silicon-Containing Block Copolymers. *Chemistry of Materials* **2016,** *28* (24), 8951-8961.

8. Yi, H.; Bao, X. Y.; Tiberio, R.; Wong, H. P., A General Design Strategy for Block Copolymer Directed Self-Assembly Patterning of Integrated Circuits Contact Holes using an Alphabet Approach. *Nano letters* **2015**.

9. Gronheid, R.; Delgadillo, P. R.; Singh, A.; Younkin, T. R.; Sayan, S.; Chan, B. T.; Van Look, L.; Bekaert, J.; Pollentier, I.; Nealey, P. F., Readying directed self-assembly for patterning in semi-conductor manufacturing. *J. Photopolym. Sci. Technol.* **2013,** *26* (6), 779-791.

10. Liu, C.-C.; Ramírez-Hernández, A.; Han, E.; Craig, G. S. W.; Tada, Y.; Yoshida, H.; Kang, H.; Ji, S.; Gopalan, P.; de Pablo, J. J.; Nealey, P. F., Chemical Patterns for Directed Self-Assembly of Lamellae-Forming Block Copolymers with Density Multiplication of Features. *Macromolecules* **2013,** *46* (4), 1415-1424.

11. Nealey, P. F.; Kang, H.; Liu, G.; Yoshida, H.; Ramirez-Hernandez, A.; De Pablo, J. J.; Tada, Y. Directed assembly of block copolymer films between a chemically patterned surface and a second surface. WO2013040483A1, 2013.

12. Suh, H. S.; Kim, D. H.; Moni, P.; Xiong, S.; Ocola, L. E.; Zaluzec, N. J.; Gleason, K. K.; Nealey, P. F., Sub-10-nm patterning via directed self-assembly of block copolymer films with a vapour-phase deposited topcoat. *Nature nanotechnology* **2017,** *12* (6), 575-581.

13. Liu, C.-C.; Thode, C. J.; Delgadillo, P. A. R.; Craig, G. S. W.; Nealey, P. F.; Gronheid, R., Towards an all-track 300 mm process for directed self-assembly. *J. Vac. Sci. Technol., B: Nanotechnol. Microelectron.: Mater., Process., Meas., Phenom.* **2011,** *29* (6), 06F203/1-06F203/6.

14. Rincon Delgadillo, P. A.; Gronheid, R.; Thode, C. J.; Wu, H.; Cao, Y.; Somervell, M.; Nafus, K.; Nealey, P. F., All track directed self-assembly of block copolymers: process flow and origin of defects. *Proc. SPIE* **2012,** *8323* (Alternative Lithographic Technologies IV), 83230D/1-83230D/9.

15. Cummins, C.; Ghoshal, T.; Holmes, J. D.; Morris, M. A., Strategies for Inorganic Incorporation using Neat Block Copolymer Thin Films for Etch Mask Function and Nanotechnological Application. *Advanced materials* **2016**.

16. Segal-Peretz, T.; Winterstein, J.; Doxastakis, M.; Ramirez-Hernandez, A.; Biswas, M.; Ren, J.; Suh, H. S.; Darling, S. B.; Liddle, J. A.; Elam, J. W.; de Pablo, J. J.; Zaluzec, N. J.; Nealey, P. F., Characterizing the Three-Dimensional Structure of Block Copolymers via Sequential Infiltration Synthesis and Scanning Transmission Electron Tomography. *ACS nano* **2015,** *9* (5), 5333-5347.

17. Tseng, Y.-C.; Peng, Q.; Ocola, L. E.; Elam, J. W.; Darling, S. B., Enhanced Block Copolymer Lithography Using Sequential Infiltration Synthesis. *The Journal of Physical Chemistry C* **2011,** *115* (36), 17725-17729.

18. Ren, J.; Zhou, C.; Chen, X.; Dolejsi, M.; Craig, G. S. W.; Rincon Delgadillo, P. A.; Segal-Peretz, T.; Nealey, P. F., Engineering the Kinetics of Directed Self-Assembly of Block Copolymers toward Fast and Defect-Free Assembly. *ACS applied materials & interfaces* **2018,** *10* (27), 23414-23423.

19. Tsai, H.; Pitera, J. W.; Miyazoe, H.; Bangsaruntip, S.; Engelmann, S. U.; Liu, C. C.; Cheng, J. Y.; Bucchignano, J. J.; Klaus, D. P.; Joseph, E. A.; Sanders, D. P.; Colburn, M. E.; Guillorn, M. A., Two-dimensional pattern formation using graphoepitaxy of PS-b-PMMA block copolymers for advanced FinFET device and circuit fabrication. *ACS nano* **2014,** *8* (5), 5227-32.

20. Suh, H.-S.; Kang, H.; Liu, C.-C.; Nealey, P. F.; Char, K., Orientation of Block Copolymer Resists on Interlayer Dielectrics with Tunable Surface Energy. *Macromolecules (Washington, DC, U. S.)* **2010,** *43* (1), 461-466.

21. Han, E.; Gopalan, P., Cross-linked random copolymer mats as ultrathin nonpreferential layers for block copolymer self-assembly. *Langmuir : the ACS journal of surfaces and colloids* **2010,** *26* (2), 1311-5.

22. In, I.; La, Y.-H.; Park, S.-M.; Nealey, P. F.; Gopalan, P., Side-chain-grafted random copolymer brushes as neutral surfaces for controlling the orientation of block copolymer microdomains in thin films. *Langmuir : the ACS journal of surfaces and colloids* **2006,** *22* (18), 7855-7860.

23. Soon, A.; Todorova, M.; Delley, B.; Stampfl, C., Thermodynamic stability and structure of copper oxide surfaces: A first-principles investigation. *Physical Review B* **2007,** *75* (12).

24. Skriver, H. L.; Rosengaard, N. M., Surface energy and work function of elemental metals. *Physical Review B* **1992,** *46* (11), 7157-7168.

25. Lopes, W. A.; Jaeger, H. M., Hierarchical self-assembly of metal nanostructures on diblock copolymer scaffolds. *Nature* **2001,** *414* (6865), 735-8.

26. Vitos, L.; Ruban, A. V.; Skriver, H. L.; Kollár, J., The surface energy of metals. *Surface Science* **1998,** *411* (1-2), 186-202.

27. Pletincx, S.; Marcoen, K.; Trotochaud, L.; Fockaert, L. L.; Mol, J. M. C.; Head, A. R.; Karslioglu, O.; Bluhm, H.; Terryn, H.; Hauffman, T., Unravelling the Chemical Influence of Water on the PMMA/Aluminum Oxide Hybrid Interface In Situ. *Sci Rep* **2017,** *7* (1), 13341.

28. Mason, M. E.; Ma, Y.; Sweis, J.; Yoshida, H.; Wang, Y.; Kye, J.; Levinson, H. J., Self-aligned double patterning (SADP) compliant design flow. **2012,** *8327*, 832706-832706-13.

29. Bohr, M. T.; Ghani, T.; Rahhal-Orabi, N. M.; Joshi, S. M.; Steigerwald, J. M.; Klaus, J. W.; Hwang, J.; Mackiewicz, R. Self-Aligned Contacts. US008436404B2, 2013.

30. Liu, C.-c.; Franke, E.; Lie, F. L.; Sieg, S.; Tsai, H.; Lai, K.; Truong, H.; Farrell, R.; Somervell, M.; Sanders, D.; Felix, N.; Guillorn, M.; Burns, S.; Hetzer, D.; Ko, A.; Arnold, J.; Colburn, M., Directed self-assembly patterning for forming fin field effect transistors. *SPIE Newsroom* **2016**.

31. Dolejsi, M.; Nealey, P. In *Utilization of metal-polymer interactions for self-aligned directed self-assembly of device relevant features (Conference Presentation)*, SPIE Advanced Lithography, SPIE: 2018; p 7.

Chapter 3: Ultrathin iCVD polymer interfacial energy control for DSA hole-shrink applications

3.1 Abstract

Integrated circuit layouts consist of patterned lines and holes, where holes define the electrical contacts between adjacent layers. Block copolymer directed self-assembly (DSA) successfully shrinks the critical dimension (CD) of these contacts beyond the resolution of conventional lithography. DSA also radically improves CD uniformity. One particularly difficult step of the DSA hole-shrink process involves establishing the correct interfacial energy throughout a lithographically templated hole to insure good assembly. Initiated chemical vapor deposition (iCVD) is a uniform, ultrathin, ultraconformal, all-organic deposition technique that allows for precise control of interfacial energy. In this work we use iCVD of polydivinylbenzene at film thicknesses below five nm to blend the interfacial energy of the coated film with that of the silicon / spin-on-carbon template. We fully characterize the iCVD surface through means of two liquid surface energy measurements. We further identify the interfacial energies presented by these functionalized templates through qualitative hole-island tests as well as quantitative harmonic mean estimations. In parallel we run TICG simulations with the determined interaction parameters and DSA experiments, and find good agreement across the range of chemistries created. Through careful control of iCVD conditions, especially filament temperature, we achieve a strongly polystyrene-preferential sidewall with a non-preferential bottom which we then demonstrate, both in simulation and in experiment, allows for a successful hole-shrink process across a wide range of template hole diameters.

3.2 Introduction

High volume manufacturing of smaller and smaller features requires increasing control over size, shape, and uniformity. Bottom-up processes such as directed self-assembly (DSA) are uniquely posed to address all three requirements. In DSA a lithographically defined template anchors and guides the self-assembly of block copolymers to form sub-lithographic features with excellent uniformity.[1-6] The patterning of contact holes or via holes is of particular interest, as multiple complex 193i exposures are required to achieve the proper density.[7-9] Even with EUV lithography, which provides the ability to pattern at higher densities, DSA hole-shrink has been shown to improve EUV local critical dimension uniformity, and repair stochastic defects such as merging vias.[10] In the DSA contact hole-shrink process, a lithographically defined template is often etched into spin-on carbon (SOC) using a spin-on glass (SOG) and SOC transfer stack.[7-9, 11] This template consists of an SOC sidewall with a silicon or silicon nitride bottom. Subsequent functionalization provides the appropriate chemical cue to the block copolymer to assemble into structures perpendicular to the surface.

In order to achieve the highest resolution features with the highest density, polystyrene-*block*-poly(methyl methacrylate) (PS-*b*-PMMA), with the appropriate size and volume fraction to form PMMA minority cylinders, is assembled inside of the functionalized template. Etching removes the PMMA cylinders and transfers their pattern into the underlying dielectric material, which is subsequently metallized to create a contact or via. Particularly advantageous to reaching high density is the ability to assemble multiple such contacts with a single lithographic template.[8-9, 12] Numerous simulations of self-assembly in confinement highlight the importance of independently functionalizing the side and bottom of the template to ensure a through-film structure.[12-15] As a result, numerous experimental efforts have focused on achieving different functionalities on the

sidewall versus the bottom of the template. Gronheid *et. al.* pioneered the sequential use of two orthogonal brush chemistries for this purpose.[9] A related approach, developed by Zhou *et. al.*, uses kinetic control to achieve differing brush thickness on the sidewall and template bottom allowing for either the interfacial energy of the brush or a mixture of the brush and substrate to be presented.[11] These efforts, as well as new simulations, have revealed unexpectedly that the strength of the sidewall preference is the key to avoid defective structures during the hole-shrink process.[11, 15]

It is thus desirable to have a more controllable process for setting the interfacial energy throughout the template. Initiated chemical vapor deposition (iCVD), is an ultrathin, ultraconformal,[16] all-organic vapor phase deposition technique that allows for precise control of interfacial energy, and has previously been integrated with DSA flows for lines and spaces.[17-20] In iCVD, a resistively heated filament cleaves a thermally labile bond in an initiator molecule. The resulting free radicals react with monomers adsorbed on a cooled growth surface to create a polymer film. The types of radicals generated and their relative concentration allows fine control of interfacial energy of the resulting polymer thin film. The radical mixture present in the chamber is largely dependent on the filament temperature.[21] In this work we deposit at varying filament temperatures iCVD films that are thin enough (~ 5 nm) to present a mixed substrate/film interfacial energy. These interfacial energies are qualitatively determined through the hole-island test,[22-24] and quantitatively determined through the harmonic mean approximation from surface energies.[25] The functionalized templates are then simulated to model the DSA process. Finally, DSA is performed, and found to be in good agreement with simulations. As a result, we identify a processing window where iCVD can be used to perfectly functionalize a template and DSA can be successfully achieved.

3.3 Experimental

In this section we describe the DSA hole-shrink process as outlined in Figure 7, as well as the ancillary experiments and simulations performed to fully describe the process.

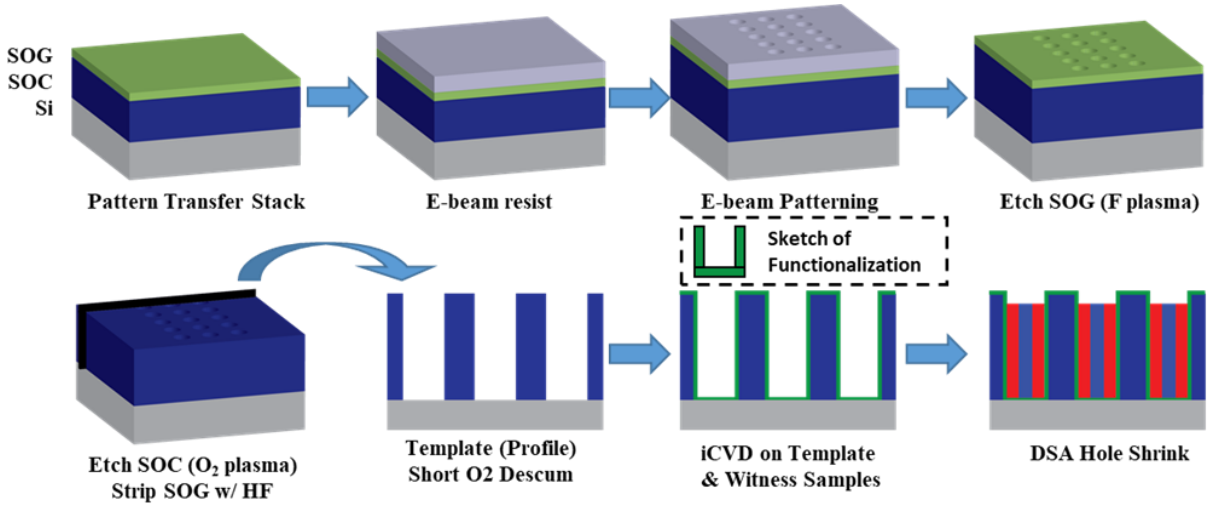

Figure 7. Schematic showing the complete DSA hole-shrink process. Inset is a sketch that will be used to depict template preferentiality throughout the paper.

3.3.1 Materials

Highly doped silicon wafers, with resistance (R) < 0.1 Ω·cm, were obtained from Pure Wafer or Silicon Materials, Inc. and cleaned with hot piranha immediately prior to use (DANGER! Reacts explosively with organics). SOC and SOG were provided by Tokyo Ohka Kogyo Co. (TOK) and used as received. Cylinder-forming PS-*b*-PMMA with a molecular weight of 50k-*b*-20k with a bulk morphological period (L_0) of 38 nm and lamellae-forming PS-*b*-PMMA with a molecular weight of 22k-*b*-22k with L_0 = 25 nm were purchased from Polymer Source and used as received. Positive e-beam resist CSAR 6200.04 was purchased from Allresist and diluted in propylene glycol monomethyl ether acetate to 2.5 wt%. DVB (80%), di-tert-butyl

peroxide (TBPO, 98%), isopropyl alcohol (IPA), deionized water (HPLC grade), and diiodomethane (99%) were purchased from Millipore Sigma and used without further purification. Oxygen (99%) and argon (99%) gases were purchased from Airgas and used without further purification.

3.3.2 Formation of hole-shrink templates

Lithographic templates were prepared following a process flow similar to that implemented by imec.[8] First SOC, and then SOG, were spin-coated and baked on a wafer in accordance with the manufacturer's instructions to yield a 100 nm thick layer of SOC and a 32 nm thick layer of SOG. A downstream oxygen clean was then used to oxidize the SOG surface to improve e-beam resist adhesion. Diluted CSAR 6200 was spin-coated to a thickness of ~55 nm and soft baked at 150 °C. The resist was then exposed on a Raith EBPG 5000+ electron beam lithography tool using a single shot exposure for each hole with an effective dose of 400–800 $\mu C/cm^2$. Development was performed in n-amyl acetate for 1 min followed by an IPA rinse and a nitrogen dry. A Plasmatherm ICP-RIE dedicated to fluorine chemistry was used to etch first the SOG with CF_4 and then the SOC with O_2 using a high bias power at low pressures. Finally, any remaining SOG was stripped in buffered HF before being shipped to MIT for iCVD deposition.

3.3.3 iCVD depositions conducted at MIT

Custom hole-shrink samples, clean silicon wafer sample, and SOC wafer samples were cleaned with an oxygen plasma (Harrick Plasma, RF Power 10.2 Watts, O_2 pressure 515-530 mTorr, 8 second exposure) prior to depositions. The samples were immediately loaded in a custom-built iCVD chamber, described elsewhere,[26] and brought under vacuum. DVB was heated to 40 °C and the resulting vapors were metered into the chamber at 0.5 sccm using a heated mass flow controller (MKS instruments). Room temperature TBPO and argon were

metered into the chamber at 3 and 6.7 sccm, respectively, using mass flow controllers. The chamber pressure was maintained at 90 mTorr using a throttling butterfly valve (MKS instruments) and the substrate temperature was fixed at 30 °C using a recirculating chiller (Thermo Scientific). A Chromaloy O filament (Goodfellow) was resistively heated to crack the peroxide bond of TBPO molecules.

Three filament temperatures (240, 270, and 300 °C) and two film thicknesses per filament temperature were used, resulting in six experimental conditions. Previously these filament temperatures were shown to yield slightly PS-preferential to very PS-preferential films.[18] The deposition time was varied to yield different film thicknesses. Films grown at higher filament temperatures required shorter deposition times. Film thickness on a reference silicon wafer (Pure Wafer) was measured ex situ using a variable angle spectroscopic ellipsometer (J. A. Woollam) at incident angles of 65°, 70°, and 75°. The data were fit to a Cauchy-Urbach isotropic model to extract the film thickness. A summary of the experimental conditions and the resulting polydivinylbenzene (PDVB) film thicknesses is given in Table 3. Atomic force microscopy (AFM) of the templates both before and after deposition was measured using an ultra-sharp, high frequency USC-F1.2-k7.3 tip on an Asylum Cypher in order to determine conformality.

Table 3. Experimental conditions and resulting PDVB film thickness.

Filament Temperature (°C)	Deposition Time (min)	Film Thickness (nm)
240	60	4.1 ± 0.5
	30	3.4 ± 0.0
270	30	5.1 ± 0.9
	15	3.6 ± 0.3
300	15	4.8 ± 0.2
	10	3.1 ± 0.3

3.3.4 Hole-island qualitative determination of interfacial energy

Symmetric PS-*b*-PMMA (22k-*b*-22k) was spin-coated to a thickness of $1.0L_0$, $1.25L_0$, and $1.5L_0$ onto both PDVB-coated silicon and SOC corresponding to each iCVD condition. Films were then annealed for 1 h in a vacuum chamber at 170 °C to induce microphase separation. Finally, films were imaged both optically and using a Zeiss Merlin SEM at a working distance of 3 mm, with an acceleration voltage of 1 keV in high-resolution mode with the InLens secondary electron detector.

3.3.5 Quantitative determination of interfacial energy

Static contact angles of water and diiodomethane on the PDVB films grown on both silicon and SOC were measured using a Model 500 Ramé-Hart Goniometer. The dispersive (γ^d), polar (γ^p), and total surface energies (γ) were calculated assuming a harmonic mean using the Drop Advanced software included with the goniometer. Interfacial energies, ($\gamma_{interfacial}$) between the substrates and either PS or PMMA were estimated using the harmonic mean equation, Eq. (1), as described previously.[25] The surface energies of PS and PMMA, Eqs. (2) and (3), were taken from the literature.[27]

$$\gamma_{interfacial} = \gamma_{poly} + \gamma_{surf} - \frac{4\gamma^d_{poly}\gamma^d_{surf}}{\gamma^d_{poly}+\gamma^d_{surf}} - \frac{4\gamma^p_{poly}\gamma^p_{surf}}{\gamma^p_{poly}+\gamma^p_{surf}}, \quad (1)$$

where

$$\gamma_{PS} = \gamma^d_{PS} + \gamma^p_{PS} = 33.9 + 6.8 = 40.7 \left(\frac{mJ}{m^2}\right), \quad (2)$$

and

$$\gamma_{PS} = \gamma^d_{PS} + \gamma^p_{PS} = 29.6 + 11.5 = 41.1 \left(\frac{mJ}{m^2}\right). \quad (3)$$

3.3.6 Directed self-assembly

Simulations of the DSA process were conducted using a theoretically informed coarse grain model previously developed to study the kinetics of assembly in the DSA hole-shrink process, which is well described elsewhere.[11, 15] In brief, *n* block copolymer chains are represented by *N* beads connected by Gaussian springs at constant temperature and volume. There is both a bonded energy associated with the polymer chain extension as well as a nonbonded interaction which accounts for melt compressibility, interchain interactions, as well as x_{AB}, which governs the incompatibility of the two blocks. Two further terms govern the interaction of the blocks with the sidewall and bottom of the template and decay exponentially with distance from the template. These interactions are calculated by a particle-to-mesh (PM_0) scheme where the interactions are locally tabulated within shifting cubic cells. The model is driven to equilibrium by a Monte Carlo simulation utilizing the Metropolis Criterion, where the probability of accepting a move is given by $p_{acc} = \exp(-\Delta H/(k_b T))$. Two moves are considered: single bead displacement and chain reptation.

DSA experiments were conducted by spin coating PMMA-cylinder-forming PS-*b*-PMMA (50k-*b*-20k) with L_0 = 38 nm on top of the iCVD hole-shrink templates. Substrates were then annealed in a nitrogen glovebox at 270 °C for 1 h before imaging on a Zeiss Merlin SEM, using the same conditions as previously described.

3.4 Results and Discussion

3.4.1 iCVD on hole-shrink template is ultra-conformal and uniform

AFM data was collected to measure the conformality of the iCVD film, as shown in Figure 8. As the profile was flat across the bottom of the holes, a true depth could be measured. If the depth of the hole decreased then additional material must have been deposited on the template bottom relative to the SOC sidewalls/top. Similarly, if the depth of the hole increased than less film must have been deposited on the template bottom relative to the SOC sidewalls/top. The thicker film depositions were measured as they were most likely to show the effect of non-conformal deposition, although a single thin condition was collected as additional validation. In all cases across more than 35 holes, the depth of the hole remained mostly constant. Some small decrease in hole depth was measured at higher temperatures suggesting a slightly increased film thickness on the template bottom relative to the sidewalls. The standard deviation of hole depths was also very small (< 0.8 nm) indicating the uniformity of the template hole depth was also unchanged as a result of the iCVD deposition.

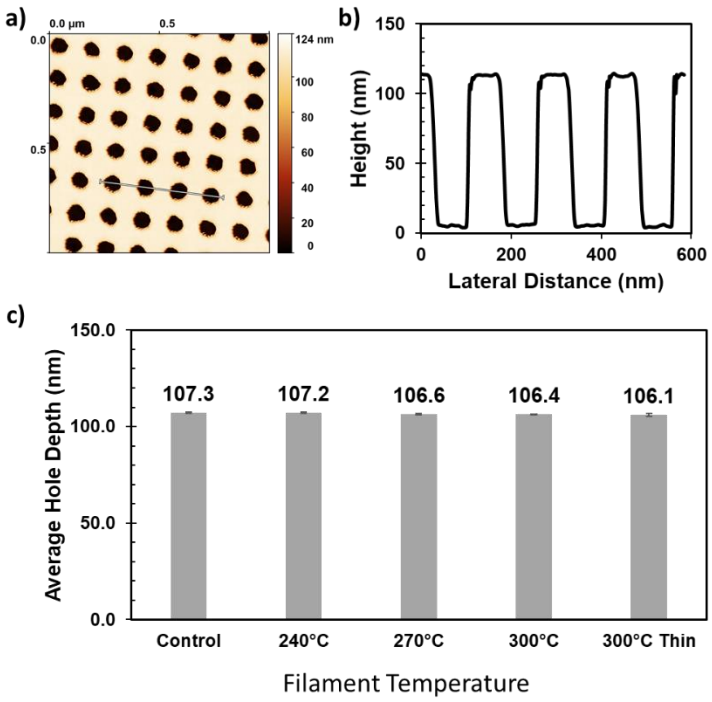

Figure 8. a) Representative AFM image from a hole-shrink template and b) the extracted profile. C) The collected hole depths as measured for a minimum of 35 holes for each thick film deposition, and for the 300°C thin film condition. Error bars represent standard deviation of 35 measurements and are less than half a nanometer in all cases.

3.3.4 Hole-Island qualitatively determines interfacial energy

Lamellae-forming block copolymers naturally form parallel domains when the surface energies of the blocks are unequal. Because the PS-*b*-PMMA (22k-*b*-22k) is annealed at 170 °C, PS has a lower surface energy and is pinned to the free interface.[28-29] If the interfacial energy of the substrate is lower towards PS than PMMA, PS is similarly pinned to the substrate, in a case called symmetric wetting. In symmetric wetting the film can only form smooth parallel lamella when the film thickness is an integer multiple of L_0 (nL_0). At incommensurate spacings, the film will either break to form a terraced structure. Alternatively, if the interfacial energy is close to

non-preferential, perpendicular assembly can be obtained at the interface.[25] If instead the interfacial energy of the substrate is lower towards PMMA than PS, PMMA is pinned to the substrate in a case called asymmetric wetting. In asymmetric wetting, the commensurate film thickness is offset by exactly $0.5L_0$ from the symmetric wetting case (nL_0+$0.5L_0$). Thus, by spin coating at thicknesses that span from the symmetric wetting commensurability condition (L_0) to the asymmetric wetting commensurability condition ($1.5L_0$), the substrate interfacial energy can be qualitatively determined.

Figure 9 And Figure 10 show the results of the hole-island test for all iCVD conditions as conducted on the SiOx and SOC samples, which mimic the template bottom and sidewall, respectively. A schematic depiction of preferentiality is shown following the previously described rules, with blue indicating PMMA preferentiality, purple indicating non-preferentiality, pink indicating slight PS preferentiality where some fingerprint pattern is still observed at all thicknesses, and red indicating full PS preferentiality.

Considering first only the SiOx results (Figure 9), increasing temperature increases PS preference in agreement with previous iCVD experiments.[18] Similarly, increasing thickness increases PS preference. However, we see that the SOC sidewall is almost always more PMMA-preferential then the SiOx bottom (Figure 10). Even more dramatic is that at a filament temperature of 300 °C, which was previously found to create very PS-preferential films, instead a PMMA-preferential sidewall is found for the thinner iCVD film. This can be explained only by the polymer interacting with both the iCVD film and the substrate during annealing. Previous work has shown that films in the thickness regime studied here often present interfacial energies as mixtures of both film and substrate as the polymer can penetrate the film during annealing and interact with the substrate.[30-31] It was also recently noted that PDVB iCVD films at these

thicknesses serve as ineffective barriers to resist processing, which further suggests the polymer may be able to contact the underlying substrate.[20] Several iCVD depositions appear to present interfacial energies that may be ideal for the DSA hole-shrink process. In particular, the 240 °C thin film deposition created a non-preferential bottom with a truly PS preferential sidewall. To better understand the true interfacial energy, quantitative measurements must be taken.

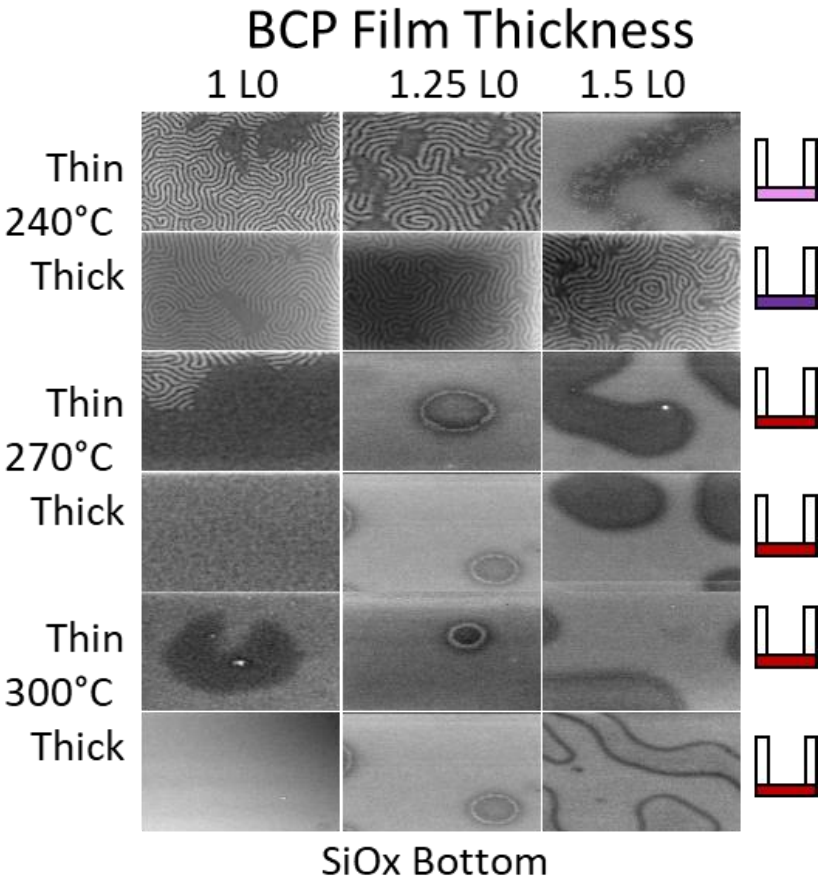

Figure 9. SEM micrographs capturing the PS-b-PMMA film assembly at different thicknesses and iCVD filament temperatures and relative thicknesses (left labels) on samples of the SiOx bottom. The sketch to the right of each row of SEM images shows the qualitative preferentiality from blue (PMMA) to red (PS) for clarity.

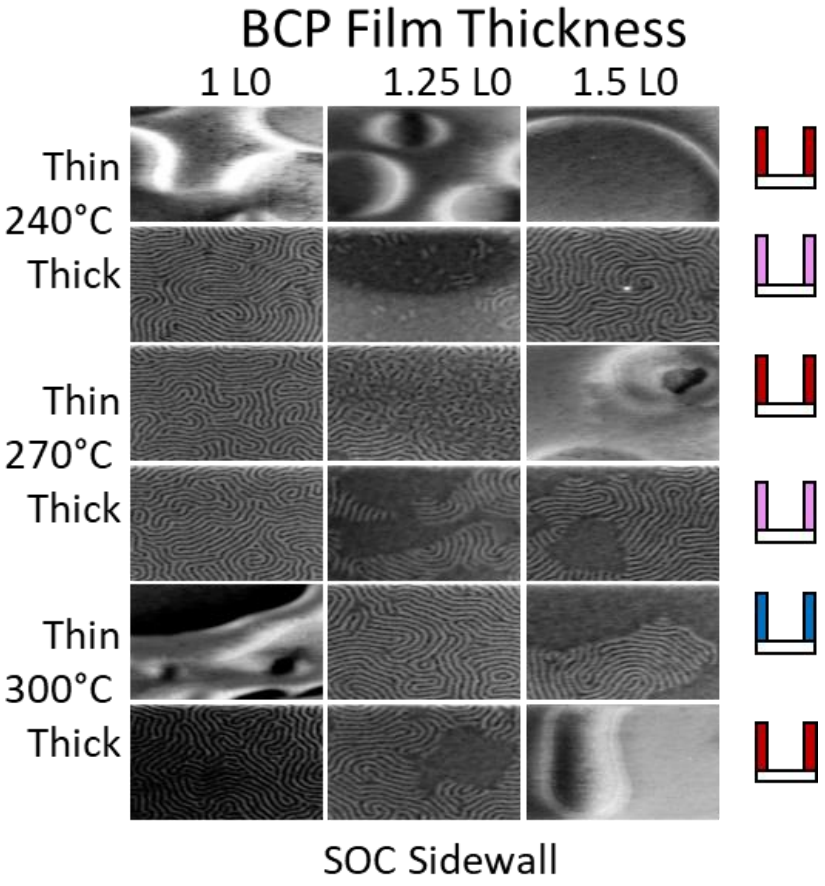

Figure 10. SEM micrographs capturing the PS-b-PMMA film assembly at different thicknesses and iCVD filament temperatures and relative thicknesses (left labels) on witness samples of the SOC sidewall. The sketch to the right of each row of SEM images shows the qualitative preferentiality from blue (PMMA) through to red (PS) for clarity.

3.3.5 Quantitative measurements confirm qualitative results

Figure 11 illustrates the effective surface energy presented by both the sidewall and bottom of the templates. The predominant measured effect of the iCVD film is to immediately drop the polar component of surface energy. One notable outlier of this rule is the 300 °C thin deposition on SOC, which still has a large polar component. There is also a subtle difference

between the surface energy of the SOC and the SiOx. To directly map the quantitative results on to the qualitative hole-island tests, the surface energy must be mapped onto an interfacial energy using the harmonic mean equation. Once the interfacial energy between the film and PS as well as the film and PMMA is calculated the difference of these interfacial energies is calculated to quantify the substrate preferentiality.

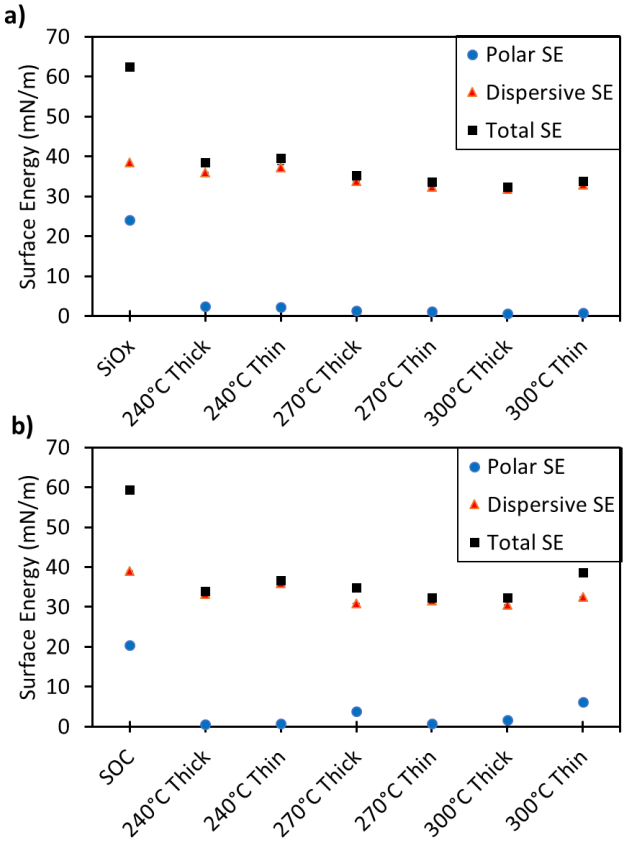

Figure 11. Calculated polar, dispersive, and total surface energy for all iCVD conditions. a) Silicon witness samples, which mimic the template bottom. b) SOC witness samples, which mimic the template sidewall. Error bars represent standard deviations of three measurements and are too small to observe.

Figure 12 shows the difference in interfacial energy along with the summarized qualitative results of the hole-island test. In the simplest case of calculating interfacial energy, we see that only the pure PS preferential conditions are adequately captured by the quantitative calculations. To correct for the observed effect of substrate/film mixed interfacial energy, the simplest approach is to average the effect of both the substrate and the film. When this is done the qualitative results are captured for all of the other films. This definitively shows the polymer must see a mixed chemistry for many of the conditions explored here. The 240 °C thinner iCVD film, which previously appeared to be promising for DSA, is found to have the largest PS-preferential sidewall, which recently has been shown to be critical for DSA hole-shrink process latitude.[15]

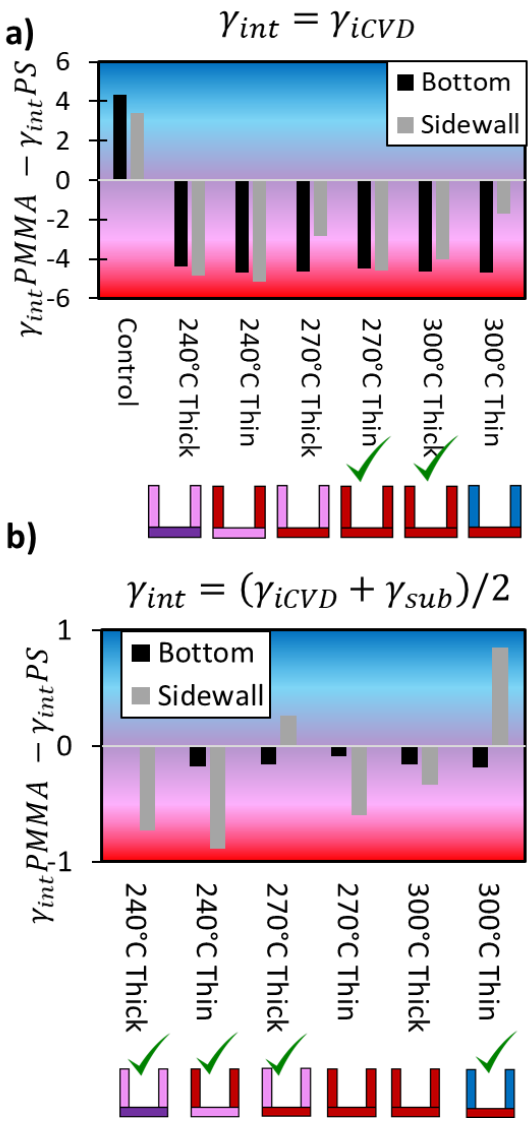

Figure 12. a) Calculated interfacial energies of both bottom (SiOx) and sidewall (SOC) of the template for both PS and PMMA. For clarity, only the difference in interfacial energy is plotted, and the color gradient indicates the relative PS preference (red) or PMMA preference (blue). b) The same calculation under the assumption that the polymer interacts with a mixture of the film and substrate. Sketches of template chemistry as determined by the qualitative hole-island test are shown for ease of comparison. A green check mark indicates agreement between quantitative and qualitative results.

3.4.4 Agreement between simulation and experiment, 240 °C thin iCVD film ideal for DSA hole-shrink

As a final test DSA was simulated and performed in experiments on the ideal 240 °C iCVD thin film sample identified in the qualitative and quantitative tests (Figure 13). The template chemistry is again shown schematically for ease of comparison. The simulation showed no defective structures *e.g*, bridging across a large range of template sizes. At larger sizes donuts eventually formed, which began to exhibit breaks as the size continued to increase. A similar trend was observed in the case of experiments in which perfect DSA was observed up until a template diameter of 70 nm. Past this diameter some shift was observed in the cylinder center, before finally a donut was formed at 100 nm. Of note is the suppression of the donut morphology in experiments relative to simulation. This could be due to the partially excluded area of the iCVD film, which the BCP can sample in experiments. In comparison, the simulation considers the walls of the template to be hard walls.

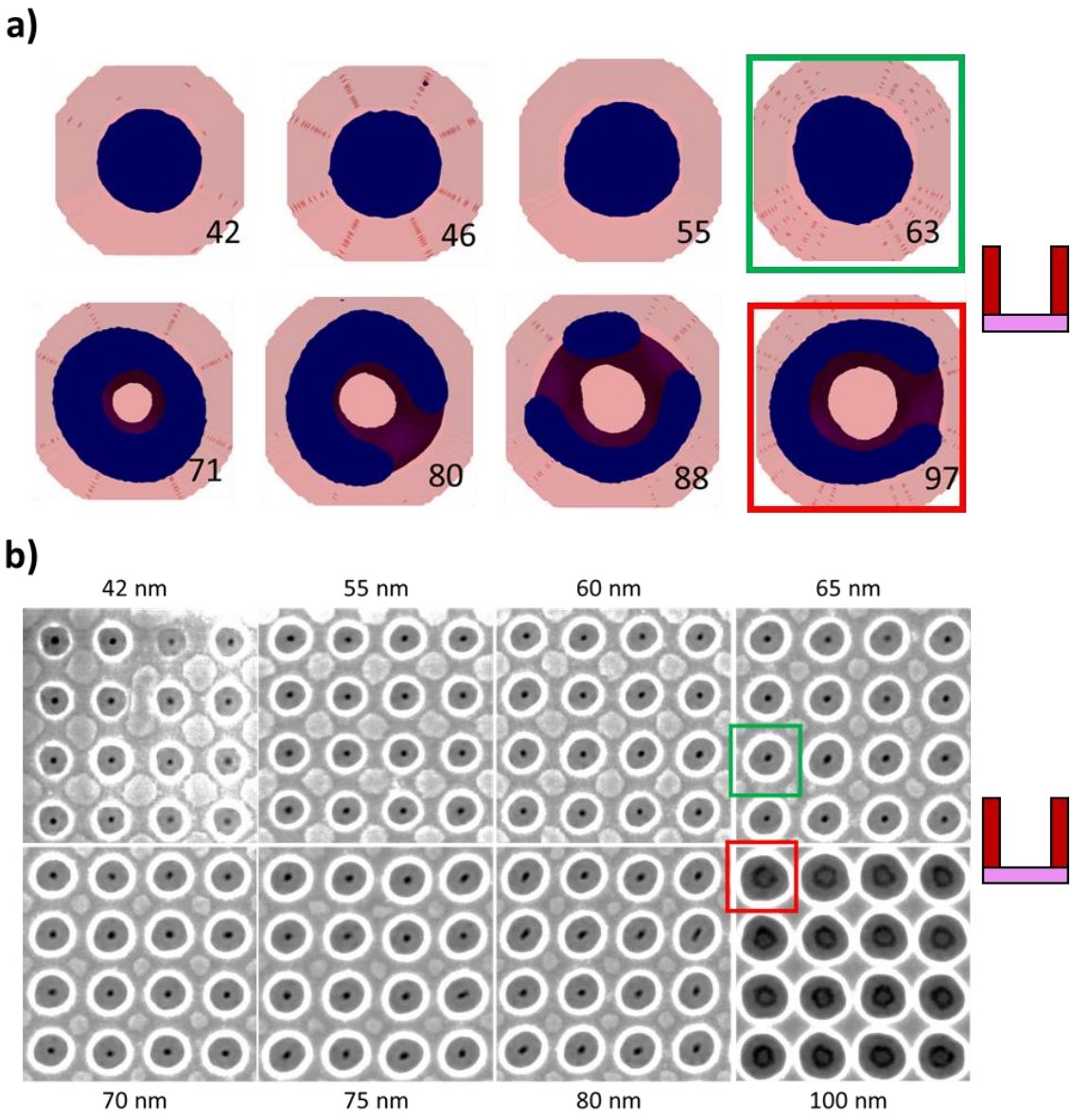

Figure 13. Comparison of simulations and experimental results of the DSA hole-shrink process with different widths of guiding holes. a) Results of simulations. b) SEM micrographs of experimental DSA results. The template holes are on a 150 nm pitch which serves as an internal scale. Both ideal assembly (green) and the eventual formation of donut (red) structures are captured in both experiments and simulations of the hole-shrink process on the 240 °C thin film processed template, whose preference is shown schematically (right).

3.5 Summary and Conclusions

In this work we have demonstrated the ability of iCVD to be used as an all-vapor chemical functionalization strategy for the DSA hole-shrink process. Both qualitative observations and quantitative measurements revealed that at a moderate temperature, 240 °C, a strongly preferential template sidewall can be created while maintaining a non-preferential template bottom. The interfacial energies generated could be explained by considering a blending of the film interfacial energy with that of the underlying substrate. Both simulation and experiment then showed how this ideally functionalized template can easily guide DSA of cylinder-forming PS-*b*-PMMA, creating much smaller contact holes. This work opens the ability of a dry process to replace one or more complex wet processing steps without impacting the DSA process.

3.6 Acknowledgements

The authors acknowledge support from the National Science Foundation **(award number: 1344891)**. Use of the Institute of Soldier Nanotechnologies is supported by the US Army Research Laboratory and the US Army Research Office Contract no. W911NF-13-D-0001. This work made use of the Pritzker Nanofabrication Facility of the Institute for Molecular Engineering at the University of Chicago, which receives support from Soft and Hybrid Nanotechnology Experimental (SHyNE) Resource **(NSF ECCS-1542205)**, a node of the National Science Foundation's National Nanotechnology Coordinated Infrastructure. We acknowledge the MRSEC Shared User Facilities at the University of Chicago (**NSF DMR-1420709**). We acknowledge Gordon S. W. Craig for helpful edits.

3.7 References

1. Liu, C.-C.; Thode, C. J.; Delgadillo, P. A. R.; Craig, G. S. W.; Nealey, P. F.; Gronheid, R., Towards an all-track 300 mm process for directed self-assembly. *J. Vac. Sci. Technol., B: Nanotechnol. Microelectron.: Mater., Process., Meas., Phenom.* **2011,** *29* (6), 06F203/1-06F203/6.

2. Somervell, M.; Gronheid, R.; Hooge, J.; Nafus, K.; Rincon Delgadillo, P.; Thode, C.; Younkin, T.; Matsunaga, K.; Rathsack, B.; Scheer, S.; Nealey, P., Comparison of directed self-assembly integrations. *Proc. SPIE* **2012,** *8325* (Advances in Resist Materials and Processing Technology XXIX), 83250G/1-83250G/14.

3. Somervell, M. H.; Gronheid, R.; Singh, A.; Younkin, T. R.; Rincon Delgadillo, P.; Nealey, P.; Chan, B. T.; Nafus, K.; Romo Negreira, A.; Somervell, M., Rectification of EUV-patterned contact holes using directed self-assembly. **2013,** *8682*, 86820A.

4. Seino, Y.; Yonemitsu, H.; Sato, H.; Kanno, M.; Kato, H.; Kobayashi, K.; Kawanishi, A.; Azuma, T.; Muramatsu, M.; Nagahara, S.; Kitano, T.; Toshima, T. In *Contact hole shrink process using graphoepitaxial directed self-assembly lithography*, SPIE: 2013; p 7.

5. Yi, H.; Bao, X. Y.; Tiberio, R.; Wong, H. P., A General Design Strategy for Block Copolymer Directed Self-Assembly Patterning of Integrated Circuits Contact Holes using an Alphabet Approach. *Nano letters* **2015**.

6. Liu, C.-C.; Franke, E.; Mignot, Y.; Xie, R.; Yeung, C. W.; Zhang, J.; Chi, C.; Zhang, C.; Farrell, R.; Lai, K.; Tsai, H.; Felix, N.; Corliss, D., Directed self-assembly of block copolymers for 7 nanometre FinFET technology and beyond. *Nature Electronics* **2018,** *1* (10), 562-569.

7. Hohle, C. K.; Gronheid, R.; Chi, C.; Liu, C.-C.; Meli, L.; Guo, J.; Parnell, D.; Mignot, Y.; Schmidt, K.; Sanchez, M.; Farrell, R.; Singh, L.; Furukawa, T.; Lai, K.; Xu, Y.; Sanders, D.; Hetzer, D.; Metz, A.; Burns, S.; Felix, N.; Arnold, J.; Corliss, D., Electrical study of DSA shrink process and CD rectification effect at sub-60nm using EUV test vehicle. **2017,** *10146*, 101460Q.

8. Doise, J.; Bekaert, J.; Chan, B. T.; Hori, M.; Gronheid, R., Via patterning in the 7-nm node using immersion lithography and graphoepitaxy directed self-assembly. *Journal of Micro/Nanolithography, MEMS, and MOEMS* **2017,** *16* (2).

9. Gronheid, R.; Hori, M.; Chan, B. T.; Doise, J., Dual brush process for selective surface modification in graphoepitaxy directed self-assembly. *Journal of Micro/Nanolithography, MEMS, and MOEMS* **2017,** *16* (03).

10. Gronheid, R.; Boeckx, C.; Doise, J.; Bekaert, J.; Karageorgos, I.; Ruckaert, J.; Chan, B. T.; Lin, C.; Zou, Y., *EUV patterned templates with grapho-epitaxy DSA at the N5/N7 logic nodes*. SPIE: 2016; Vol. 9776.

11. Zhou, C.; Kurosawa, T.; Dazai, T.; Doise, J.; Ren, J.; Bezik, C.; Segal-Peretz, T.; Gronheid, R.; Rincon-Delgadillo, P.; Yamazaki, A.; de Pablo, J.; Nealey, P. F., Studying the effects of chemistry and geometry on DSA hole-shrink process in three-dimensions. *Journal of Micro/Nanolithography, MEMS, and MOEMS* **2018,** *17* (03).

12. Doise, J.; Bezik, C.; Hori, M.; de Pablo, J. J.; Gronheid, R., Influence of Homopolymer Addition in Templated Assembly of Cylindrical Block Copolymers. *ACS nano* **2019,** *13* (4), 4073-4082.

13. Yu, B.; Sun, P.; Chen, T.; Jin, Q.; Ding, D.; Li, B.; Shi, A. C., Confinement-induced novel morphologies of block copolymers. *Phys Rev Lett* **2006,** *96* (13), 138306.

14. Laachi, N.; Delaney, K. T.; Kim, B.; Hur, S.-M.; Bristol, R.; Shykind, D.; Weinheimer, C. J.; Fredrickson, G. H., Self-consistent field theory investigation of directed self-assembly in cylindrical confinement. *Journal of Polymer Science Part B: Polymer Physics* **2015,** *53* (2), 142-153.

15. Bezik, C. T.; Garner, G. P.; de Pablo, J. J., Mechanisms of Directed Self-Assembly in Cylindrical Hole Confinements. *Macromolecules* **2018,** *51* (7), 2418-2427.

16. Servi, A. T.; Guillen-Burrieza, E.; Warsinger, D. M.; Livernois, W.; Notarangelo, K.; Kharraz, J.; Lienhard V, J. H.; Arafat, H. A.; Gleason, K. K., The effects of iCVD film thickness and conformality on the permeability and wetting of MD membranes. *Journal of Membrane Science* **2017,** *523*, 470-479.

17. Moni, P.; Mohr, A. C.; Gleason, K. K., Growth Rate and Cross-Linking Kinetics of Poly(divinyl benzene) Thin Films Formed via Initiated Chemical Vapor Deposition. *Langmuir : the ACS journal of surfaces and colloids* **2018,** *34* (23), 6687-6696.

18. Moni, P.; Suh, H. S.; Dolejsi, M.; Kim, D. H.; Mohr, A. C.; Nealey, P. F.; Gleason, K. K., Ultrathin and Conformal Initiated Chemical-Vapor-Deposited Layers of Systematically Varied Surface Energy for Controlling the Directed Self-Assembly of Block CoPolymers. *Langmuir : the ACS journal of surfaces and colloids* **2018,** *34* (15), 4494-4502.

19. Moni, P.; Al-Obeidi, A.; Gleason, K. K., Vapor deposition routes to conformal polymer thin films. *Beilstein J Nanotechnol* **2017,** *8*, 723-735.

20. Suh, H. S.; Kim, D. H.; Moni, P.; Xiong, S.; Ocola, L. E.; Zaluzec, N. J.; Gleason, K. K.; Nealey, P. F., Sub-10-nm patterning via directed self-assembly of block copolymer films with a vapour-phase deposited topcoat. *Nature nanotechnology* **2017,** *12* (6), 575-581.

21. Ozaydin-Ince, G.; Gleason, K. K., Transition between kinetic and mass transfer regimes in the initiated chemical vapor deposition from ethylene glycol diacrylate. *Journal of Vacuum Science & Technology A: Vacuum, Surfaces, and Films* **2009,** *27* (5), 1135-1143.

22. Maher, M. J.; Self, J. L.; Stasiak, P.; Blachut, G.; Ellison, C. J.; Matsen, M. W.; Bates, C. M.; Willson, C. G., Structure, Stability, and Reorganization of 0.5 L0 Topography in Block Copolymer Thin Films. *ACS nano* **2016**.

23. Peters, R. D.; Yang, X. M.; Nealey, P. F., Morphology of Thin Films of Diblock Copolymers on Surfaces Micropatterned with Regions of Different Interfacial Energy. *Macromolecules* **2002,** *35* (5), 1822-1834.

24. Smith, A. P.; Douglas, J. F.; Meredith, J. C.; Amis, E. J.; Karim, A., High-throughput characterization of pattern formation in symmetric diblock copolymer films. *J Polym Sci Pol Phys* **2001,** *39* (18), 2141-2158.

25. Suh, H. S.; Kang, H.; Nealey, P. F.; Char, K., Thickness Dependence of Neutral Parameter Windows for Perpendicularly Oriented Block Copolymer Thin Films. *Macromolecules* **2010,** *43* (10), 4744-4751.

26. Tenhaeff, W. E.; Gleason, K. K., Initiated Chemical Vapor Deposition of Alternating Copolymers of Styrene and Maleic Anhydride. *Langmuir* **2007,** *23* (12), 6624-6630.

27. Wu, S., *Polymer Interface and Adhesion*. 2017.

28. Mansky, P., Controlling Polymer-Surface Interactions with Random Copolymer Brushes. *Science* **1997,** *275* (5305), 1458-1460.

29. Han, E.; Stuen, K. O.; Leolukman, M.; Liu, C.-C.; Nealey, P. F.; Gopalan, P., Perpendicular Orientation of Domains in Cylinder-Forming Block Copolymer Thick Films by Controlled Interfacial Interactions. *Macromolecules* **2009,** *42* (13), 4896-4901.

30. Xiong, S.; Chapuis, Y. A.; Wan, L.; Gao, H.; Li, X.; Ruiz, R.; Nealey, P. F., Directed self-assembly of high-chi block copolymer for nano fabrication of bit patterned media via solvent annealing. *Nanotechnology* **2016,** *27* (41), 415601.

31. Han, E.; Stuen, K. O.; La, Y.-H.; Nealey, P. F.; Gopalan, P., Effect of Composition of Substrate-Modifying Random Copolymers on the Orientation of Symmetric and Asymmetric Diblock Copolymer Domains. *Macromolecules (Washington, DC, U. S.)* **2008,** *41* (23), 9090-9097.

Chapter 4 Confinement of Bottlebrush Block Copolymers Promotes Re-Arrangement of Backbones

4.1 Abstract

Graft polymers present a unique architecture for self-assembly where large features (100 nm +) can be rapidly formed from high molecular weight (1000 kg/mol +) materials. The assembly of a representative graft(polystyrene)-*block*-graft(polylacticacid), gPS-*b*-gPLA, is thoroughly studied in the thin film (< 100 nm) in the absence of solvent effects using a combination of GISAXS and SEM. Under out-of-plane confinement imposed by film thickness, graft polymers are observed to form features with an in-plane spacing approximately double that of the bulk. This expansion was found to be far more dramatic for PLA preferential substrates. Under the in-plane confinement imposed by a chemical pattern, the graft polymers form a non-bulk cylindrical morphology with PLA cores and PS coronas. These results show the incredible ability of these large polymers, once thought of as stiff, to undergo remarkable changes in morphology under confinement.

4.2 Introduction

Advances in polymerization chemistry have made it possible to investigate the effects of polymer architecture on material properties.[1-2] One particularly interesting architecture is that of graft polymers, or bottlebrush polymers, so called because they possess a grafted oligomeric pendant group on each backbone and thus resemble a bottlebrush. Block copolymers of bottlebrushes have been shown to rapidly self-assemble even above 1000 kg/mol into large (100 nm+) features forming photonic crystals.[3-4] The ability to selectively modify the pendant groups

orthogonal to the backbone has allowed graft polymers to find further use in fluorescent dyes, quantum dot arrays,[5] polymer electrolytes,[6] and drug delivery vehicles.[7-8] If the unique chemical platform presented by graft polymers could be directed to assemble in an aligned way across a large area, these properties could be incorporated into a functional device such as lab-on-chip or photonic interconnects. Even without added functionality, understanding how the unique architecture effects the directed assembly at the nanoscale is of tremendous interest.

This bottlebrush architecture presents new rules governing self-assembly, with the lamellar period now dependent on the backbone length and grafting density while the sidechain length can be freely varied to control other properties.[9-10] As an example, if the side chain is below its own entanglement weight, increasing grafting density prohibits chain entanglement of the graft polymer backbone even when the graft polymers total molecular weight is in the 1000 kg / mol range.[11-12] Increasing sidechain grafting density can also dramatically increase the polymers radius of gyration due to steric crowding.[12-13] Interestingly simulations of bottlebrushes in solution have shown that decreasing excluded volume dramatically modulates this steric crowding effect, as the side chains begin to screen each other.[14] Conceptually this is similar to the well-known effect of 'crowding agents' in proteins, where homopolymer additives screen amino acid interactions resulting in radical changes in folding dynamics.[15-18] Nonetheless in the bulk, the added stiffness of the polymer backbone due to this steric repulsion results in a markably expanded lamellar domain window which is of key interest for directed self-assembly.[19-20]

However, to date there are fewer studies of the effect of confining these large polymers within a thin film. There are three predominant configurations for lamellar BCPs in thin films, those with parallel orientations will exhibit either symmetric or asymmetric wetting, while equal surface energies for both blocks will lead to perpendicular lamellae.[21-22] Beginning with the

parallel orientations: if the same block prefers both the substrate and the free interface, it is called symmetric wetting and well ordered parallel lamellae are formed at film thickness of nL_0; where n is any integer and L_0 is again the innate lamellar period of the BCP. If one block prefers the substrate and the other block prefers the free interface it is called asymmetric wetting and the resulting layers are $(n+1/2)L_0$ thick. Intermediate thicknesses will result in the formatiuo nof islands or holes at the top of the film to alleviate the stresses induced by confinement. When a symmetric wetting condition is exposed to confinement commensurate with asymmetric wetting or vice versa the competing effects often cancel out to form perpendicular assembly.[23] Only in the case of nearly equal surface energies, and nearly equal substrate interactions can perpendicular assembly be obtained across film thicknesses.[24-26] Due to the importance of controlling orientation when utilizing BCP thin films an extensive toolset has been developed to control the BCP orientation. The surface free energy is inherent in the block chemistry[27] and can be tuned via solvent annealing[28-29] or addressed via top coat approaches.[30-31] Numerous approaches have been utilized to control these interactions such as random copolymer brushes or mats,[32-34] surface energy tunable SAMs [35] or orthosilicates,[36] metals and graphene.[37-38] When considering the surface energy of graft polymers, it is known that the polymer sidechains are strongly entropically driven to the free interface, and that in thin films the backbone can bend as needed to minimize surface energy.[39-41] Some work has also been done in solvent annealing conditions, but far less is known in the case of thermal annealing where solvent effects no longer dominate the film morphology. [42]

Understanding how the concepts of commensurability and surface energy translate to graft polymers is of critical importance for controlled large scale patterning of these materials through directed self-assembly (DSA). DSA of BCPs is a self-aligned density multiplication technique in which self-assembling BCPs can be used to shrink the pitch of a lithographically defined

template.[43-47] In the benchmark process, a linear PS-*b*-PMMA with an innate 28 nm lamellar period, or L_0, is directed to form well-ordered perpendicular features by a 3x (84 nm pitch or L_s) template patterned by 193 nm immersion (193i) photolithography.[48] Sufficient commensurability between the polymer and template periodicities are critical for achieving defect free assembly. Linear polymer can tolerate a few nanometers of incommensurability, with a slightly larger tolerance for compression compared to stretching.[49-50] The DSA of bottlebrush polymers has not yet been demonstrated and could open the door to unique length scales, kinetics, and functionality, thereby improving patterning and producing new devices.

In this work, we study the effects of both out-of-plane and in-plane confinement on thin film assembly of a bottlebrush BCP with a polynorbornene backbone where the first half of the pendent groups consists of tethered polystyrene and the second half consists of tethered polylactic acid (gPS-*b*-gPLA) and compare them with previous bulk studies [3, 10, 51] To understand the effect of out-of-plane confinement we spun coat the polymer to both commensurate and incommensurate film thicknesses on substrates that induce both symmetric and asymmetric wetting. Due to the differing orientations of chain ends relative to the backbone presented by the bottle brush architecture we expected to see an enhanced perpendicular assembly as the pendent side chains are entropically driven to the free surface. Next, to understand the effect of in-plane confinement a hybrid epitaxial guiding pattern was created with spacing both commensurate and incommensurate with L_0.

4.3 Methods

4.3.1 Preparation of Substrates

Prime grade N-type doped silicon wafers were purchased from Pure Wafer or Silicon Materials.[52] Wafers were cleaned using piranha at 130°C for five minutes and used within one week of cleaning. DANGER: Piranha is explosive if incorrectly mixed or if excess organics are added. Crosslinked polystyrene (xPS) and crosslinked PMMA (xPMMA), random copolymers of PS and PMMA with four percent glycidyl methacrylate as a crosslinking moiety were prepared in accordance with previous literature[53]. Solutions of 0.5 w% in toluene were prepared and spuncoat within a day to prevent solution crosslinking to a nominal thickness of 10 nm. Short chain hydroxy terminated PS (PSOH) brushes (M_w 1.6kg/mol) were prepared in accordance with previous literature.[54] Solutions of 1 w% in toluene were prepared and spuncoat to a thickness of 20 nm. All films were crosslinked (xPS, xPMMA) or attached (PSOH) at 250°C for 5 minutes in an inert environment, and then sonicated 3x in toluene to remove any free polymer.

4.3.2 Preparation of gPS-b-gPLA

Bottlebrush polymer consisting of a polynorbornene backbone with grafted PS and grafted PLA domains were prepared in accordance with previous literature and full details are available in the supplemental material. Briefly, short side chains of PS (35 repeat units) and PLA (42 repeat units) of approximately equal volume were grafted onto norbornene to form a macromonomer, which was then polymerized into a symmetric volume fraction bottlebrush polymer with 100% grafting density. The bulk phase behavior has been previously reported.[9]

4.3.3 Preparation of gPS-b-gPLA thin films

Solutions of gPS-b-gPLA at varying concentrations in chlorobenzene were prepared and spuncoat. Films were soft baked at 80°C for a few minutes in order to minimize the effect of trapped solvent volume on the film thickness, or the post assembled film morphology. This soft bake resulted in an approximately 10% decrease in film volume. Films were first prepared at 1.25 L_0 in order to determine asymmetric/wetting preference using the Hole-Island test well detailed elsewhere [23, 34]. Films were prepared at other thicknesses to more completely explore the thin film behavior. Films were thermally annealed at 170°C for one hour in a custom-made vacuum chamber, which was cycled three times with nitrogen to minimize oxygen exposure before being left under vacuum. Separately TGA was performed at identical conditions to insure polymer degradation was not occurring (Figure 20Figure 20. TGA of gPS-b-gPLA.). Due to the chamber's thermal mass, the heating ramp rate is 30 minutes and the cooling ramp rate is an hour and half. Any solvent which was not removed during the soft bake will be removed under vacuum during the initial ramp to temperature.

4.3.4 Grazing Incidence Small X-ray Scattering (GISAXS)

GISAXS measurements were conducted at the Advanced Photon Source at Argonne National Lab at sector 8 ID-E.[55] Thin films of gPS-b-gPLA were prepared on roughly 2 cm square chips as previously described. The photon energy was 10.915 KeV, and the sample to detector distance used was 2183.42 mm. At these energies, the critical angle of the block copolymer film is approximately 0.12°, and so exposures were taken both above (0.14°) and below (0.10°) in order to probe the full film and surface morphology respectively. Data was analyzed by averaging across q_y in the vicinity of the first order peak and locating the first order peak intensity corresponding to in plane structure using the GIXSGUI UI and API.[56] Additional SAXS

experiments were performed at the DuPont−Northwestern−Dow Collaborative Access Team (DND-CAT) Synchrotron Research Center located at Sector 5 of the APS. For SAXS the energy was 16.4 keV, and scattering intensities were monitored with a CCD area detector at a sample to detector distance of 850 cm. To obtain 1-D spectra the 2-D scattering patterns were azimuthally integrated to give the scattering intensity with respect to the scattering vector (q).

4.3.5 Directed Self-Assembly Template Creation

Crosslinked polystyrene substrates were prepared as previously described. On top of this mat, all-resist N7520.07 Neu was diluted with PGMEA and spuncoat to a thickness of ~60 nm and then soft-baked at 150°C for 1 minute. The samples were then exposed on a Raith EBPG using a pattern CD of 14 nm on a varying pitch with a resolution of 2 nm, and a dose of 800-1300 $\mu C/cm^2$. After exposure patterns were developed using MIF 726 for 1 minute, before a 30 second vigorous DI rinse, followed by an immediate nitrogen dry. Patterns were then imaged to determine the width of resulting lines as a function of dose (~ 30 nm). The patterned lines were then transferred from the resist down into the xPS using an oxygen plasma trim etch in a plasmatherm ICP RIE, with a 65 w bias, 10 sccm Oxygen, at 10 mTorr for ~15 seconds. The trim etch length is specifically controlled to shrink the line width to the well known 0.75 L_0 DSA window.[49] After trim etch the remaining resist is stripped with NMP, before the non-preferential short PS brush is grafted back into the exposed silicon following the same procedure as previously described.

4.3.6 Characterizations

The surface morphologies of BCP thin films were obtained with a Scanning Electron Microscope (SEM Zeiss Merlin), an Atomic Force Microscope (AFM, Asylum, Cypher) in tapping mode, and a laser scanning confocal microscope (Olympus LEXT). Thicknesses were measured with a JA Woolam Alpha SE ellipsometer, and fit using a compound silicon/SiOx (1.5 nm)/Cauchy film model. Images were adjusted for brightness and contrast in Gwyddion[57] (AFM) or FIJI[58] (SEM). Sequential Infilitration Synthesis (SIS) Alumina was performed in accordance with the literature using an Ultratech/Cambridge Savannah ALD System utilizing two supercycles of TMA/Water for PLA selective staining.[54, 59-60]

4.4 Results & Discussion

4.4.1 Determining symmetric and Assymetric wetting conditions

The first step towards understanding the effects of confinement on the sample was to conduct the classic island-hole experiment, where the polymer is assembled at a thickness of 1.25 L0 on substrates with a range of surface energies. Films were prepared on three different substrates: silicon oxide (SiOx) which is hydrophilic, crosslinked polystyrene (xPS) which is hydrophobic, and short hydroxyl-terminated polystyrene brush (1.6k PSOH) which presents an intermediate surface energy**.** Figure 14 shows the results of the classic hole island experiment conducted for gPS-b-gPLA films that are 1.25 L_0 thick. Because this thickness is incommensurate with the BCP lamellar period, the film terraces to form features that are either odd-integer multiples of half L_0 (e.g. 0.5L_0 or 1.5L_0) which are indicators of asymmetric wetting or even-integer multiples of half L_0 (e.g. 1L_0 or 2 L_0) which indicates symmetric wetting. In the case of symmetric or asymmetric wetting the majority of the film adopts a 1L_0 or 1.5L_0 thickness respectively. The remainder of the film adopts the next close commensurate condition, either 2L_0 or 0.5L_0, respectively. Figure 14A

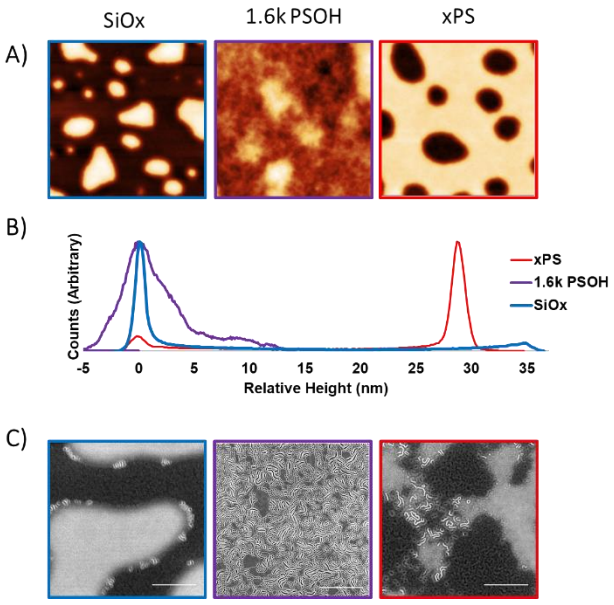

Figure 14. A) 20x20 um AFM height images showing the film topography on top of 1.25 L0 thick gPS-b-gPLA films on three representative substrates. B) The histogram of film height demonstrating islands on silicon oxide, and holes on xPS indicative of symmetric and asymmetric wetting behavior. C) 5 um wide SEM images showing the BCP microstructure (scalebar is 1 um).

shows the AFM of gPS-*b*-gPLA on the SiOx substrate where the presence of islands with a step height of ~1L_0 is observed, consistent with symmetric wetting. In comparison the AFM of gPS-*b*-gPLA on the xPS substrate demonstrates the presence of holes with a step depth of ~1L_0 consistent with asymmetric wetting conditions.

The short PS brush surface presents a chemistry that is a mixture of PS and the silicon substrate resulting in a non-preferential substrate as is demonstrated by the surface roughening as opposed to terracing[54]. The asymmetric wetting found on xPS shows that for our polymers the gPLA rich block presents a slightly lower surface energy consistent with the literature.[61-62] Figure 14B shows AFM height histograms which demonstrate the terrace step height, associated with L_0, is 7 nm shorter on xPS (28nm) than on SiOx (35 nm).

This can be explained in part by considering the architecture of the bottlebrush polymer. The morphology of islands have been described as causing encourage chain crowding.[21-22] MD simulations of bottlebrushes in solutions has found that at increasing concentrations in solution, analogous to chain crowding in the thin film, the excluded volume between the side chains is decreases causing intramolecular screening. This screening changes the conformation from a self-avoiding walk into a random walk effectively reducing the mean-square size of the bottle brush.[14] This is similar to a previously mentioned effect observed in proteins where the addition of 'crowding agents' such as PEO is used to reduce excluded volume and produce a decrease in the radius of gyration of proteins[15].

4.4.2 Bottlebrush polymers have extended perpendicular structure under out-of-plane confinement

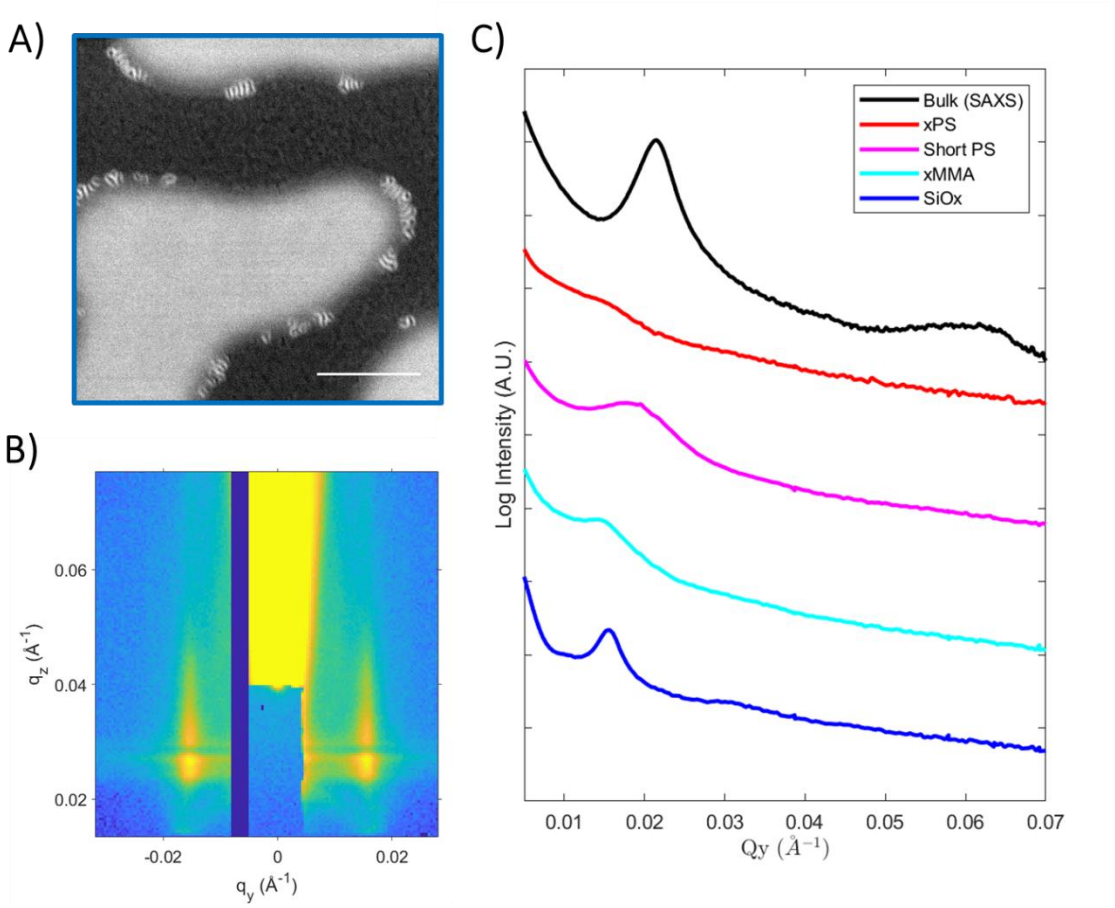

Figure 15. A) Example 5 um wide SEM images showing the BCP microstructure on SiOx at a thickness of 1.25 L_0 identical to that shown in Figure 1C (scalebar is 1 um). B) GISAXS scattering data collected at APS at an incident angle $\theta > \theta_c$ capturing the full film morphology. C) Extracted line cuts along Q_y for GISAXS captured on 1.25 L_0 thick films.

While AFM data allows for an understanding of the polymers coiling when the backbone is in plane, SEM imaging also revealed an extensive in plane morphology is formed especially on the non-preferential surface. SEM is limited in that a polymer may not produce adequate contrast, and due to the forward electron scattering it is hard to determine whether the morphology imaged

occurs in the film or at the film's surface. Grazing incidence small angle x-ray scattering (GISAXS) was conducted in order to fully capture the in plane periodicity, d*, of the bottlebrush BCP (Figure 15). In GISAXS, at incident angles below the polymer film's critical angle the incident wave is completely reflected by the surface, allowing for probing only the top few nanometers of the film. If the angle is increased to be above the film's critical angle but below that of the silicon wafer, the incident wave is instead reflected by the wafer allowing the full film to be probed. Data was captured both above and below the critical angle of the film in order characterize both surface and film assembly. We observe that the d* for the non-preferential surface was closest to that of the bulk polymer (29.3 nm as measured by bulk SAXS). In comparison the peak shifted on all other substrates towards smaller q_y resulting in an approximately 35% expansion in d* relative to the non-preferential surface or nearly 50% to in comparison to the bulk. This effect is not observed in linear polymers. Next the width of the peak can be used as a measure of the distribution of periodicities in the film. In particular we find that increasing substrate PLA affinity especially on SiOx vs xPS resulted in a tigher distribution of d*. This tighter distribution coincided with a larger expansion in period relative to the bulk SAXS. Compression of the polymer relative to the bulk pitch is never observed suggesting the bottlebrush is sterically hindered from compressing. However, an expansion of up to 50% is observed at these conditions, with thinner films (Figure 16) showing a maximum expansion of 100% relative to the bulk lamellar spacing.

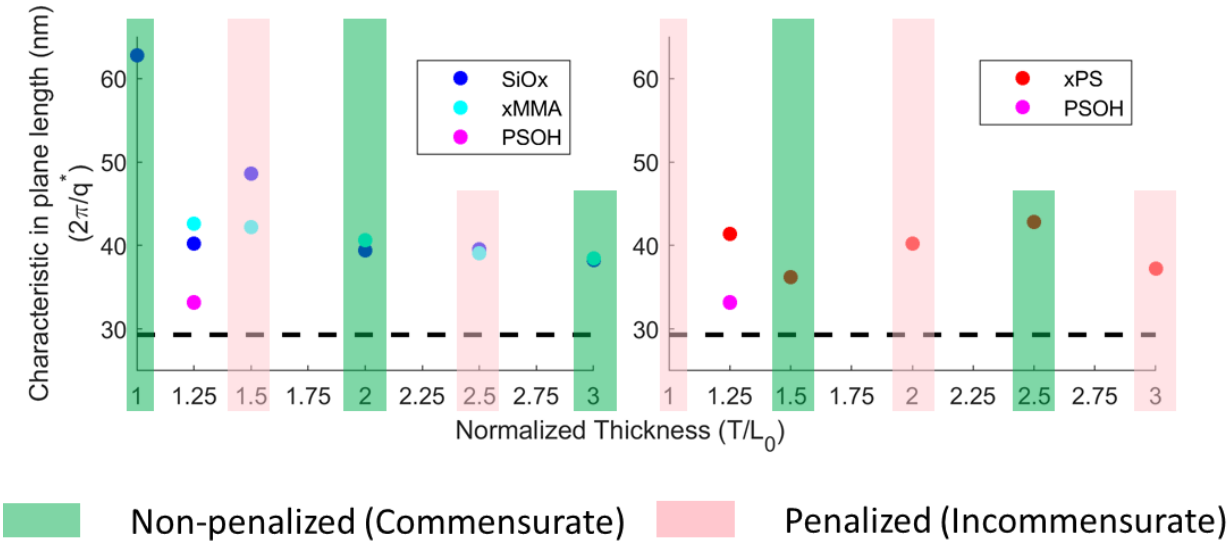

Figure 16. Polymer characteristic length scale in the in-plane direction as measured via GISAXS for gPS-*b*-gPLA on SiOx (dark blue), xMMA (teal), xPS (red), and short PSOH (purple). The bulk periodicity as measured via SAXS is indicated with a black dashed line.

Figure 16 shows GISAXS data collected at different film thicknesses demonstrating that expansion of the statistical length scale becomes more significant at thinner film thicknesses, especially on the silicon substrates. The need for the pendant groups to demix to form expanded spacing structures also helps to explain the differences in morphology observed in the case of out-of-plane confinement. Here the bottlebrush polymer is driven to form perpendicular features even at commensurate spacings perhaps due to the strong surface-active effect of the pendant sidechains in addition to the relative small differences in surface energy between PS and PLA.[39-40, 63] The formation of these in-plane features is not however solely due to this effect as GISAXS revealed the perpendicular morphology in all cases persists throughout the film thickness (Figure 21). Here a non-preferential substrate presented a boundary similar to the bulk which allowed for the

smallest, and closest to bulk, lamellar spacing to be obtained. Similarly, soft substrates (xPS, xMMA) allow the bottle brush polymer to form parallel features and thus there are no peaks corresponding to perpendicular morphology, while the hard SiOx instead causes the largest deviation from bulk behavior. The SiOx substrate also shows some effect of commensurability on the in-plane spacing, with the incommensurate thickness of 1.5 L_0 presenting an expanded pitch relative to either 1.25 L_0 or 2 L_0.

One possibility for the expanded lamellar period observed is that strong substrate interaction have been shown to increase the glass transition temperature of the block pinned at the interface and decrease it for the not favorable block.[64-67] This can lead to changes in free volume causing a change in side chain screening. Effectively this is the reverse of what was observed in considering the height of the terraced structures. Again, in line with simulation slight changes in excluded volume can cause outsized changes in the polymer period. Further evidence that the volume of the bottlebrush is changing, and specifically that it is changing asymmetrically can be seen directly in the x-ray scattering. The bulk scattering shows an absence of the second order peak, indicating very symmetric lamella, but in the thin film we see a slight second order peak visible in the GISAXS on the silicon substrate, indicating assymetric lamella.

In addition, Sheiko *et. al.* have specifically shown how strong absorption energies alters the free energy landscape for bottlebrush polymers by pulling the sidechains towards the surface in order to maximize the number of chains absorbed which results in full extension of the sidechains.[68] Hence the difference between chain extension on the xPMMA and the SiOx surface may be due solely to the increased interfacial energy present on the freshly piranha cleaned and thus very hydrophilic surface of the SiOx. A further factor is the ability of interfacial interactions to alter the

bending modulus of backbone, which has been shown to spontaneously curve on surfaces to maximize intramolecular sidechain interactions.[69-70]

4.4.3 Bottlebrush polymers exhibit non-bulk morphologies under in-plane confinement

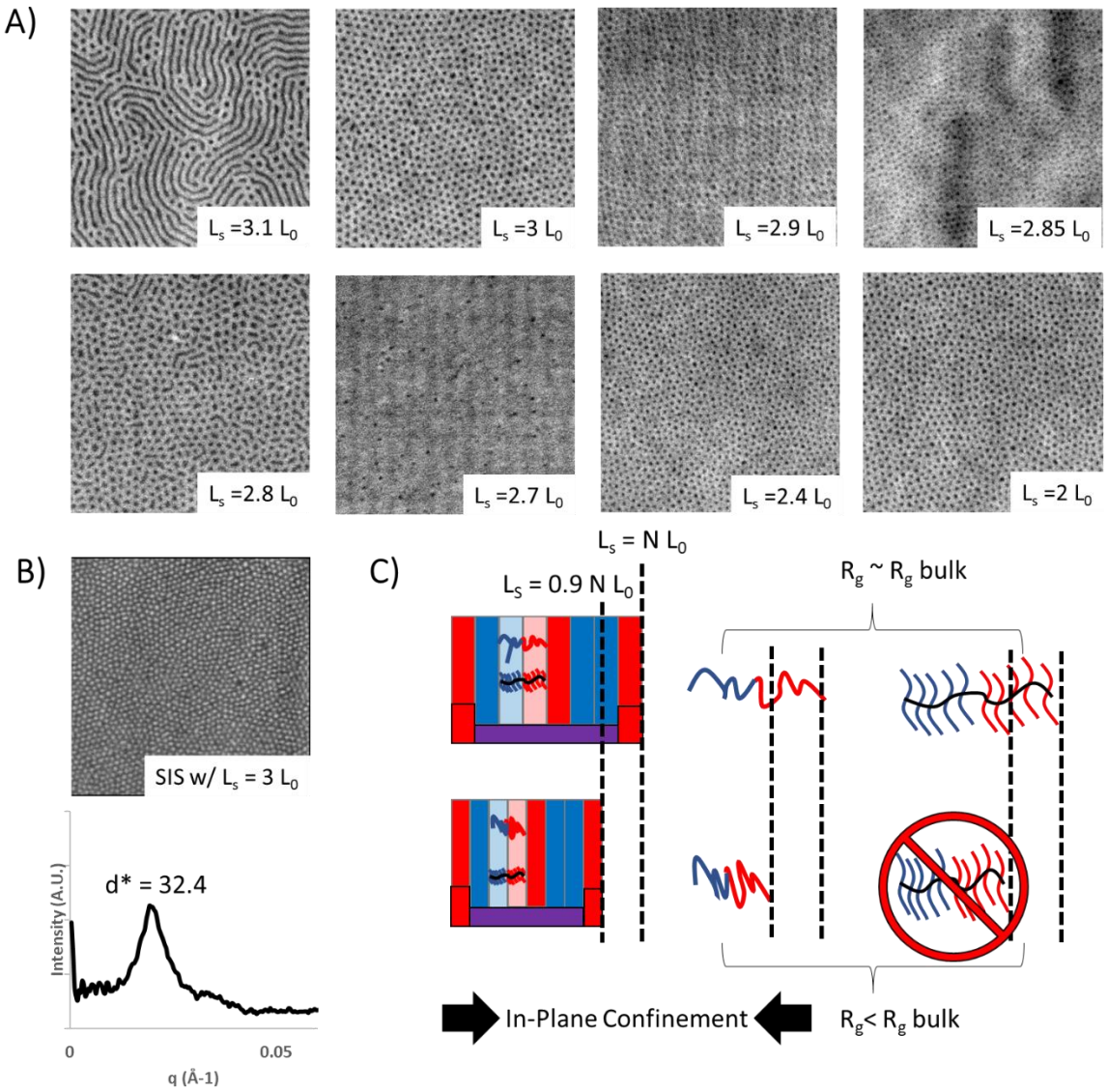

Figure 17. A) 1x1 um SEM images of BCP assembled on top of chemical patterns at decreasing spacings (L_s) relative to L_0. B) SEM of BCP after selectively staining PLA with SIS alumina, and the radial power spectral density showing lamellar period expansion C) Schematic showing the confining effect of the chemical pattern.

The most direct test of DSA, is to perform it using a hybrid epitaxial pattern with both topographic and chemical features presented on a spacing (L_s) that is an integer multiple of L_0. [71] Here preferential guides (xPS) approximately 0.75 L_0 wide stand a few nm above the non-preferential backfill brush (PSOH). When a linear lamellar forming polymer is put on such a pattern which presents the appropriate cues, it will readily form well-ordered lamella. For linear polymers, as L_s is decreased and becomes incommensurate, the polymer adopts a smaller equilibrium lamellar period as the polymer adopts a tighter coil (R_g < R_g bulk); however, we hypothesized the steric hindrances of the bottlebrush sidechains will prohibit such a shrink.[72-73]

Figure 17A shows SEM images of the assembled polymer structure on such a pattern, which reveal that even when the guiding pitch is commensurate with the bulk lamellar period, in the thin film gPS-b-gPLA prefers to adapt a non-bulk morphology resembling hexagonally close packed cylinders. To understand which domains forms the core the film was stained using alumina Sequential Infiltration Synthesis (SIS) which specifically stains the hydrophilic PLA.[60] SIS staining with alumina showed that PLA formed the core of the structures seen (Figure 17B). Interestingly, the associated 1D radial power spectral density exhibits only a first order peak; whereas, a true perpendicular cylinder structure would exhibit peaks at $1, \sqrt{3}, 2, \sqrt{7}$. The lack of higher order peaks is in agreement with the GISAXS taken during the out-of-plane confinement experiments detailed earlier during which only a primary peak was found. As chemical pattern pitch (L_s) continues to decrease this non-bulk cylindrical like morphology is lost and parallel morphology appears. Figure 17C schematically compares this confinement effect with that of linear polymers, where the polymer compresses and contracts under DSA confinement from L_s/L_0 of 2.85 to 3.1[74].

The presence of the new morphology is due to the unique architecture of the bottlebrush. The surface of the chemical pattern is PS rich relative to the non-preferential brush alone due to the presence of the xPS guide stripes. Similar to what was observed in the case of GISAXS scattering, the excess PS can facilitate re-arrangement of the bottlebrush PS sidechains forming globular domains with the non-interacting PLA forming a core.[75-76] The re-arrangment of the sidechains also likely affects the statistical segment length of the backbone. Here it is well known in linear polymers that stiffening one block can cause a shift in the equilibrium phase space and push the cylinder phase towards equal volume fractions. This also results in a thinning of the cylinder corona region where local volume is created due to differences in statistical segment length between the two blocks.[77] Bottlebrush polymers are uniquely sensitive to such changes in volume due to dominant effect their sidechains can have on L_0 which may also partially explain the large increased in periodicity observed varying confinement.

4.5 Conclusions

In this work we studied the effect of thin film confinement on bottlebrush polymers. We found that these polymers formed perpendicular features under out-of-plane confinement, even at film thicknesses that should be commensurate with parallel assembly. These perpendicular features possessed only short-range order and were associated in all cases with an expansion of the block copolymers natural periodicity. These expanded features were found to occur both in the film and at the free interface and were thus not only due to the surface-active effect of the bottlebrush polymer's pendant groups. This extension was minimized on non-preferential substrates, but drastically increased on substrates which strongly interacted with the PLA block. These strongly interacting substrates allow for the creation of more excluded volume between pendant groups and facilitate side chain re-arrangement in the bottlebrush allowing for an increase in the in plane

periodicity as measured via GISAXS. Utilizing a hybrid epitaxy DSA scheme it was found that in-plane confinement also resulted in bottlebrush expansion and the creation of excluded volume, and the PS groups selectively demixed to yield PLA core structures with no long-range order. These features were found to persist across large ranges of chemical pattern pitches relative to the bulk spacing. It is clear that for lamella forming graft block copolymers to be successfully assembled into large defect free structures, care must be taken to insure that excluded volume changes present in bottle brush BCP thin films are suppressed or at least symmetric.

4.6 Acknowledgements

We acknowledge the MRSEC Shared User Facilities at the University of Chicago (NSF DMR-1420709) for SEM, AFM, and optical characterization. Additional SAXS experiments were performed at the DuPont−Northwestern−Dow Collaborative Access Team (DND-CAT) Synchrotron Research Center located at Sector 5 of the APS. DND-CAT is supported by the E.I. DuPont de Nemours & Co., The Dow Chemical Company, the U.S. National Science Foundation through Grant DMR-9304725, and the State of Illinois through the Department of Commerce and the Board of Higher Education Grant IBHE HECA NWU 96. Use of the APS was supported by the U.S. Department of Energy, Office of Science, Office of Basic Energy Sciences, under Contract DE-AC02-06CH11357. Funding support was provided by CHiMad which is supported by U.S. Department of Commerce, National Institute of Standards and Technology under financial assistance award number 70NANB14H012.

4.8 Supplemental Information

4.8.1 Materials

The third-generation Grubbs catalyst, **G3** [$(H_2IMes)(pyr)_2(Cl)_2Ru{=}CHPh$], was prepared according to previously reported procedures.[78] The ω-norbornenyl polystyrene (**PS**)[79] and poly(D,L-lactide) (**PLA**)[80] macromonomers were likewise prepared according to reported procedure. Anhydrous dichloromethane was obtained from a solvent purification system and stored in a glovebox.

4.8.2 Synthesis of gPS-*b*-gPLA Brush Block Polymer

gPS-*b*-gPLA was synthesized by the grafting-through ring-opening metathesis polymerization (ROMP) of PS and PLA macromonomers.

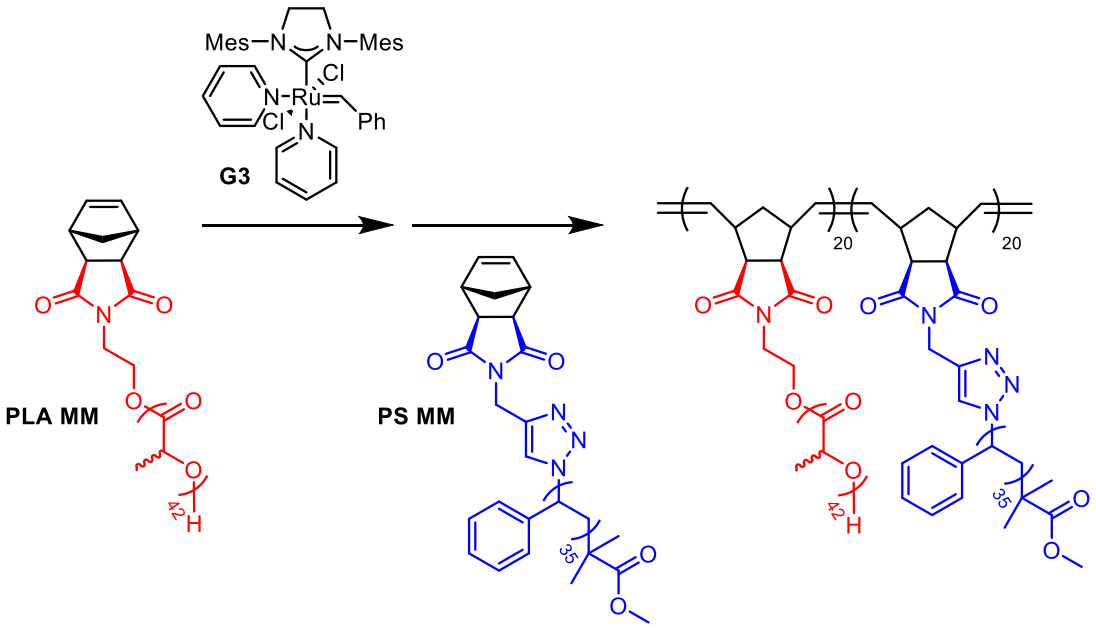

Figure 18. Synthesis of gPS-b-gPLA brush block polymer by sequential grafting-through ring-opening metathesis polymerization.

In an argon glovebox, 40 mg of the PLA macromonomer (3230 g/mol, 0.0125 mmol) was transferred to a 4 mL vial equipped with a stir bar. The macromonomer was dissolved in 0.25 mL dichloromethane ([**PLA**] = 0.050 M). In a separate vial, 50 mg of the PS macromonomer (3990 g/mol, 0.0125 mmol) was dissolved in 0.25 mL dichloromethane ([**PS**] = 0.050 M). In a third vial, 12.6 mg of the **G3** catalyst was dissolved in 0.50 mL dichloromethane ([**G3**] = 0.034 M). To initiate the polymerization, 16.5 μL of the catalyst stock solution was added to the rapidly stirring vial of the PLA macromonomer. After 30 minutes, the solution of the PS macromonomer was quickly added. The needle and syringe were flushed to ensure complete transfer. After 1 hour, the polymerizations were quenched outside the glovebox by rapidly adding a large excess of ethyl vinyl ether (≈ 0.2 mL). After stirring for 5 minutes, a silica-bound metal scavenger (SiliaMetS DMT) was added. The quenched ruthenium complex adsorbs to the silica and can be removed by filtration. The **gPS-*b*-gPLA** brush block polymer was isolated by precipitation into 50 mL cold (−78 °C) methanol. The precipitate was isolated by centrifugation, dried under high vacuum for 24 hours, then freeze-dried from benzene.

4.8.3 Size-Exclusion Chromatography

SEC data were collected using two Agilent PLgel MIXED-B 300 × 7.5 mm columns with 10 μm beads. The columns were connected in series with an Agilent 1260 pump, Wyatt 18-angle DAWN HELEOS light scattering detector, and Optilab rEX differential refractive index detector. The mobile phase was THF, and the flow rate was 1 mL/min.

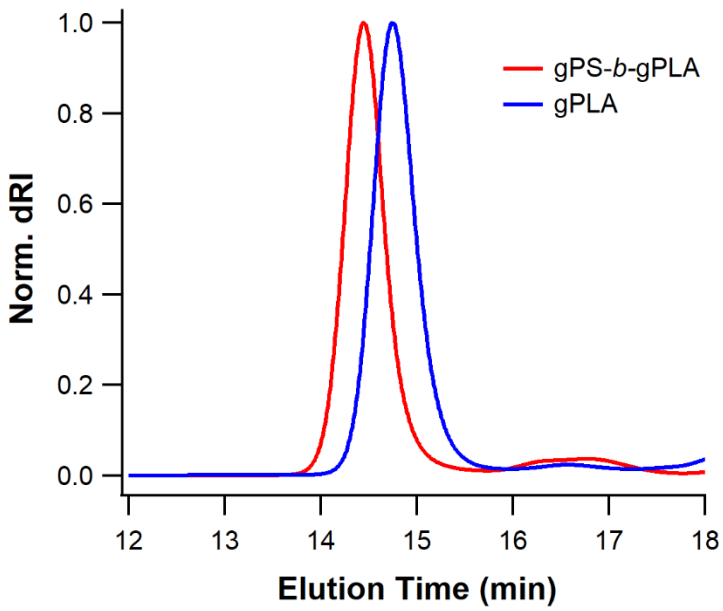

Figure 19. Size-exclusion chromatography data for *(red)* gPS-*b*-gPLA and *(blue)* gPLA (prior to addition of the PS macromonomer).

Table 4. Backbone degrees of polymerization (N_{bb}), total molar mass, and dispersity determined by size-exclusion chromatography.

ID	$N_{bb,PS}$	$N_{bb,PLA}$	**Total M_w (kDa)**	$Đ$
gPS-*b*-gPLA	20	20	140	1.03
gPLA	–	20	67	1.02

4.8.4 TGA of polymer at annealing conditions

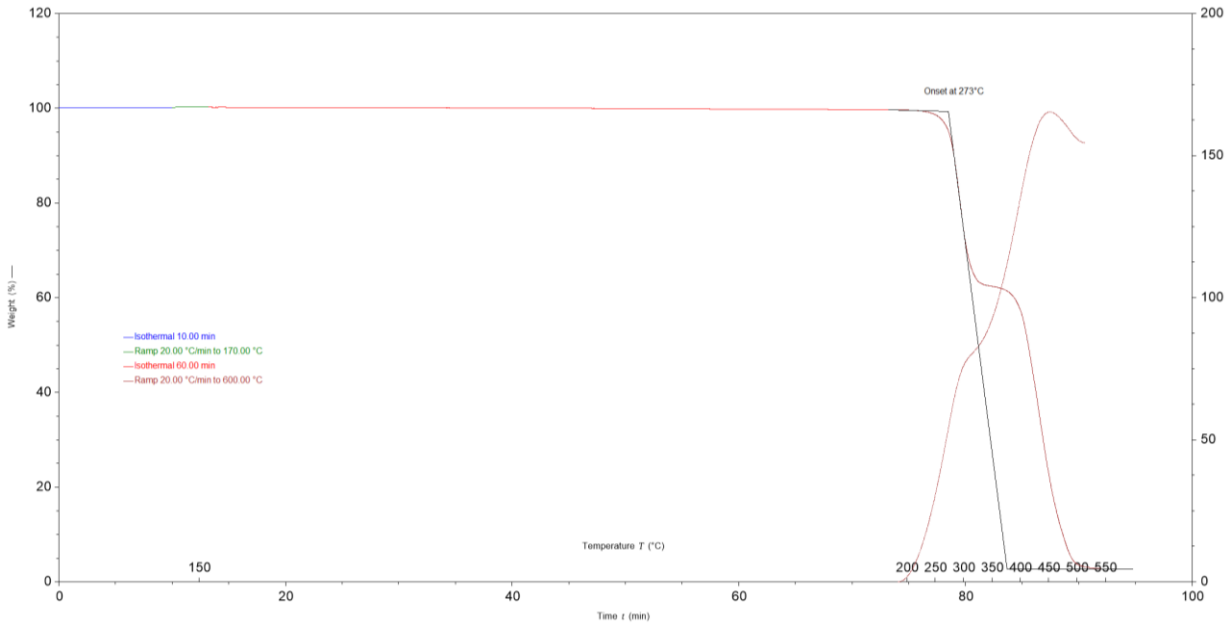

Figure 20. TGA of gPS-b-gPLA.

In order to insure no degradation was occurring during annealing a TGA run was set up which followed the annealing temperature profile. During the one hour spent at 170°C no degradation was observed. After this pseudo-annealing process the polymer was ramped up to 600°C to definitively observe the polymer degradation, which begins at approximately 270°C

4.8.5 GISAXS comparison of film and surface morphology.

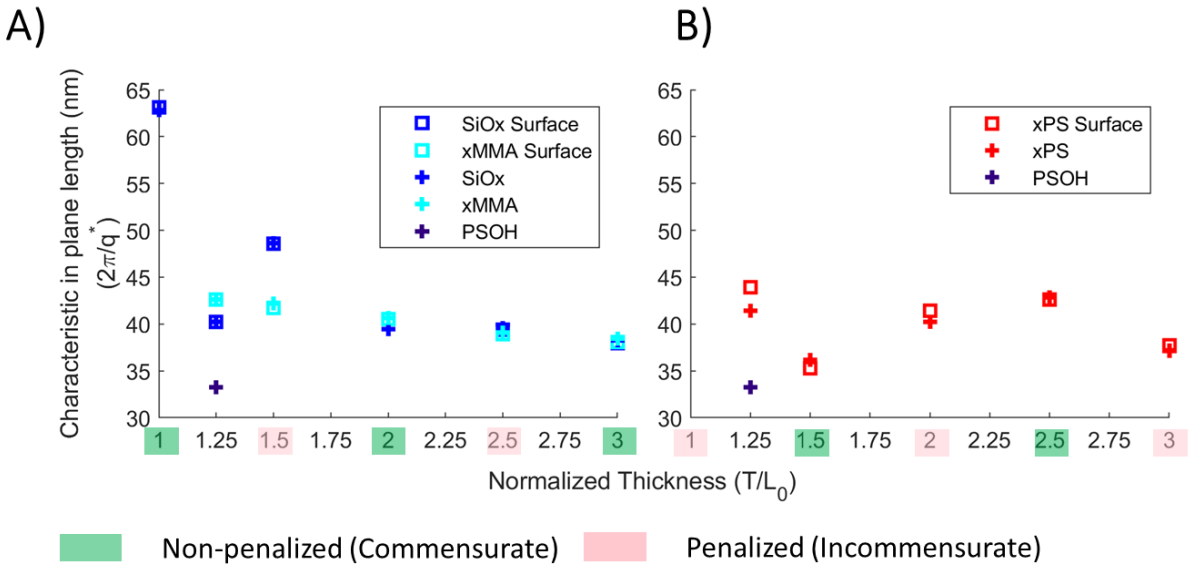

Figure 21. GISAXS taken both above (full film) and below (surface) the critical angle of the polymer film for both symmetric (A) and assymetric (B) wetting conditions. In general there is good agreement between surface and full film measurements. Surface morphology is never observed without bulk morphology.

4.7 References

1. Polymeropoulos, G.; Zapsas, G.; Ntetsikas, K.; Bilalis, P.; Gnanou, Y.; Hadjichristidis, N., 50th Anniversary Perspective: Polymers with Complex Architectures. *Macromolecules* **2017,** *50* (4), 1253-1290.

2. Matyjaszewski, K., Chemistry. Architecturally complex polymers with controlled heterogeneity. *Science* **2011,** *333* (6046), 1104-5.

3. Sveinbjornsson, B. R.; Weitekamp, R. A.; Miyake, G. M.; Xia, Y.; Atwater, H. A.; Grubbs, R. H., Rapid self-assembly of brush block copolymers to photonic crystals. *Proceedings of the National Academy of Sciences of the United States of America* **2012,** *109* (36), 14332-6.

4. Chae, C.-G.; Yu, Y.-G.; Seo, H.-B.; Kim, M.-J.; Grubbs, R. H.; Lee, J.-S., Experimental Formulation of Photonic Crystal Properties for Hierarchically Self-Assembled POSS–Bottlebrush Block Copolymers. *Macromolecules* **2018,** *51* (9), 3458-3466.

5. Song, D.-P.; Shahin, S.; Xie, W.; Mehravar, S.; Liu, X.; Li, C.; Norwood, R. A.; Lee, J.-H.; Watkins, J. J., Directed Assembly of Quantum Dots Using Brush Block Copolymers for Well-Ordered Nonlinear Optical Nanocomposites. *Macromolecules* **2016,** *49* (14), 5068-5075.

6. Bates, C. M.; Chang, A. B.; Schulze, M. W.; Momčilović, N.; Jones, S. C.; Grubbs, R. H., Brush polymer ion gels. *Journal of Polymer Science Part B: Polymer Physics* **2016,** *54* (2), 292-300.

7. Johnson, J. A.; Lu, Y. Y.; Burts, A. O.; Xia, Y.; Durrell, A. C.; Tirrell, D. A.; Grubbs, R. H., Drug-loaded, bivalent-bottle-brush polymers by graft-through ROMP. *Macromolecules* **2010,** *43* (24), 10326-10335.

8. Johnson, J. A.; Lu, Y. Y.; Burts, A. O.; Lim, Y. H.; Finn, M. G.; Koberstein, J. T.; Turro, N. J.; Tirrell, D. A.; Grubbs, R. H., Core-clickable PEG-branch-azide bivalent-bottle-brush polymers by ROMP: grafting-through and clicking-to. *J Am Chem Soc* **2011,** *133* (3), 559-66.

9. Lin, T. P.; Chang, A. B.; Luo, S. X.; Chen, H. Y.; Lee, B.; Grubbs, R. H., Effects of Grafting Density on Block Polymer Self-Assembly: From Linear to Bottlebrush. *ACS nano* **2017,** *11* (11), 11632-11641.

10. Gu, W.; Huh, J.; Hong, S. W.; Sveinbjornsson, B. R.; Park, C.; Grubbs, R. H.; Russell, T. P., Self-assembly of symmetric brush diblock copolymers. *ACS nano* **2013,** *7* (3), 2551-8.

11. Hu, M.; Xia, Y.; McKenna, G. B.; Kornfield, J. A.; Grubbs, R. H., Linear Rheological Response of a Series of Densely Branched Brush Polymers. *Macromolecules* **2011,** *44* (17), 6935-6943.

12. Haugan, I. N.; Maher, M. J.; Chang, A. B.; Lin, T. P.; Grubbs, R. H.; Hillmyer, M. A.; Bates, F. S., Consequences of Grafting Density on the Linear Viscoelastic Behavior of Graft Polymers. *Acs Macro Letters* **2018,** *7* (5), 525-530.

13. Paturej, J.; Sheiko, S. S.; Panyukov, S.; Rubinstein, M., Molecular structure of bottlebrush polymers in melts. *Sci Adv* **2016,** *2* (11), e1601478.

14. Paturej, J.; Kreer, T., Hierarchical excluded volume screening in solutions of bottlebrush polymers. *Soft Matter* **2017,** *13* (45), 8534-8541.

15. Soranno, A.; Koenig, I.; Borgia, M. B.; Hofmann, H.; Zosel, F.; Nettels, D.; Schuler, B., Single-molecule spectroscopy reveals polymer effects of disordered proteins in crowded environments. *Proceedings of the National Academy of Sciences of the United States of America* **2014,** *111* (13), 4874-9.

16. Kuznetsova, I. M.; Turoverov, K. K.; Uversky, V. N., What macromolecular crowding can do to a protein. *Int J Mol Sci* **2014,** *15* (12), 23090-140.

17. Christiansen, A.; Wang, Q.; Cheung, M. S.; Wittung-Stafshede, P., Effects of macromolecular crowding agents on protein folding in vitro and in silico. *Biophys Rev* **2013,** *5* (2), 137-145.

18. Minton, A. P., Excluded volume as a determinant of macromolecular structure and reactivity. *Biopolymers* **1981,** *20* (10), 2093-2120.

19. Rzayev, J., Synthesis of Polystyrene−Polylactide Bottlebrush Block Copolymers and Their Melt Self-Assembly into Large Domain Nanostructures. *Macromolecules* **2009,** *42* (6), 2135-2141.

20. Chang, A. B.; Bates, C. M.; Lee, B.; Garland, C. M.; Jones, S. C.; Spencer, R. K. W.; Matsen, M. W.; Grubbs, R. H., Manipulating the ABCs of self-assembly via low-chi block polymer design. *Proceedings of the National Academy of Sciences of the United States of America* **2017,** *114* (25), 6462-6467.

21. Smith, A. P.; Douglas, J. F.; Meredith, J. C.; Amis, E. J.; Karim, A., High-throughput characterization of pattern formation in symmetric diblock copolymer films. *J Polym Sci Pol Phys* **2001,** *39* (18), 2141-2158.

22. Russell, T. P.; Menelle, A.; Anastasiadis, S. H.; Satija, S. K.; Majkrzak, C. F., Unconventional Morphologies of Symmetric, Diblock Copolymers Due to Film Thickness Constraints. *Macromolecules* **1991,** *24*, 6263-6269.

23. Suh, H. S.; Kang, H.; Nealey, P. F.; Char, K., Thickness Dependence of Neutral Parameter Windows for Perpendicularly Oriented Block Copolymer Thin Films. *Macromolecules* **2010,** *43* (10), 4744-4751.

24. Anastasiadis, S. H.; Russell, T. P.; Satija, S. K.; Majkrzak, C. F., Neutron reflectivity studies of the surface-induced ordering of diblock copolymer films. *Phys Rev Lett* **1989,** *62* (16), 1852-1855.

25. Anastasiadis, S. H.; Russell, T. P.; Satija, S. K.; Majkrzak, C. F., The Morphology of Symmetric Diblock Copolymers as Revealed by Neutron Reflectivity. *Journal of Chemical Physics* **1990,** *92* (9), 5677-5691.

26. Coulon, G.; Russell, T. P.; Deline, V. R.; Green, P. F., Surface-Induced Orientation of Symmetric, Diblock Copolymers - a Secondary Ion Mass-Spectrometry Study. *Macromolecules* **1989,** *22* (6), 2581-2589.

27. Kim, S.; Nealey, P. F.; Bates, F. S., Decoupling Bulk Thermodynamics and Wetting Characteristics of Block Copolymer Thin Films. *ACS Macro Lett.* **2012,** *1* (1), 11-14.

28. Leolukman, M.; La, Y.-H.; Nealey, P. F.; Gopalan, P. In *Solvent annealing of poly(styrene-b-tert-butylacrylate) thin films: Effect of casting and annealing solvent on morphology*, American Chemical Society: 2006; pp POLY-128.

29. Albert, J. N.; Bogart, T. D.; Lewis, R. L.; Beers, K. L.; Fasolka, M. J.; Hutchison, J. B.; Vogt, B. D.; Epps, T. H., Gradient solvent vapor annealing of block copolymer thin films using a microfluidic mixing device. *Nano letters* **2011,** *11* (3), 1351-7.

30. Suh, H. S.; Kim, D. H.; Moni, P.; Xiong, S.; Ocola, L. E.; Zaluzec, N. J.; Gleason, K. K.; Nealey, P. F., Sub-10-nm patterning via directed self-assembly of block copolymer films with a vapour-phase deposited topcoat. *Nature nanotechnology* **2017,** *12* (6), 575-581.

31. Seshimo, T.; Bates, C. M.; Dean, L. M.; Cushen, J. D.; Durand, W. J.; Maher, M. J.; Ellison, C. J.; Willson, C. G., Block Copolymer Orientation Control Using a Top-Coat Surface Treatment. *Journal of Photopolymer Science and Technology* **2012,** *25* (1), 125-129.

32. Han, E.; Stuen, K. O.; La, Y.-H.; Nealey, P. F.; Gopalan, P., Effect of Composition of Substrate-Modifying Random Copolymers on the Orientation of Symmetric and Asymmetric Diblock Copolymer Domains. *Macromolecules (Washington, DC, U. S.)* **2008,** *41* (23), 9090-9097.

33. Kim, S. H.; Misner, M. J.; Russell, T. P., Controlling Orientation and Order in Block Copolymer Thin Films. *Advanced materials* **2008,** *20* (24), 4851-4856.

34. Mansky, P., Controlling Polymer-Surface Interactions with Random Copolymer Brushes. *Science* **1997,** *275* (5305), 1458-1460.

35. Peters, R. D.; Yang, X. M.; Kim, T. K.; Sohn, B. H.; Nealey, P. F., Using Self-Assembled Monolayers Exposed to X-rays To Control the Wetting Behavior of Thin Films of Diblock Copolymers. *Langmuir : the ACS journal of surfaces and colloids* **2000,** *16* (10), 4625-4631.

36. Suh, H.-S.; Kang, H.; Liu, C.-C.; Nealey, P. F.; Char, K., Orientation of Block Copolymer Resists on Interlayer Dielectrics with Tunable Surface Energy. *Macromolecules (Washington, DC, U. S.)* **2010,** *43* (1), 461-466.

37. Chang, T.-H.; Xiong, S.; Jacobberger, R. M.; Mikael, S.; Suh, H. S.; Liu, C.-C.; Geng, D.; Wang, X.; Arnold, M. S.; Ma, Z.; Nealey, P. F., Directed self-assembly of block copolymer films on atomically-thin graphene chemical patterns. *Sci. Rep.* **2016,** *6*, 31407.

38. Dolejsi, M.; Nealey, P., Utilization of metal–polymer interactions for self-aligned directed self-assembly of device relevant features. *Journal of Micro/Nanolithography, MEMS, and MOEMS* **2018,** *17* (03), 1.

39. Mah, A. H.; Afzali, P.; Qi, L.; Pesek, S.; Verduzco, R.; Stein, G. E., Bottlebrush Copolymer Additives for Immiscible Polymer Blends. *Macromolecules* **2018,** *51* (15), 5665-5675.

40. Pesek, S. L.; Lin, Y.-H.; Mah, H. Z.; Kasper, W.; Chen, B.; Rohde, B. J.; Robertson, M. L.; Stein, G. E.; Verduzco, R., Synthesis of bottlebrush copolymers based on poly(dimethylsiloxane) for surface active additives. *Polymer* **2016,** *98*, 495-504.

41. Sunday, D. F.; Chang, A. B.; Liman, C. D.; Gann, E.; Delongchamp, D. M.; Thomsen, L.; Matsen, M. W.; Grubbs, R. H.; Soles, C. L., Self-Assembly of ABC Bottlebrush Triblock Terpolymers with Evidence for Looped Backbone Conformationse. *Macromolecules* **2018,** *51* (18), 7178-7185.

42. Hong, S. W.; Gu, W.; Huh, J.; Sveinbjornsson, B. R.; Jeong, G.; Grubbs, R. H.; Russell, T. P., On the self-assembly of brush block copolymers in thin films. *ACS nano* **2013,** *7* (11), 9684-92.

43. Williamson, L. D.; Seidel, R. N.; Chen, X.; Suh, H. S.; Rincon Delgadillo, P.; Gronheid, R.; Nealey, P. F., Three-Tone Chemical Patterns for Block Copolymer Directed Self-Assembly. *ACS applied materials & interfaces* **2016,** *8* (4), 2704-12.

44. Wan, L.; Ruiz, R.; Gao, H.; Patel, K. C.; Albrecht, T. R.; Yin, J.; Kim, J.; Cao, Y.; Lin, G., The Limits of Lamellae-Forming PS-b-PMMA Block Copolymers for Lithography. *ACS nano* **2015,** *9* (7), 7506-14.

45. Wan, L.; Ruiz, R.; Gao, H.; Patel, K. C.; Lille, J.; Zeltzer, G.; Dobisz, E. A.; Bogdanov, A.; Nealey, P. F.; Albrecht, T. R., Fabrication of templates with rectangular bits on circular tracks by combining block copolymer directed self-assembly and nanoimprint lithography. *J. Micro/Nanolithogr., MEMS, MOEMS* **2012,** *11* (3), 031405/1-031405/5.

46. Rincon Delgadillo, P. A.; Gronheid, R.; Thode, C. J.; Wu, H.; Cao, Y.; Somervell, M.; Nafus, K.; Nealey, P. F., All track directed self-assembly of block copolymers: process flow and origin of defects. *Proc. SPIE* **2012,** *8323* (Alternative Lithographic Technologies IV), 83230D/1-83230D/9.

47. Liu, C.-C.; Thode, C. J.; Delgadillo, P. A. R.; Craig, G. S. W.; Nealey, P. F.; Gronheid, R., Towards an all-track 300 mm process for directed self-assembly. *J. Vac. Sci. Technol., B: Nanotechnol. Microelectron.: Mater., Process., Meas., Phenom.* **2011,** *29* (6), 06F203/1-06F203/6.

48. Sanchez, M. I.; Panning, E. M.; Kitano, T.; Ido, Y.; You, G.; Nishi, T.; Muramatsu, M., Defect and roughness reduction of chemo-epitaxy DSA pattern. In *Novel Patterning Technologies 2018*, 2018.

49. Garner, G. P.; Rincon Delgadillo, P.; Gronheid, R.; Nealey, P. F.; de Pablo, J. J., Design of surface patterns with optimized thermodynamic driving forces for the directed self-assembly of block copolymers in lithographic applications. *Mol. Syst. Des. Eng.* **2017**.

50. Suh, H. S.; Nair, A.; Delgadillo, P. R.; Doise, J.; Lorusso, G.; Nealey, P.; Monreal, V.; Baskaran, D.; Cao, Y.; Padmanaban, M.; Li, J.; Kato, T.; Sutani, T.; Ishimoto, T.; Ikota, M.; Koshihara, S., *Impact of annealing temperature on DSA process: toward faster assembly kinetics (Conference Presentation)*. SPIE: 2018; Vol. 10586.

51. Matson, J. B.; Grubbs, R. H., Synthesis of fluorine-18 functionalized nanoparticles for use as in vivo molecular imaging agents. *J Am Chem Soc* **2008,** *130* (21), 6731-3.

52. Certain Commercial Equipment, Instruments, or Materials Are Identified in This Paper in Order to Specify the Experimental Procedure Adequately. Such Identification Is Not Intended to Imply Recommendation or Endorsement by the National Institute of Standards and Technology, nor Is It Intended to Imply That the Materials or Equipment Identified Are Necessarily the Best Available for the Purpose.

53. Han, E.; Gopalan, P., Cross-linked random copolymer mats as ultrathin nonpreferential layers for block copolymer self-assembly. *Langmuir : the ACS journal of surfaces and colloids* **2010,** *26* (2), 1311-5.

54. Xiong, S.; Chapuis, Y. A.; Wan, L.; Gao, H.; Li, X.; Ruiz, R.; Nealey, P. F., Directed self-assembly of high-chi block copolymer for nano fabrication of bit patterned media via solvent annealing. *Nanotechnology* **2016,** *27* (41), 415601.

55. Jiang, Z.; Li, X.; Strzalka, J.; Sprung, M.; Sun, T.; Sandy, A. R.; Narayanan, S.; Lee, D. R.; Wang, J., The dedicated high-resolution grazing-incidence X-ray scattering beamline 8-ID-E at the Advanced Photon Source. *J Synchrotron Radiat* **2012,** *19* (Pt 4), 627-36.

56. Jiang, Z., GIXSGUI: a MATLAB toolbox for grazing-incidence X-ray scattering data visualization and reduction, and indexing of buried three-dimensional periodic nanostructured films. *Journal of Applied Crystallography* **2015,** *48* (3), 917-926.

57. Necas, D.; Klapetek, P., Gwyddion: an open-source software for SPM data analysis. *Cent Eur J Phys* **2012,** *10* (1), 181-188.

58. Schindelin, J.; Arganda-Carreras, I.; Frise, E.; Kaynig, V.; Longair, M.; Pietzsch, T.; Preibisch, S.; Rueden, C.; Saalfeld, S.; Schmid, B.; Tinevez, J. Y.; White, D. J.; Hartenstein, V.; Eliceiri, K.; Tomancak, P.; Cardona, A., Fiji: an open-source platform for biological-image analysis. *Nat Methods* **2012,** *9* (7), 676-82.

59. Segal-Peretz, T.; Winterstein, J.; Doxastakis, M.; Ramirez-Hernandez, A.; Biswas, M.; Ren, J.; Suh, H. S.; Darling, S. B.; Liddle, J. A.; Elam, J. W.; de Pablo, J. J.; Zaluzec, N. J.; Nealey, P. F., Characterizing the Three-Dimensional Structure of Block Copolymers via Sequential Infiltration Synthesis and Scanning Transmission Electron Tomography. *ACS nano* **2015,** *9* (5), 5333-47.

60. Tseng, Y.-C.; Peng, Q.; Ocola, L. E.; Elam, J. W.; Darling, S. B., Enhanced Block Copolymer Lithography Using Sequential Infiltration Synthesis. *The Journal of Physical Chemistry C* **2011,** *115* (36), 17725-17729.

61. Ringard-Lefebvre, C.; Baszkin, A., Behavior of Poly(D,L-lactic acid) Monolayers at the Air-Water Interface. Effect of Spreading Solvents. *Langmuir : the ACS journal of surfaces and colloids* **1994,** *10* (7), 2376-2381.

62. Wu, S., *Polymer Interface and Adhesion*. 2017.

63. Li, X.; Liu, Y.; Wan, L.; Li, Z.; Suh, H.; Ren, J.; Ocola, L. E.; Hu, W.; Ji, S.; Nealey, P. F., Effect of Stereochemistry on Directed Self-Assembly of Poly(styrene-b-lactide) Films on Chemical Patterns. *ACS Macro Lett.* **2016,** *5* (3), 396-401.

64. Efremov, M. Y.; Kiyanova, A. V.; Last, J.; Soofi, S. S.; Thode, C.; Nealey, P. F., Glass transition in thin supported polystyrene films probed by temperature-modulated ellipsometry in vacuum. *Phys. Rev. E: Stat., Nonlinear, Soft Matter Phys.* **2012,** *86* (2-1), 021501/1-021501/11.

65. Fryer, D. S.; Peters, R. D.; Kim, E. J.; Tomaszewski, J. E.; de Pablo, J. J.; Nealey, P. F.; White, C. C.; Wu, W.-l., Dependence of the Glass Transition Temperature of Polymer Films on Interfacial Energy and Thickness. *Macromolecules* **2001,** *34* (16), 5627-5634.

66. Tate, R. S.; Fryer, D. S.; Pasqualini, S.; Montague, M. F.; de Pablo, J. J.; Nealey, P. F., Extraordinary elevation of the glass transition temperature of thin polymer films grafted to silicon oxide substrates. *J. Chem. Phys.* **2001,** *115* (21), 9982-9990.

67. Kim, J. H.; Jang, J.; Zin, W.-C., Thickness Dependence of the Glass Transition Temperature in Thin Polymer Films. *Langmuir : the ACS journal of surfaces and colloids* **2001,** *17* (9), 2703-2710.

68. Brush Molecules at Flat Interfaces. *Macromolecules* **2001**.

69. R., S., *Phys Rev E Stat Nonlin Soft Matter Phys* **2001**.

70. Spontaneous Curvature of Comblike Polymers. *Macromolecules* **2004**.

71. Ren, J.; Zhou, C.; Chen, X.; Dolejsi, M.; Craig, G. S. W.; Rincon Delgadillo, P. A.; Segal-Peretz, T.; Nealey, P. F., Engineering the Kinetics of Directed Self-Assembly of Block Copolymers toward Fast and Defect-Free Assembly. *ACS applied materials & interfaces* **2018,** *10* (27), 23414-23423.

72. Xiong, S.; Wan, L.; Ishida, Y.; Chapuis, Y.-A.; Craig, G. S. W.; Ruiz, R.; Nealey, P. F., Directed Self-Assembly of Triblock Copolymer on Chemical Patterns for Sub-10-nm Nanofabrication via Solvent Annealing. *ACS nano* **2016,** *10* (8), 7855-7865.

73. Moni, P.; Suh, H. S.; Dolejsi, M.; Kim, D. H.; Mohr, A. C.; Nealey, P. F.; Gleason, K. K., Ultrathin and Conformal Initiated Chemical-Vapor-Deposited Layers of Systematically Varied Surface Energy for Controlling the Directed Self-Assembly of Block CoPolymers. *Langmuir : the ACS journal of surfaces and colloids* **2018,** *34* (15), 4494-4502.

74. Rincon, P. ORIGIN OF DEFECTS IN DIRECTED SELF-ASSEMBLY OF DIBLOCK COPOLYMERS USING FEATURE MULTIPLICAITON. University of Chicago, 2014.

75. Potemkin, I. I.; Khokhlov, A. R.; Prokhorova, S.; Sheiko, S. S.; Moller, M.; Beers, K. L.; Matyjaszewski, K., Spontaneous curvature of comblike polymers at a flat interface. *Macromolecules* **2004,** *37* (10), 3918-3923.

76. Sheiko, S. S.; Prokhorova, S. A.; Beers, K. L.; Matyjaszewski, K.; Potemkin, I. I.; Khokhlov, A. R.; Moller, M., Single molecule rod-globule phase transition for brush molecules at a flat interface. *Macromolecules* **2001,** *34* (23), 8354-8360.

77. Matsen, M. W.; Bates, F. S., Conformationally asymmetric block copolymers. *Journal of Polymer Science Part B: Polymer Physics* **1997,** *35* (6), 945-952.

78. Love, J. A.; Morgan, J. P.; Trnka, T. M.; Grubbs, R. H., A Practical and Highly Active Ruthenium-Based Catalyst that Effects the Cross Metathesis of Acrylonitrile. *Angew. Chem. Int. Ed.* **2002,** *41* (21), 4035–4037.

79. Bates, C. M.; Chang, A. B.; Momčilović, N.; Jones, S. C.; Grubbs, R. H., ABA Triblock Brush Polymers: Synthesis, Self-Assembly, Conductivity, and Rheological Properties. *Macromolecules* **2015,** *48* (14), 4967-4973.

80. Sveinbjörnsson, B. R.; Weitekamp, R. A.; Miyake, G. M.; Xia, Y.; Atwater, H. A.; Grubbs, R. H., Rapid self-assembly of brush block copolymers to photonic crystals. *Proc. Natl. Acad. Sci. U.S.A.* **2012,** *109*, 14332–14336.

Chapter 5: Facile control of block surface energy *via* clickable modification of poly (styrene-*block*-butadiene) enabling topcoat-free directed self-assembly with thermal annealing

5.1 Abstract

A versatile protocol is outlined to create **A-*b*-(B-*r*-C)** block copolymers with differing Flory-Huggins parameters, χ, and equal surface free energies (SFE). Thiol-ene click is used to modify polybutadiene **(PB)** homopolymer to rapidly create **B-*r*-C** blocks with varying composition, φ. Water contact angle (WCA) is used to identify the composition that results in a similar surface free energy (SFE) to the **A** block, polystyrene (**PS**). Small angle X-ray scattering was then carried out to determine the effect of modification on the morphology. Two different **A-*b*-(B-*r*-C)** polymers are identified and synthesized *via* the thiol-ene "click" reaction with mercaptoethanol (**MEA**) and 1-thioglycerol (**MGA**) from the same parent PS-*b*-PB block copolymer. Both polymers show a linear dependence in SFE and a second order dependence in χ with composition, enabling χ to be fully decoupled from the processing restraints required for topcoat free directed self-assembly (DSA) with thermal annealing. The radical scavenger, butylated hydroxy toluene (BHT), was added to suppress the crosslinking of unreacted double bonds enabling 1 □m defect free pattern using the Liu-Nealey (LiNe) DSA process flow.

5.2 Introduction

As the semiconductor industry continuously moves toward ever-shrinking feature sizes, directed self-assembly (DSA) of block copolymers (BCPs) has emerged as a promising approach for the patterning of sub-lithographic features. In DSA a lithographically defined template is

subdivided through the guided self-assembly of BCPs and has been investigated in high volume manufacturing (HVM) using the Liu-Nealey (LiNe) process flow, with the model BCP poly(styrene-*block*-methyl methacrylate) (PS-*b*-PMMA).[1-3] However, the model BCP PS-*b*-PMMA can only form features down to a lamellar period, or full pitch, of approximately 20 nm, on account of its low Flory-Huggins parameter, χ.[4] As such, significant efforts have focused on the development of higher χ BCPs over the last few years.[5] For example, Yu et al synthesized poly(solketal methacrylate-*block*-styrene) with a χ of 0.438 at 25 °C.[6] Kwak *et al.* reported a lamellar structure with a full pitch of 5.7 nm using poly(dihydroxystyrene-*block*-styrene) (PDHS-*b*-PS). PDHS-*b*-PS has a χ of 0.7 at 170 °C.[7] Other high χ BCPs can also be accessed by adding ionic liquids to PS-*b*-PMMA,[8] replacing PS with silylated variants,[9] or making architectural changes.[10] However, a main issue associated with high χ BCPs is that the two block also tend to have dissimilar surface free energies (SFE, γ). As a result, parallel orientation rather than the desired perpendicular orientation is observed upon self-assembly. In addition, while numerous BCPs exist with high χ, simulations have shown that a high χN is strongly associated with increased defect formation suggesting that each pitch may have an optimum χ associated with it,[11] and as such, to access ever smaller defect free pitch sizes using DSA requires more than maximizing the χ in a BCP.

To realize perpendicular orientation, several strategies have been developed to cope with BCPs having dissimilar SFE. Solvent vapor can be used to change the polymer-air interface into a polymer-solvent interface, which helps to modulate differences in SFE.[12-13] However, the addition of solvent also brings shortcomings such as long annealing times, deformation of structures, and incompatibility with industrial nanofabrication processes.[14] Another strategy is the use of topcoat layers which can present a balanced interfacial energy to the BCP.[15-19] Recent work has even

shown how initiated chemical vapor deposition (iCVD) could be used to crosslink the BCP turning any BCP into its own non-preferential topcoat.[20] However, the compositions of topcoats must be very carefully tailored to produce a non-preferential surface for a specific BCP. Furthermore, these approaches all required additional processing steps and therefore cost. As such, it would be ideal to use BCPs that can form perpendicular orientation solely *via* (industrially friendly) thermal annealing. This requires a BCP, in which both blocks have equal SFE: a difference of less than 10% can be sufficient to induce parallel assembly.[21] Unfortunately, only a few BCPs such as PS-*b*-PMMA, poly(styrene-*block*-lactic acid), and poly(styrene-*block*-propylene carbonate) exhibit equal SFE.[22-23]

Recently, Kim *et al.* proposed a novel strategy to decouple the bulk thermodynamics of a BCP and its SFE by employing a **A-*b*-(B-*r*-C)** polymer.[24] The key to this strategy is the selection of the B and C components, which should be less and more polar than the A block, respectively. The theory has shown that while SFE is strictly an additive function of composition, χ has a non-linear dependence on the composition.[25-26] Therefore, equal SFE can be achieved at a certain compositional ratio of B to C in B-*r*-C block. This prior work showed that the partial epoxidation of the polyisoprene block in a poly (styrene-*block*-isoprene) (PS-*b*-PI) copolymer does allow access to a BCP with equal SFE and slightly enhanced χ. However, the thermodynamic versatility for this particular system is limited, i.e. χ_{AB}, χ_{AC}, and χ_{BC} is restricted due to limited compositional flexibility. Presented herein is the development of a high throughput, versatile synthetic approach that can be employed to allow access to many BCPs with varying chemistries and unique thermodynamic pathways, each of which contains an **A** block and **(B-*r*-C)** block with equal SFE and enhanced χ (**Scheme 1**). To realize this approach, facile thiol-ene click chemistry[27-28] is used

to modify an alkene-containing parent polymer, poly(styrene-*block*-1,2-butadiene) (PS-*b*-PB) (1,2 content of the PB block is 90 mol %), with a wide variety of thiols ranging from non-polar to polar.

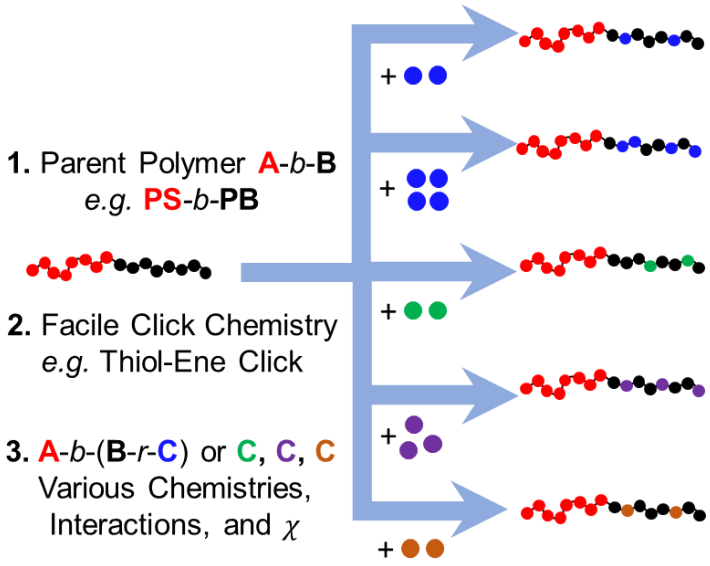

Figure 22. A high throughput synthetic approach to differently functionalized block copolymers used for screen for block copolymers which possess equal surface energy for Directed Self-Assembly applications.

5.3 Results and discussion

An illustration of the specific protocol utilized in this work is outlined in Figure 22. First, a homopolymer analogue of the **B** block, here 1,2-polybutadiene (PB) (90 mol% of 1,2 content), is modified *via* thiol-ene click chemistry to create a **B-*r*-C** copolymer with different degrees of functionalization (φ), which is realized by altering the reaction time. Thiol-ene chemistry was employed on account of its robustness and tolerance to a wide variety of functional groups.[29-30] A series of these polymers are prepared with a range of φ and the water contact angle (WCA) of this **B-*r*-C** block is then compared to that of the **A** block to determine if the approximated surfaces free energies are close. If they are not, then the thiol-ene reaction is repeated to alter φ. Once the

relationship between φ and WCA is known, then the parent **A-*b*-B** polymer is modified with the conditions necessary to achieve the φ at which the WCA for the two blocks is equal. At this point, small angle X-ray scattering (SAXS) is used to verify the morphology and χ of the resulting **A-*b*-(B-*r*-C)** polymer. The desired morphology is lamellar. The hole-island test is then carried out at elevated temperatures on silicon in order to verify the SFE is equal enough for both blocks to wet the free interface. This polymer is then tested on differing random copolymer substrates to identify a strongly preferential substrate, as well as a non-preferential substrate. Finally, this preferential substrate is patterned with e-beam lithography, and a non-preferential material is backfilled in to create a LiNe process flow chemical pattern,[2] to allow for the DSA.

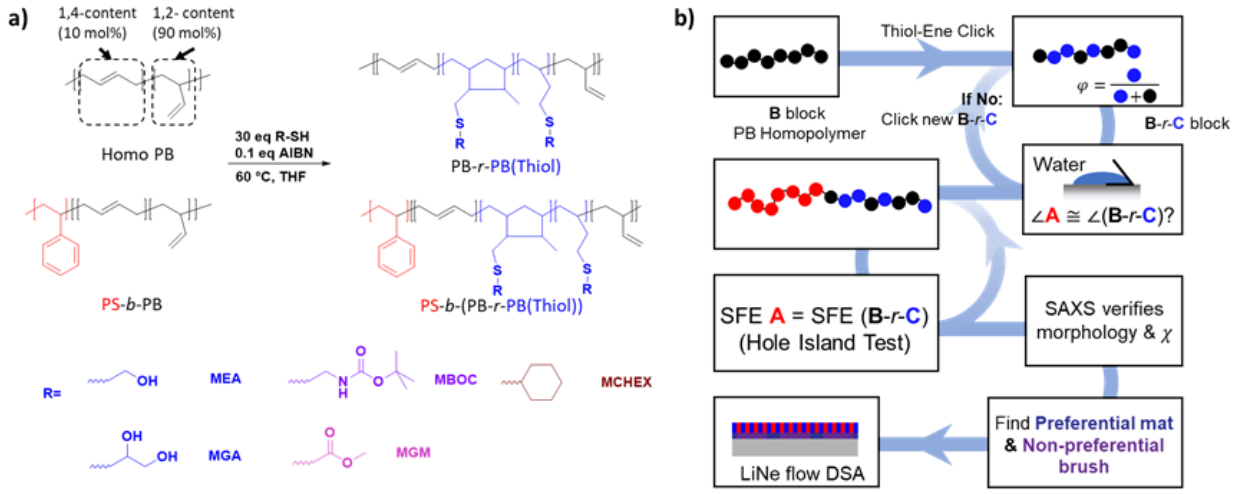

Figure 23. a) Synthetic scheme of thiols modified PB homopolymer and PS-*b*-PB using thiol-ene "click" chemistry. b) Overall protocol for the creation and DSA of A-*b*-(B-*r*-C) with equal SFE. Each box shows the key experimental question or outcome of a given step and is labeled with the figure in which the data is presented for ease of reference.

While true SFE consists of the sum of thermodynamic interactions between the polymer components and the free interface, WCA provides a quick and easy, though indirect, method to reliably probe the surface wetting behavior.[31] Since both homo PB and and PB block in the PS-*b*-

PB used in this work have similar molecular weight and microstructure (90 mol% of 1,2-content) and only φ is varied, the WCA-φ relationship of the modified homo PB is assumed to be similar to that of modified PS-*b*-PB. Therefore, homo PB was used to rapidly evaluate the effect that varying thiol functionalities and φ has on the WCA, and thus SFE. In a good agreement with theory, Figure 24 demonstrates a linear relationship between φ and WCA of the **(B-*r*-C)** analogue material (**PB**-*r*-**PB(Thiol)**). The measured WCA of homo PS and homo PB are 90° and 101 °, respectively. When the homo PB is modified by a less polar thiol, MCHEX, its WCA increases, moving it further away from PS and indicating that it cannot be used to create an equal SFE **PS-*b*-(PB**-*r*-**PB(Thiol))**. In comparison, modifying the homo-PB with polar thiols results in a reduction of the WCA, with more polar moieties producing a greater reduction in WCA at an equivalent φ. A series of **PB**-*r*-**PB(Thiol)** with different functional groups and degree of functionalization φ were synthesized shown in Figure 1. From the WCA data shown in Figure 1 it is estimated that a φ of 25 %, 24%, 20 %, and 15% for MGM, MBOC, MEA, and MGA, respectively, would result in the WCA of the **PB**-*r*-**PB(Thiol)** block being close to that of the **A** block, PS. Using these WCA relationships as guides, a PS-*b*-PB block copolymer (M_n= 16.5 kg/mol, PS:PB molar ratio= 0.356:0.644, Đ= 1.10, 90 mol% of 1,2-content in PB block) was functionalized *via* thiol-ene chemisty in a similar manner as used to functionalize the homo-PB polymer. To allow a more complete study in addition to the **PS-*b*-(PB**-*r*-**PB(Thiol))** with φ close to the above determined point of crossover, *i.e.* 25 % for MGM, 24 % for MBOC, 20 % for MEA, and 15 % for MGA, **PS-*b*-(PB**-*r*-**PB(Thiol))s** with other φ values were also synthesized.

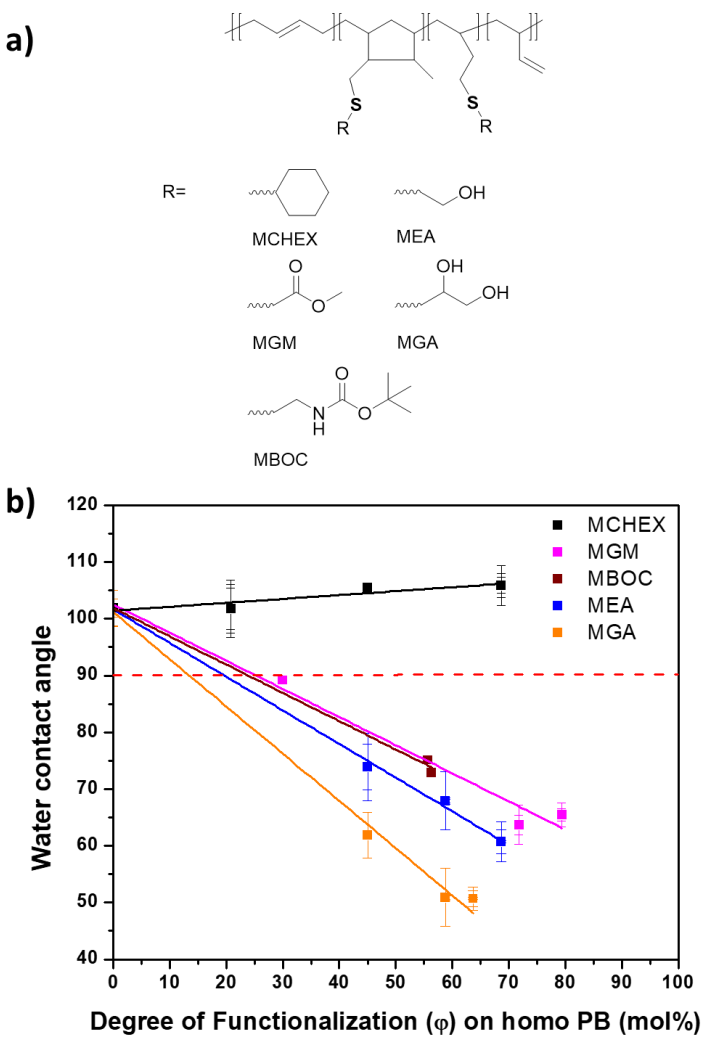

Figure 24. a) Chemical structures of thiols modified homo PB. b) Water contact angle of thiols modified PB (red dashed line represents the WCA of homo PS).

SAXS was performed to determine the effect of modification on the BCPs morphology **(**Figure 25**)**. It was found by SAXS (Figure) that at a level of φ predicted to have equal SFEs for the MGM and MBOC-modified BCPs resulted in a change in morphology from lamellae to hexagonally closed packed cylinders. This transformation is presumably a consequence of the shift in volume fraction after attaching these bulky thiols. In addition, no higher order scattering peaks were observed for φ = 24.7-51.9 for PS-*b*-(PB-*r*-PB(MGM)) and 35.3-64.7 for PS-*b*-(PB-*r*-

PB(MBOC)), indicating the absence of strong microphase separation and therefore much smaller χ_{eff}. Only PS-*b*-PB modified using the two less bulky and more polar thiols, MEA and MGA, maintained lamellar morphology. Therefore, these two materials were selected for further study. The first thing to note is that the lamellar periodicity ($L_0=2\pi/q^*$, where q^* is the principle Bragg reflection) changes with different φ, indicating that the χ_{eff} of the resulting materials changes on account of the thiol addition. In addition, there is a general shift from equally spaced lamella (no second order peak in SAXS) to asymmetric lamella (second order peak observed) upon increasing the amount of polar thiol added to the backbone. This indicates the added volume of the thiol moiety directly affects the morphology and should be taken into account when considering the χ_{eff} of the polymer. The addition of the thiol also results in the appearance of higher ordering scattering, which is directly related to the bulk grain size and is often qualitatively related back to a change in χ_{eff}.[32]

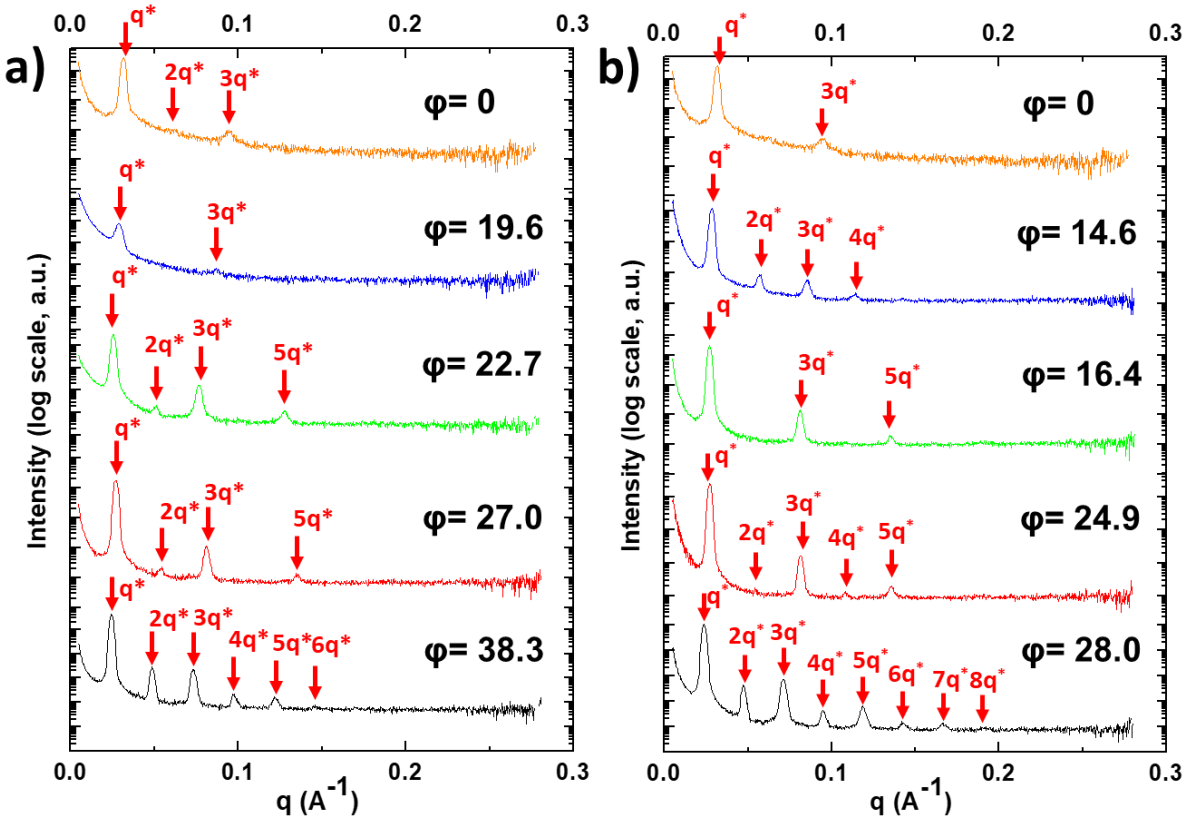

Figure 25. a) SAXS of PS-b-(PB-r-PB(MEA)) and b) PS-b-(PB-r-PB(MGA)). The curves were shifted vertically for clarity.

To more quantitatively investigate the effect of thiol addition on χ_{eff}, we employed the previously reported binary interaction model.[25, 33-34] One can more completely probe the dependence of χ_{eff} on φ by using the SCFT derived relationship (**Eqn. 1**):

$$L_0 = 1.10aN^{\frac{2}{3}}\chi^{\frac{1}{6}} \qquad (1)$$

Where L_0 is the lamellar period, a is the statistical segment chain length, and N is the number of standard lattice volumes occupied by the polymer rather than the degree of polymerization. Here it is important to be be careful about notations and definitions, and be clear on any assuptioms

being made. First, it is assumed that the SCFT relationship holds at the value of χN of these polymers, which is commonly done throughout the literature.[8, 35-36]

Next, it is assumed that the thiol-ene modification does not drastically alter the backbone stiffness as reflected in the statistical segment length, a, which allows us to rearrange the equation to be equal to a constant **(Eqn. 2)**. This is a reasonable assumption give the relatively low degree of modification, φ, in these materials. If this is done then it is possible to directly compare with the known qualities of the well studied **A-*b*-B** parent polymer **(Eqn. 3)**.

$$L_0/(N^{\frac{2}{3}}\chi^{\frac{1}{6}}) = 1.10a \qquad (2)$$

$$\hat{L}_0/(\hat{N}^{\frac{2}{3}}\hat{\chi}^{\frac{1}{6}})\ [\text{Modified}] = L_0/(N^{\frac{2}{3}}\chi^{\frac{1}{6}})\ [\text{Parent}] \qquad (3)$$

Finally, the SAXS data clearly shows that it is important to take into account the added volume of the thiol addition. Assuming that densities do not change significantly, and the volume of the thiol is directly added onto the volume of the BCP it is possible to say that N of the modified polymer is directly equal to N of the parent polymer plus N of the thiol added and arrive at the final equation used to calculate χ_{eff}.

$$\hat{L}_0/((N + N_{thiol})^{\frac{2}{3}}\hat{\chi}^{\frac{1}{6}}) = L_0/(N^{\frac{2}{3}}\chi^{\frac{1}{6}}) \qquad (4)$$

Figure 26 shows χ_{eff} of the final products calculated using equation 4 with published $\chi_{PS\text{-}b\text{-}PB}$ = 0.055.[37] The effect of the addition of thiols on the lamellar periodicity quantitatively shows a second order effect on χ_{eff}, again in good agreement with theory as well as the qualitative SAXS results. This second order dependence of χ on φ along with the first order dependence of WCA and thus SFE on φ is the critical property of an **A-*b*-(B-*r*-C)** architecture when viewed for DSA applications.

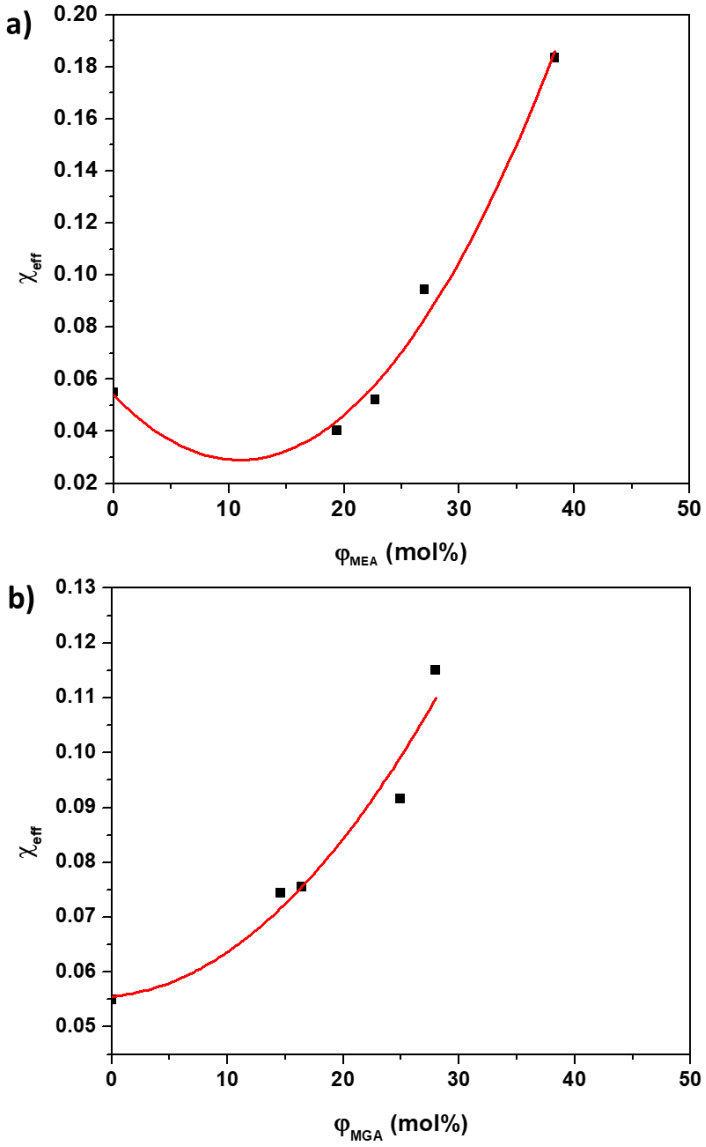

Figure 26. The effect of thiols and φ on χeff calculated: χeff vs a) φMEA and b) φMGA. (χeff was calculated using eq. 4)

As shown in Figure 27, the wetting behavior of modified PS-*b*-PB was further investigated using a so-called "Hole-Island" test.[38-39] The key of this test is the formation of topography in the BCP thin films that depends upon the BCP as-cast film thickness relative to its lamellar periodicity (L_0) and the wetting preferences at both interfaces. Here, 1.75 L_0 (as-cast) thin film was annealed

at 165 °C on crosslinked PS (x-PS). The thermal properties of these two materials are shown in Figure . After annealing, holes formed from pristine PS-*b*-PB, indicating a symmetric wetting condition with polybutadiene at both the top and bottom interfaces (Figure 27a). As more MEA is attached to the PB block, a transition from holes to islands (Figure 27c and d) is observed suggesting that the SFE of the **(B-*r*-C)** block starts to increase until it is eventually higher than that of PS. At an intermediate composition (φ=19.6 mol% and 14.6 mol% for MEA and MGA, respectively) we find 0.5 L_0 topography indicative of equal SFE, with one block still preferentially wetting the substrate. These compositions were very close to those predicted by WCA measurements discussed previously. In addition, the χ_{eff} at these compositions were calculated to be 0.041 and 0.074 for PS-*b*-(PB-*r*-PB(MEA)) and PS-*b*-(PB-*r*-PB(MGA)), respectively at 165 °C.

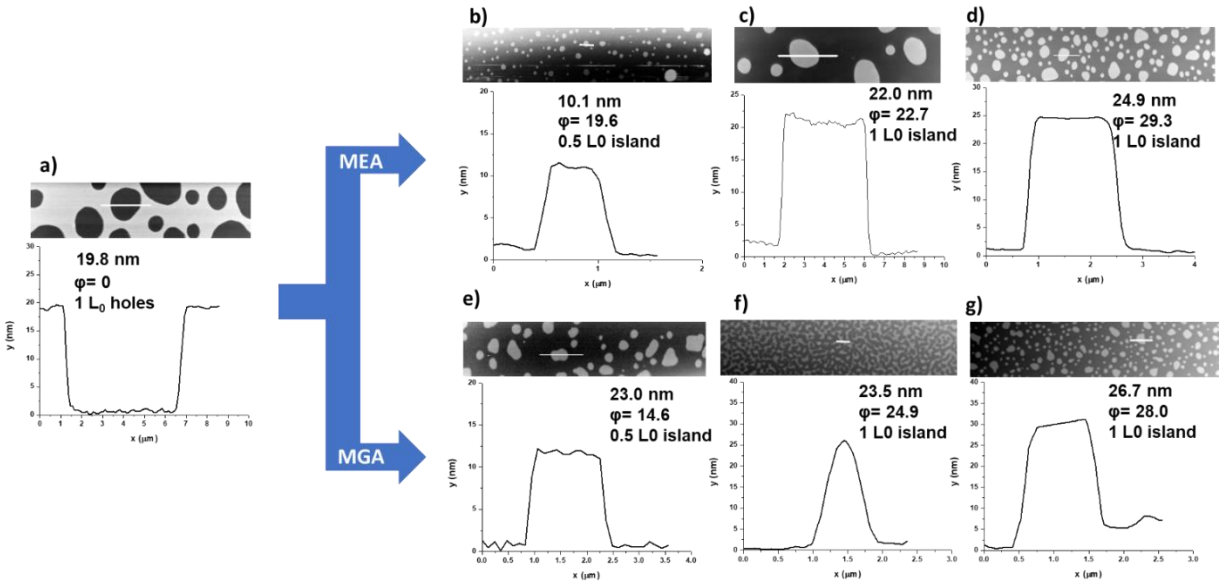

Figure 27. AFM height traces of a) PS-b-PB, b-d) PS-b-(PB-r-PB(MEA)) with different degree of functionalization φ, and e-g) PS-b-(PB-r-PB(MGA)) with different degree of functionalization φ on x-PS coated silicon wafer.

The bottom interfacial energy is then fine tuned to also be non-preferential through the use of poly(t-butyl styrene)-*r*-poly(methyl methacrylate) which bears an azide-based crosslinker (see Figure for the synthetic details).[40] Figure 28 shows that as the t-butyl styrene (tBS) content was increased, the topography vanished and fingerprint patterns were observed under SEM. The tBS composition required to achieve this was from 28.3 to 42.5 mol% for PS-*b*-(PB-*r*-PB(MEA)) and 24.0 to 38.5 mol% for PS-*b*-(PB-*r*-PB(MGA)). As a comparison, the non-preferential tBS window for lamellar forming PS-*b*-PMMA is 19.0- 29.5 mol%. It is worthwhile noting that further increasing content of tBS eventually caused the film to become optically cloudy after annealing, indicating the presence of dewetting.

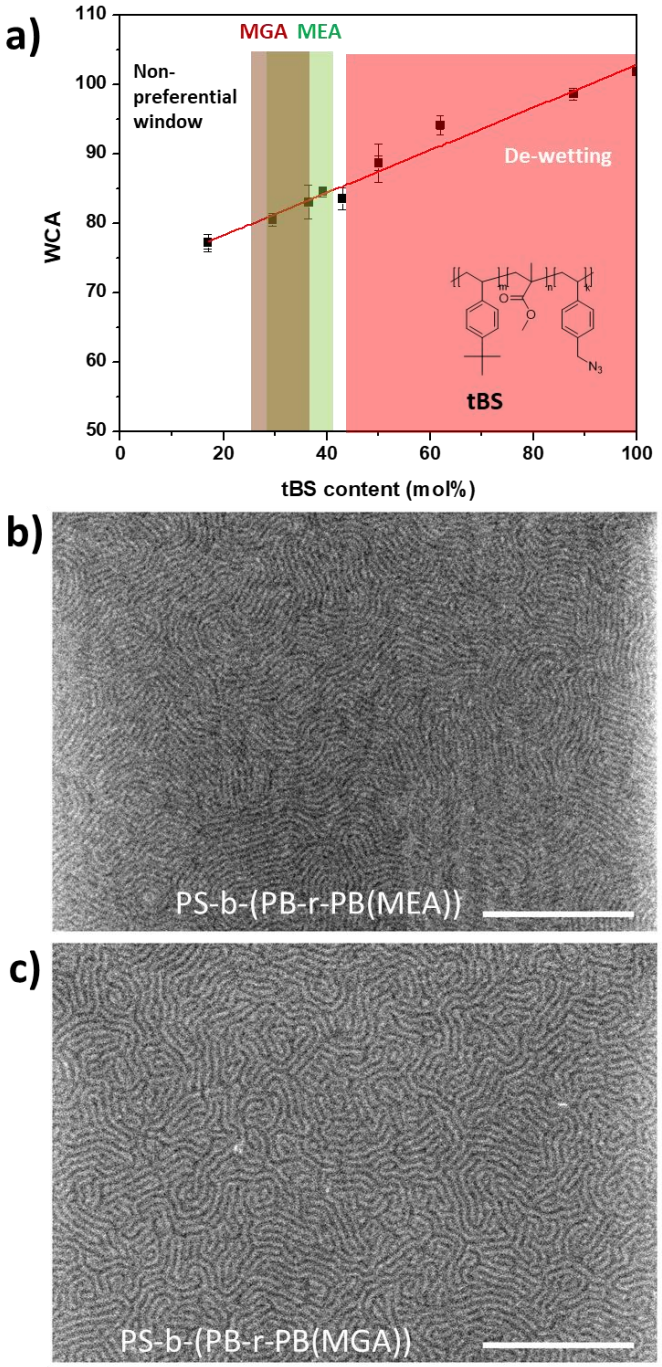

Figure 28. a) Water contact angles for the random copolymer mat with different tBS content. (The mat chemical structure is shown in the inlet and the non-preferential window for two materials marked). b) Top-down SEM images of PS-b-(PB-r-PB(MEA)) and c) PS-b-(PB-r-PB(MGA)) indicative of assembly within the non-preferential window. Scale bar is 500 nm.

In both representative samples, (PS-*b*-(PB-*r*-PB(MEA)) and PS-*b*-(PB-*r*-PB(MGA))), there are residue unreacted double bonds, which are known to crosslink at elevated temperature.[41-42] To verify that crosslinking was occurring at the same time scale as the assembly process, the post annealing block copolymer was washed from the surface using toluene/DMF mixture solvent. Upon doing this it was found that a significant amount of residue remained on the surface **(**Figure **)**. If the film crosslinks too quickly it will negatively affect the DSA process by 'freezing' in an incompletely assembled structure. To probe this crosslinking behavior in more detail, rheology experiments were undertaken. Figure 29 shows the storage modulus and tan δ captured from frequency sweep rheology performed at 150 °C, which allows a quantitative evaluation of the crosslinking during the annealing process. The storage modulus rapidly increases with crosslinking, at the same time the tan δ first increases as the film phase separates and then rapidly decreases as the film crosslinks and becomes more elastic.[43-44] The decrease is observed within a half hour at high frequencies, which probe the smallest length scales. Assuming a doubling of kinetics with every 10 °C, this corresponds to an onset of crosslinking within minutes at 200 °C which was the ultimate temperature used for DSA. Okhrimenko suggested a radical mechanism for this thermal crosslink.[45] Simply adding 0.1 % BHT by weight relative to the BCP slows the cross linking as indicated by the much slower rise in storage modulus as well as the flattening of the peak in tan δ observed at 100 Rad/s and the complete absence of a tan δ peak at either 10 Rad/s or 1 Rad/s. To verify the effect is controlled by the PB domain, homopolymer PS was also tested for comparison and showed a pure liquid like behavior (Figure).

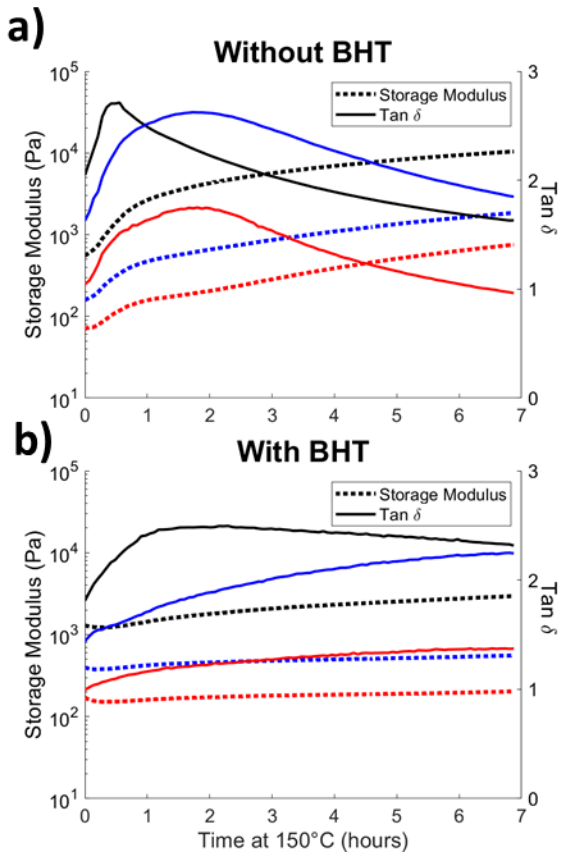

Figure 29. Rheology showing the storage modulus (dotted lines) and Tan δ (solid lines) at 100 rad/s (black), 10 rad/s (blue), and 1 rad/s (red) both with (a) and without (b) 0.1% BHT. Data was obtained at 150 °C and the x axis is shared between the two figures.

Having found conditions that will minimize this crosslinking, it was then important to investigate the DSA capability of this new **A-*b*-(B-*r*-C)** platform. **PS-*b*-(PB-*r*-PB(MEA))** was chosen to go through LiNe DSA process. Figure 30 outlines the basic steps of LiNe DSA flow that are more completely described in the methods. In this process a pattern pitch L_S was used that is four times that of the BCP natural lamellar period L_0. After the trim etch step, which establishes the guide stripe width, the pattern is inspected *via* SEM. The trim etch time was adjusted to achieve 1.5 L_0 wide guide stripes. While 0.5 – 1 L_0 wide is ideal, this is often difficult to achieve when L_0 is small without collapse of the resist pattern.[46] After creation of the chemical pattern, a non-

preferential brush with a composition in the window previously found was grafted between the guide stripes. On top of this complete chemical pattern **PS-*b*-(PB-*r*-PB(MEA))** was spin coated both with and without BHT in order to further validate the rheometry results vis-à-vis crosslinking. After annealing for 200°C for 1 hour it was found that without BHT some registration was achieved, however, by adding 0.1 wt % BHT perfect 1 □m wide DSA could be achieved.

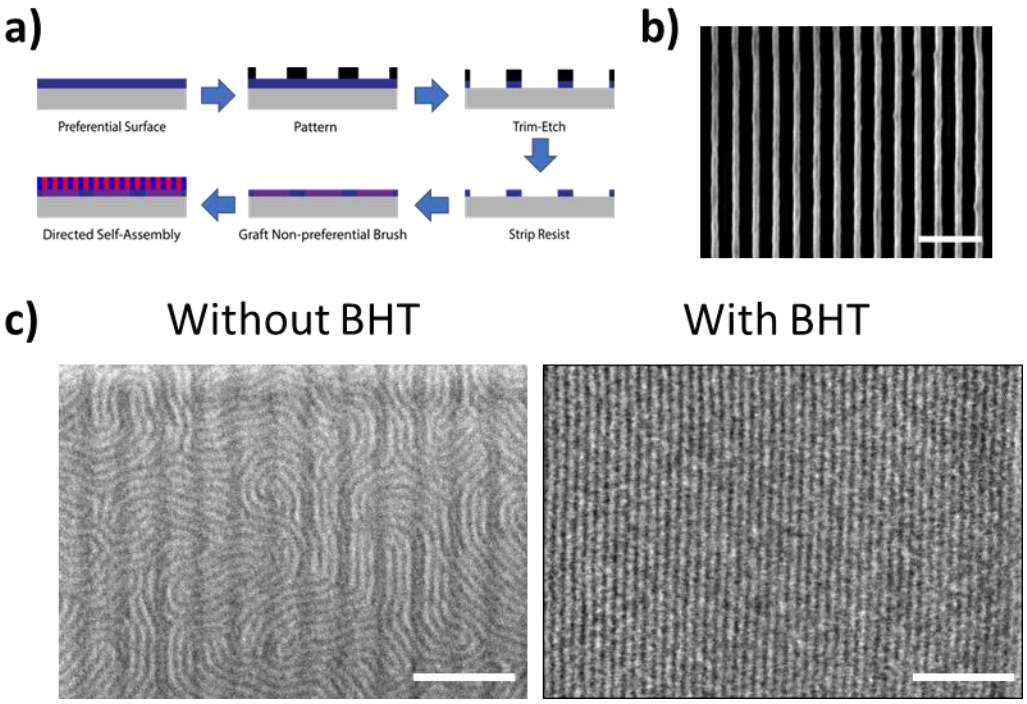

Figure 30. a) The LiNe flow schematic outlining the creation of a chemoepitaxial pattern. b) SEM inspection of the guide strip pattern with a pitch of 82 nm immediately following trim etch. c) SEM of DSA of PS-b-(PB-r-PB(MEA)) with and without 0.1% BHT. Scale bar is 250 nm.

5.4 Conclusions

Here a simple and robust protocol has been demonstrated which allows the facile creation of new equal surface energy block copolymers fit for DSA. Using thiol-ene click chemistry, **B**-*r*-**C** (**PB**-*r*-**PB(Thiol)**) blocks were created with varying φ. WCA was used to quickly iterate through

the various compositions to identify that closest to the **A (PS)** block, as well as to show the linear dependence of WCA on φ. It is also worth noting that the volume fraction change after thiol-ene chemistry especially using bulky thiols could lead to non-lamellar morphology. Nonetheless, using smaller and more polar thiols and the WCA determined composition as a target, two different **A**-*b*-(**B**-*r*-**C)** polymers were synthesized and definitively shown to have equal SFE through the Hole-Island test. The χ_{eff} of these blocks was probed through SCFT, and the second order dependence of χ_{eff} on φ was both qualitatively and quantitatively verified in agreement with theory. The Hole-Island test was then used again to identify both preferential and non-preferential substrates for DSA. The addition of BHT was found to slow vinyl crosslinking suggested by rheology results (quantitative) and rinse tests (qualitative). The combination of **PS**-***b***-**(PB**-***r***-**PB(MEA))** with BHT allowed for perfect 1 □m wide DSA without topcoat**.**

5.5 Acknowledgement

We acknowledge the MRSEC Shared User Facilities at the University of Chicago (NSF DMR-1420709). This work made use of the Pritzker Nanofabrication Facility of the Institute for Molecular Engineering at the University of Chicago, which receives support from Soft and Hybrid Nanotechnology Experimental (SHyNE) Resource (**NSF ECCS-1542205**), a node of the National Science Foundation's National Nanotechnology Coordinated Infrastructure. We also thank Intel Corporation and Semiconductor Research Corporation for the support. Part of this work were carried out at the Soft Matter Characterization Facility of the University of Chicago.

5.6 Supplemental Information

5.6.1 Methods

Surface Preparation

All surfaces were prepared on freshly hot piranha cleaned (DANGER!) silicon using wafers purchased from silicon materials or Pure Wafer (previously WRS materials). Brushes were spun coat to a thickness > 30 nm to ensure sufficient material for grafting, whereas cross-linkable mats were spun coat to the desired thickness (~10 nm). Brushes were grafted by heating the wafer to 200 °C for one hour under vacuum in a custom annealing chamber equivalent to a hotplate which had been pump/purged with nitrogen. Similarly, mats were crosslinked at 250°C for 30 minutes. After grafting or crosslinking the surfaces were sonicated 3 times in the spin coating solvent to ensure the removal of unattached material.

5.6.2 Metrology

Film thicknesses were measured using a J.A. Woollam Alpha SE ellipsometer, and fitted using a Si-SiO_x-Cauchy model where the native oxide thickness was preset at 1.5 nm. For films under 10 nm the optical constants were first fit to thick films, and then locked to more accurately capture the film thickness. AFM was conducted on films using a Bruker multimode 5 in tapping mode. SEM images were captured on a Zeiss Merlin using a 1 – 1.5 KeV accelerating voltage at a working distance below 3 mm using the in-lens secondary electron detector, brightness and contrast were adjusted for presentation. Rheometry measurements were performed using the TA Instruments ARES-G2 strain-controlled shear rheometer with the sample temperature regulated by a forced convection oven. Frequency sweep measurements from 0.3–100 rad/s were performed at small

strains (in the linear viscoelastic region) continually over the course of several hours under N_2 environment.

5.6.3 LiNe flow DSA

Following Figure 30, first a surface was prepared with a preferential crosslinked mat. Allresist AR-N 7520 was spun on top of this mat and soft baked at 150°C for one minute, which yielded a 60 nm thick film. As AR-N 7520 is also light sensitive, the sample was stored in a light tight container to minimize exposure. Films were exposed on a Raith EBPG 5300+ using a pattern dimension of 14 nm, with a 2 nm resolution, a 1 nA current and a dose of 800-1300 $\mu C/cm^2$. The patterns were then developed in MIF 726 for 1 minute, before being quickly rinsed with water (15 seconds) and dried with N_2. Patterns were trim etched into the preferential mat using a Plasmatherm RIE with pure oxygen plasma at a pressure of 10 mTorr, and a bias of 65 watts for 15 seconds. After etching, the remaining resist was stripped by sonicating three times in NMP for 5 minutes. After drying with N_2, a non-preferential brush was back grafted into the pattern as previously described. The pattern was then again sonicated three times in a good solvent for the brush to insure no un-grafted material remained. Finally, the block copolymer solution was spun on and annealed at 200°C for 1 hour in a vacuum chamber, though glovebox gave similar results.

5.6.4 Polymer synthesis and characterization

Materials. Mercaptoethanol (MEA, 99%, Aldrich), 1-thioglycerol (MGA, 97%, Aldrich), methyl thioglycolate (MGM, 95%, Aldrich), and 2-(boc-amino) ethanethiol (MBOC, 97%, Aldrich) were used as received. 2,2-Azobis(2-methylpropionitrile) (AIBN, 98%, Aldrich) was recrystallized from methanol before use. Polybutadiene (PB, 90 mol% of 1,2-content) was purchased from Aldrich. Poly(styrene-*b*-butadiene) (PS-*b*-PB, M_n= 8500 g/mol -*b*-8000 g/mol, 90 mol% of 1,2-content) was purchased from Polymer Source Inc.

Polymer synthesis. A typical thiol-ene modification on PB is described as follows: to a two-neck round bottom flask was added PB (0. 2 g, 3.7 mmol), MEA (8.67 g, 111.1 mmol, 30eq), AIBN (6.0 mg, 0.036 mmol, 0.01 eq), and THF (20 mL). The mixture was purged with anhydrous N_2 for 30 min and stir for 2h at 60 °C. The reaction was then quenched using liquid N_2, concentrated and precipitated into H_2O.

A typical thiol-ene modification on PS-*b*-PB is described as follows: to a two-neck round bottom flask was added PS-*b*-PB (0. 15 g, 1.34 mmol), MEA (3.15 g, 40.3 mmol, 30 eq), AIBN (2.2 mg, 0.013 mmol, 0.01 eq), and THF (15 mL). The mixture was purged with anhydrous N_2 for 30 min and stir for 2h at 60 °C. The reaction was quenched using liquid N_2, concentrated and precipitated into methanol.

The molecular weight and polydispersity indices (Đ) were measured using a Shimadzu gel permeation chromatography system equipped with a Wyatt DAWN HELEOS II Multi-Angle Light Scattering detector, a Wyatt ViscoStar III differential viscometer, a Wyatt Optilab T-rEX differential refractive index detector, and a Shimadzu SPD-M_{30}A Photodiode Array detector (200-800 nm) dynamic light scattering detector. THF was used as the eluent and columns sets are: 2 Agilent PLgel 5 um MIXED-D plus guard. Nuclear magnetic resonance spectroscopy (NMR) was recorded on a Bruker AVANCE II+ 500 at room temperature. The samples were dissolved in $CDCl_3$. The degree of functionalization φ was calculated using ^{1}H-NMR integrals.

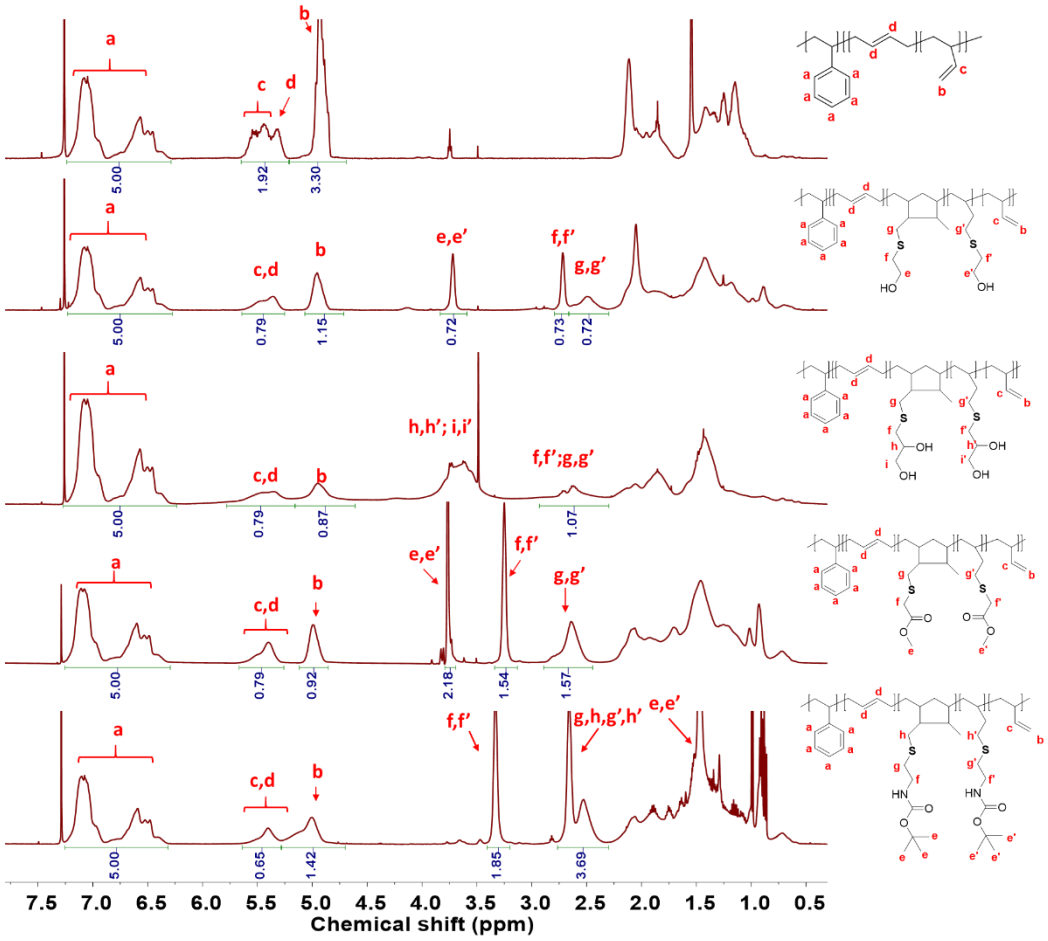

Figure 31. From top to bottom: 1H-NMR of PS-b-PB, PS-b-(PB-r-PB(MEA)), PS-b-(PB-r-PB(MGA)), PS-b-(PB-r-PB(MGA)), PS-b-(PB-r-PB(MGM)), PS-b-(PB-r-PB(MBOC)) in CDCl3.

Degree of functionalization of MEA is calculated as follows:

$$\varphi_{MEA} = \frac{\frac{0.72}{2}}{\frac{3.39}{2} + \frac{1.97 - \frac{3.39}{2}}{2}} = 19.6\ \%$$

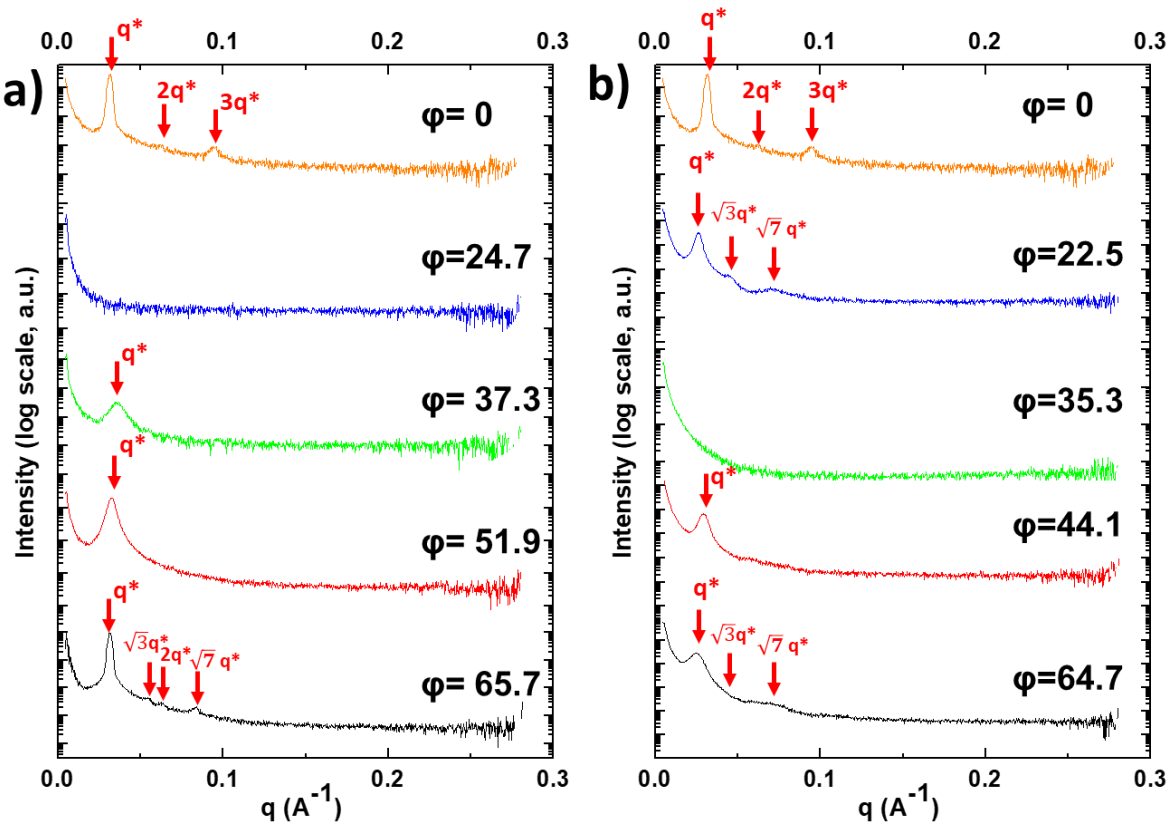

Figure 32. The SAXS of PS-b-(PB-r-PB(MGM)) (left) and PS-b-(PB-r-PB(MBOC)) (right). Curves were shifted vertically for clarity.

Table 5. Summary of BCPs used in this work.

Sample ID	φ	M_n Kg/mol	Đ
PS-*b*-PB	0	16.5	1.10
PS-*b*-(PB-*r*-PB(MEA))	19.6	18.8	1.12
PS-*b*-(PB-*r*-PB(MGA))	14.6	18.9	1.13

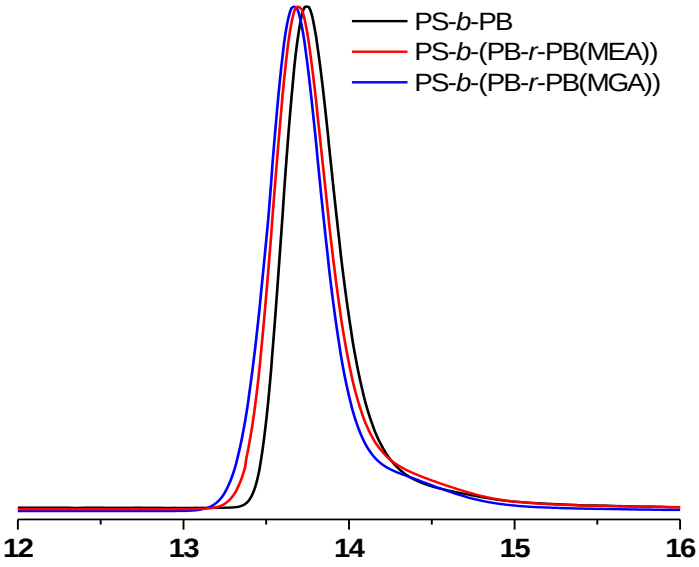

Figure 33. The SEC profile of PS-b-PB (black), PS-b-(PB-r-PB(MEA)) (red), and PS-b-(PB-r-PB(MGA)) (blue).

Thermal properties.

Differential scanning calorimetry (DSC) was performed on a TA Discovery DSC 2500. The samples were equilibrated at 150 °C for 5 min to eliminate thermal history then cooled to -80 °C at a rate of 10 °C/min and equilibrated for another 5 min followed by a heating cycle at 10 °C/min. The glass transitions were measured on the heating cycle. Thermal gravimetric analysis (TGA) was recorded on a TA Discovery TGA. The samples were equilibrated at 105 °C for 5 min to remove any moisture followed by a heating rate of 10 °C/min to 600 °C under N_2 atmosphere. Small-Angle X-ray scattering was recorded on a SAXSLAB (XENOCS)'s GANESHA with a Cu Kα (λ= 1.54 Å) X-ray source. The samples were annealed at 165 °C for 20h under vacuum before measurement. The exposure time was 33 min for each sample.

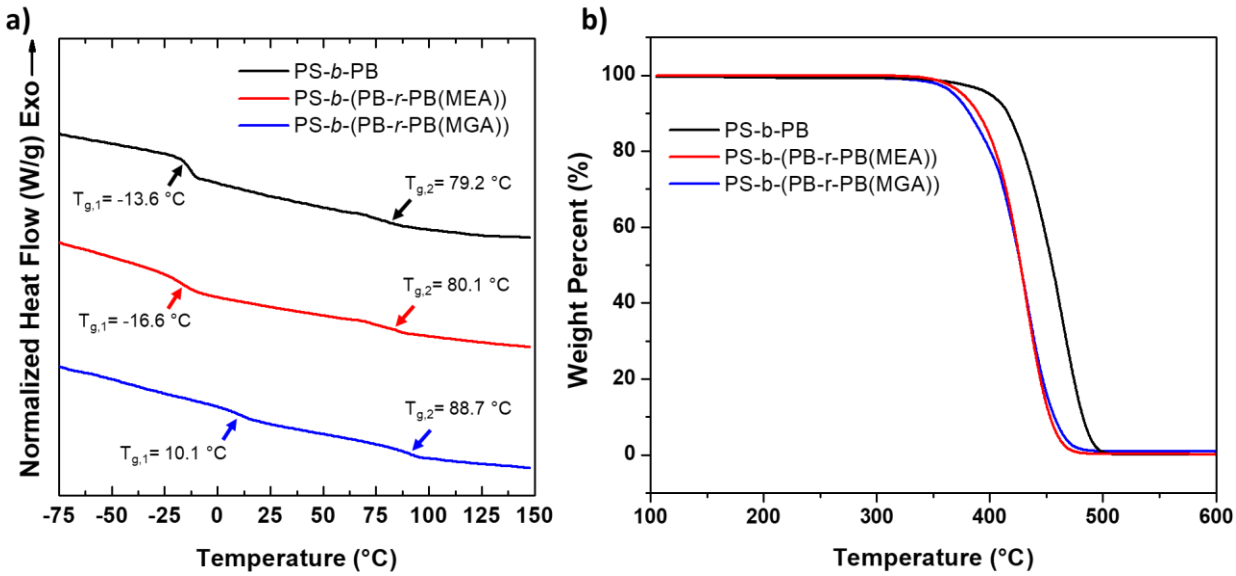

Figure 34. a) DSC profile of PS-b-PB, PS-b-(PB-r-PB(MEA)) and PS-b-(PB-r-PB(MGA)). Lines shifted vertically for clarity. b) TGA curves of PS-b-PB, PS-b-(PB-r-PB(MEA)) and PS-b-(PB-r-PB(MGA)).

Synthesis of poly (t-butyl styrene-*random*- methyl methacrylate) (xSTM-N_3). The synthetic procedure was reported elsewhere.[1]

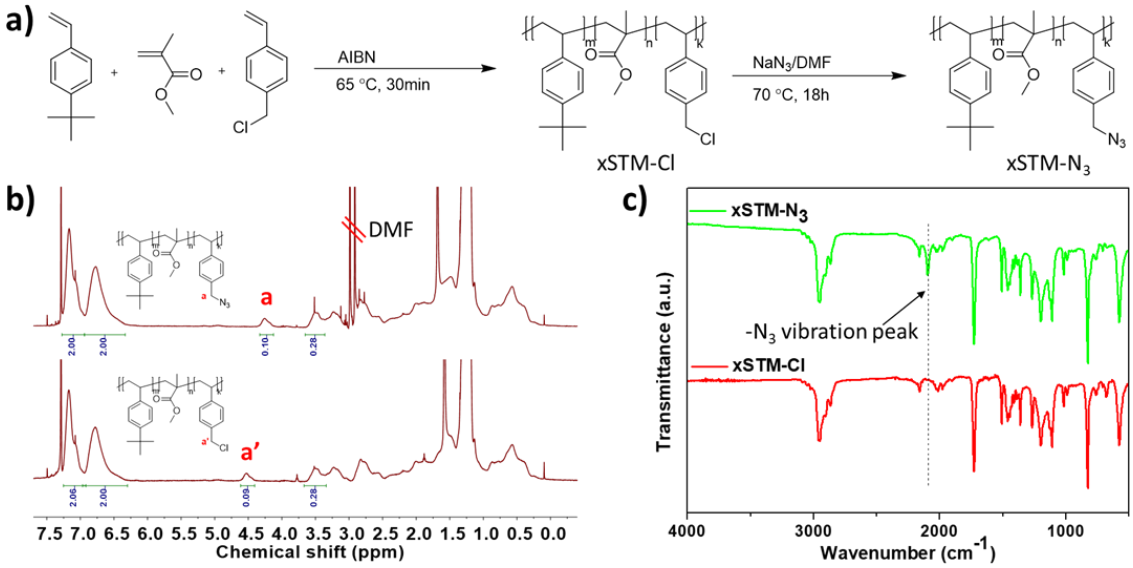

Figure 35. a) Synthetic scheme of xSTM-N3; b) 1H-NMR of xSTM-N3 (top) and xSTM-Cl (bottom) in CDCl3; c) FT-IR spectra of xSTM-N3 (top) and xSTM-Cl (bottom).

Polymer Crosslinking Study

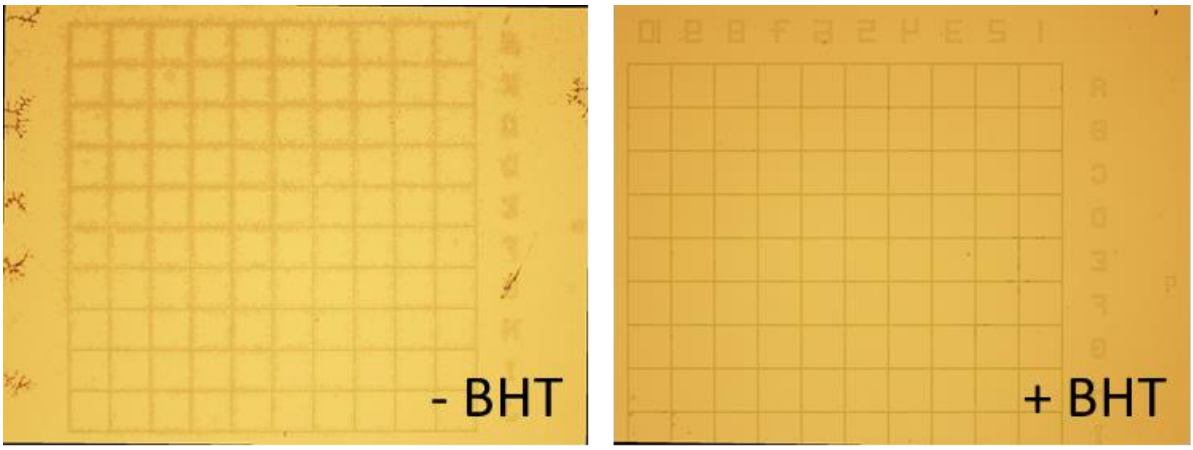

Figure 36. Qualitative crosslinking test shows areas of insoluble material after annealing which is completely suppressed by the addition of BHT. (Each square is 200 µm wide.)

PS-*b*-(PB-*r*-PB(MEA)) films which were annealed at 200°C for 1 hour as part of the DSA optimization experiments were subsequently rinsed and sonicated with increasing polarity mixtures of toluene: DMF (1:0, 2:1, 1;1, 1:2, 1:9, 0:1). Images were taken after final sonication showing clear residue without BHT.

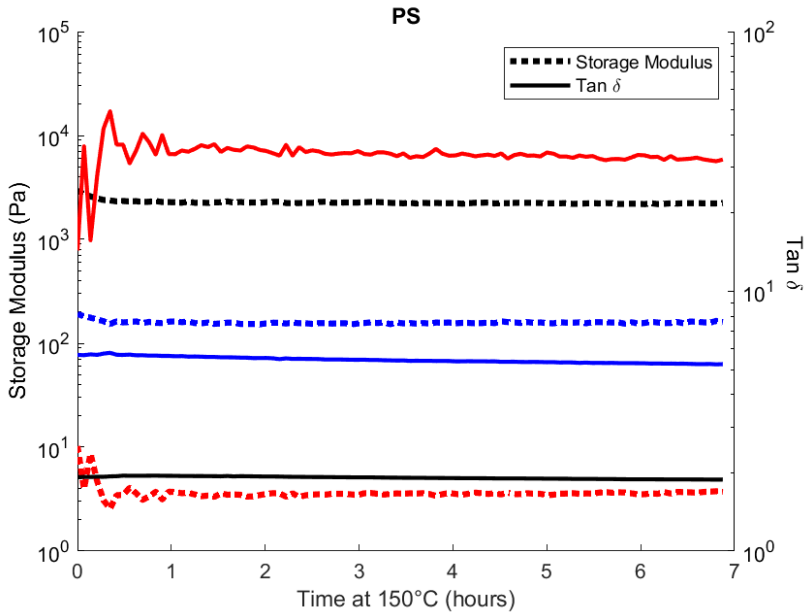

Figure 37. Rheology showing the storage modulus (dotted lines) and Tan δ (solid lines) at 100 Rad/s (black), 10 Rad/s (blue), and 1 Rad/s (red) for homo PS. Data was obtained at 150 °C.

5.7 References

1. Ren, J.; Zhou, C.; Chen, X.; Dolejsi, M.; Craig, G. S. W.; Rincon Delgadillo, P. A.; Segal-Peretz, T.; Nealey, P. F., Engineering the Kinetics of Directed Self-Assembly of Block Copolymers toward Fast and Defect-Free Assembly. ACS applied materials & interfaces 2018, 10 (27), 23414-23423.

2. Liu, C.-C.; Ramírez-Hernández, A.; Han, E.; Craig, G. S. W.; Tada, Y.; Yoshida, H.; Kang, H.; Ji, S.; Gopalan, P.; de Pablo, J. J.; Nealey, P. F., Chemical Patterns for Directed Self-Assembly of Lamellae-Forming Block Copolymers with Density Multiplication of Features. Macromolecules 2013, 46 (4), 1415-1424.

3. Augsburg, A.; Grundke, K.; Pöschel, K.; Jacobasch, H. J.; Neumann, A. W., Determination of contact angles and solid surface tensions of poly(4-X-styrene) films. Acta Polymerica 1998, 49 (8), 417-426.

4. Wan, L.; Ruiz, R.; Gao, H.; Patel, K. C.; Albrecht, T. R.; Yin, J.; Kim, J.; Cao, Y.; Lin, G., The Limits of Lamellae-Forming PS-b-PMMA Block Copolymers for Lithography. ACS nano 2015, 9 (7), 7506-14.

5. Feng, H. B.; Lu, X. Y.; Wang, W. Y.; Kang, N. G.; Mays, J. W., Block Copolymers: Synthesis, Self-Assembly, and Applications. Polymers 2017, 9 (10), 494.

6. Yoshida, K.; Tian, L.; Miyagi, K.; Yamazaki, A.; Mamiya, H.; Yamamoto, T.; Tajima, K.; Isono, T.; Satoh, T., Facile and Efficient Modification of Polystyrene-block-poly (methyl methacrylate) for Achieving Sub-10 nm Feature Size. Macromolecules 2018, 51 (20), 8064-8072.

7. Kwak, J.; Mishra, A. K.; Lee, J.; Lee, K. S.; Choi, C.; Maiti, S.; Kim, M.; Kim, J. K., Fabrication of Sub-3 nm Feature Size Based on Block Copolymer Self-Assembly for Next-Generation Nanolithography. Macromolecules 2017, 50 (17), 6813-6818.

8. Chen, X.; Zhou, C.; Chen, S. J.; Craig, G. S. W.; Rincon-Delgadillo, P.; Dazai, T.; Miyagi, K.; Maehashi, T.; Yamazaki, A.; Gronheid, R.; Stoykovich, M. P.; Nealey, P. F., Ionic Liquids as Additives to Polystyrene- Block-Poly(Methyl Methacrylate) Enabling Directed Self-Assembly of Patterns with Sub-10 nm Features. ACS applied materials & interfaces 2018, 10 (19), 16747-16759.

9. Bates, C. M.; Pantoja, M. A. B.; Strahan, J. R.; Dean, L. M.; Mueller, B. K.; Ellison, C. J.; Nealey, P. F.; Willson, C. G., Synthesis and thin-film orientation of poly(styrene-block-trimethylsilylisoprene). J. Polym. Sci., Part A: Polym. Chem. 2013, 51 (2), 290-297.

10. Kawamoto, K.; Zhong, M.; Gadelrab, K. R.; Cheng, L. C.; Ross, C. A.; Alexander-Katz, A.; Johnson, J. A., Graft-through Synthesis and Assembly of Janus Bottlebrush Polymers from A-Branch-B Diblock Macromonomers. J Am Chem Soc 2016, 138 (36), 11501-4.

11. Hur, S.-M.; Thapar, V.; Ramirez-Hernandez, A.; Khaira, G.; Segal-Peretz, T.; Rincon-Delgadillo, P. A.; Li, W.; Muller, M.; Nealey, P. F.; de Pablo, J. J., Molecular pathways for defect annihilation in directed self-assembly. Proc. Natl. Acad. Sci. U. S. A. 2015, 112 (46), 14144-14149.

12. Xiong, S.; Wan, L.; Ishida, Y.; Chapuis, Y.-A.; Craig, G. S. W.; Ruiz, R.; Nealey, P. F., Directed Self-Assembly of Triblock Copolymer on Chemical Patterns for Sub-10-nm Nanofabrication via Solvent Annealing. ACS nano 2016, 10 (8), 7855-7865.

13. Kim, S. H.; Misner, M. J.; Russell, T. P., Controlling Orientation and Order in Block Copolymer Thin Films. Advanced materials 2008, 20 (24), 4851-4856.

14. Paik, M. Y.; Bosworth, J. K.; Smilges, D.-M.; Schwartz, E. L.; Andre, X.; Ober, C. K., Reversible morphology control in block copolymer films via solvent vapor processing: An in situ GISAXS study. Macromolecules 2010, 43 (9), 4253-4260.

15. Sunday, D. F.; List, S.; Chawla, J. S.; Kline, R. J., Evaluation of the effect of data quality on the profile uncertainty of critical dimension small angle x-ray scattering. J Micro-Nanolith Mem 2016, 15 (1).

16. Kim, E.; Kim, W.; Lee, K. H.; Ross, C. A.; Son, J. G., A Top Coat with Solvent Annealing Enables Perpendicular Orientation of Sub-10 nm Microdomains in Si-Containing Block Copolymer Thin Films. Advanced Functional Materials 2014, 24 (44), 6981-6988.

17. Yoshida, H.; Suh, H. S.; Ramirez-Hernandez, A.; Lee, J. I.; Aida, K.; Wan, L.; Ishida, Y.; Tada, Y.; Ruiz, R.; de Pablo, J.; Nealey, P. F., Topcoat approaches for directed self-assembly of strongly segregating block copolymer thin films. J. Photopolym. Sci. Technol. 2013, 26 (1), 55-58.

18. Seshimo, T.; Bates, C. M.; Dean, L. M.; Cushen, J. D.; Durand, W. J.; Maher, M. J.; Ellison, C. J.; Willson, C. G., Block Copolymer Orientation Control Using a Top-Coat Surface Treatment. Journal of Photopolymer Science and Technology 2012, 25 (1), 125-129.

19. Zhang, J.; Clark, M. B.; Wu, C.; Li, M.; Trefonas III, P.; Hustad, P. D., Orientation control in thin films of a high-χ block copolymer with a surface active embedded neutral layer. Nano Lett. 2015, 16 (1), 728-735.

20. Suh, H. S.; Kim, D. H.; Moni, P.; Xiong, S.; Ocola, L. E.; Zaluzec, N. J.; Gleason, K. K.; Nealey, P. F., Sub-10-nm patterning via directed self-assembly of block copolymer films with a vapour-phase deposited topcoat. Nat Nanotechnol 2017, 12 (6), 575-581.

21. Albert, J. N.; Baney, M. J.; Stafford, C. M.; Kelly, J. Y.; Epps, T. H., Generation of monolayer gradients in surface energy and surface chemistry for block copolymer thin film studies. ACS nano 2009, 3 (12), 3977-86.

22. Zhang, X.; He, Q.; Chen, Q.; Nealey, P. F.; Ji, S., Directed Self-Assembly of High χ Poly (styrene-b-(lactic acid-alt-glycolic acid)) Block Copolymers on Chemical Patterns via Thermal Annealing. ACS Macro Lett. 2018, 7 (6), 751-756.

23. Yang, G.-W.; Wu, G.-P.; Chen, X.; Xiong, S.; Arges, C. G.; Ji, S.; Nealey, P. F.; Lu, X.-B.; Darensbourg, D. J.; Xu, Z.-K., Directed self-assembly of polystyrene-b-poly (propylene carbonate) on chemical patterns via thermal annealing for next generation lithography. Nano Lett. 2017, 17 (2), 1233-1239.

24. Kim, S.; Nealey, P. F.; Bates, F. S., Decoupling Bulk Thermodynamics and Wetting Characteristics of Block Copolymer Thin Films. ACS Macro Lett. 2012, 1 (1), 11-14.

25. Ren, Y.; Lodge, T. P.; Hillmyer, M. A., Synthesis, Characterization, and Interaction Strengths of Difluorocarbene-Modified Polystyrene− Polyisoprene Block Copolymers. Macromolecules 2000, 33 (3), 866-876.

26. Ten Brinke, G.; Karasz, F. E.; MacKnight, W. J., Phase behavior in copolymer blends: poly (2, 6-dimethyl-1, 4-phenylene oxide) and halogen-substituted styrene copolymers. Macromolecules 1983, 16 (12), 1827-1832.

27. Hoyle, C. E.; Bowman, C. N., Thiol–ene click chemistry. Angew. Chem., Int. Ed. 2010, 49 (9), 1540-1573.

28. Michal, B. T.; Brenn, W. A.; Nguyen, B. N.; McCorkle, L. S.; Meador, M. A. B.; Rowan, S. J., Thermoresponsive shape-memory aerogels from thiol–ene networks. Chem. Mater. 2016, 28 (7), 2341-2347.

29. Uygun, M.; Tasdelen, M. A.; Yagci, Y., Influence of type of initiation on thiol–ene "click" chemistry. Macromolecular Chemistry and Physics 2010, 211 (1), 103-110.

30. Silverstein, J. S.; Casey, B. J.; Natoli, M. E.; Dair, B. J.; Kofinas, P., Rapid Modular Synthesis and Processing of Thiol–Ene Functionalized Styrene–Butadiene Block Copolymers. Macromolecules 2012, 45 (7), 3161-3167.

31. Williamson, L. D.; Seidel, R. N.; Chen, X.; Suh, H. S.; Rincon Delgadillo, P.; Gronheid, R.; Nealey, P. F., Three-Tone Chemical Patterns for Block Copolymer Directed Self-Assembly. ACS Appl Mater Interfaces 2016, 8 (4), 2704-12.

32. Chintapalli, M.; Chen, X. C.; Thelen, J. L.; Teran, A. A.; Wang, X.; Garetz, B. A.; Balsara, N. P., Effect of Grain Size on the Ionic Conductivity of a Block Copolymer Electrolyte. Macromolecules 2014, 47 (15), 5424-5431.

33. Roe, R.-J.; Zin, W.-C., Determination of the Polymer-Polymer Interaction Parameter for the Polystyrene-Polybutadiene Pair. Macromolecules 1980, 13 (5), 1221-1228.

34. Kambour, R. P.; Bendler, J. T.; Bopp, R., Phase behavior of polystyrene, poly (2, 6-dimethyl-1, 4-phenylene oxide), and their brominated derivatives. Macromolecules 1983, 16 (5), 753-757.

35. Keen, I.; Yu, A.; Cheng, H. H.; Jack, K. S.; Nicholson, T. M.; Whittaker, A. K.; Blakey, I., Control of the orientation of symmetric poly(styrene)-block-poly(D,L-lactide) block copolymers using statistical copolymers of dissimilar composition. Langmuir : the ACS journal of surfaces and colloids 2012, 28 (45), 15876-88.

36. Semenov, A., Contribution to the theory of microphase layering in block-copolymer melts. Zh. Eksp. Teor. Fiz 1985, 88 (4), 1242-1256.

37. Schwahn, D.; Willner, L., Phase Behavior and Flory− Huggins Interaction Parameter of Binary Polybutadiene Copolymer Mixtures with Different Vinyl Content and Molar Volume. Macromolecules 2002, 35 (1), 239-247.

38. Russell, T., TP Russell, G. Coulon, VR Deline, and DC Miller, Macromolecules 22, 4600 (1989). Macromolecules 1989, 22, 4600.

39. Coulon, G.; Russell, T.; Deline, V.; Green, P., Surface-induced orientation of symmetric, diblock copolymers: a secondary ion mass-spectrometry study. Macromolecules 1989, 22 (6), 2581-2589.

40. Bang, J.; Bae, J.; Löwenhielm, P.; Spiessberger, C.; Given-Beck, S. A.; Russell, T. P.; Hawker, C. J., Facile routes to patterned surface neutralization layers for block copolymer lithography. Adv. Mater. 2007, 19 (24), 4552-4557.

41. Bellander, M.; Stenberg, B.; Persson, S., Crosslinking of polybutadiene rubber without any vulcanization agent. Polymer Engineering & Science 1998, 38 (8), 1254-1260.

42. Uhl, F. M.; McKinney, M. A.; Wilkie, C. A., Polybutadiene cross-linked with various diols—effect on thermal stability. Polym. Degrad. Stab. 2000, 70 (3), 417-424.

43. Raghavan, S. R.; Chen, L. A.; McDowell, C.; Khan, S. A.; Hwang, R.; White, S., Rheological study of crosslinking and gelation in chlorobutyl elastomer systems. Polymer 1996, 37 (26), 5869-5875.

44. De Rosa, M. E.; Winter, H. H., The effect of entanglements on the rheological behavior of polybutadiene critical gels. Rheologica Acta 1994, 33 (3), 220-237.

45. Okhrimenko, I., The Vulcanization of Rubber under High Pressure. Rubber Chem. Technol. 1960, 33 (4), 1019-1028.

46. Garner, G. P.; Delgadillo, P. R.; Gronheid, R.; Nealey, P. F.; de Pablo, J. J., Design of surface patterns with optimized thermodynamic driving forces for the directed self-assembly of block copolymers in lithographic applications. Molecular Systems Design & Engineering 2017, 2 (5), 567-580.

Chapter 6: Freeing Directed Self-Assembly from Surface and Interfacial Energies

6.1 Abstract

Directed Self-Assembly (DSA) of block copolymers (BCPs) is a promising technique for cheaply creating nanoscale features. However, the use of BCPs for this application requires both blocks have equal surface free energies (SFE), controllable substrate wetting including both preferential and non-preferential, high etch contrast, as well as a Flory-Huggins parameter, χ, high enough for moderate phase separation, but not so high as to prohibit defect annihilation. To date, the BCPs that meets these requirements is still very limited. Here we demonstrate a high throughput approach to create a series of BCPs on one parent platform that meet all industrial requirements. These materials are also capable of forming their own non-preferential brush layer, simplifying the synthetic requirements for DSA as well as the process flow. Lastly the capability of incorporation of etch resistant chemistries is shown to enable direct pattern transfer. We believe the work here will broaden the scope for DSA suitable materials and promote the next-generation of nanolithography.

6.2 Introduction

Directed self-assembly (DSA) of block copolymers (BCPs) is a promising nano-patterning technique due to not only its ability to form well-ordered and perfectly aligned nanostructures over a large areas but also its low cost and high throughput capability.[1-3] The ideal block copolymers for DSA are high χ, with equal surface free energy (SFE), and innately controllable interfacial energy so that small feature size and perpendicular orientation can be achieved *via* thermal anneal

without additional steps such as top-coat, solvent annealing or brush grafting. Without precisely engineering the polymer architecture it has been difficult to achieve just two of these three requirements, In particular high χ arises from dissimilar chemistries which often results in large differences in SFE. These differences in surface free energy can be corrected for through replacing the free interface with a solvent,[4-7] or top-coat interface which presents a balanced interfacial interaction.[8-11] Top-coat methods have recently gained interest due to the ability to crosslink the BCP itself prior to annealing so that it presents itself as a non-preferential top interface.[8] While these methods allow for the creation of through film structures, which necessarily requires balanced SFE and interfacial energies, it is of note that only polystyrene-*block*-polymethylmethacrylate (PS-*b*-PMMA) which requires neither topcoat or solvent annealing, is the only platform which has been implemented in an all track process with in depth defectivity and kinetics studies.[12-16] Furthermore it is only PS-*b*-PMMA which has been integrated and electrically validated in semiconductor manufacturing processes for the creation of sublithographic vias and transistors.[17-21] This must be in no small part due to the ease of processing a material with innately equal surface energies which can simply be thermally annealed. When considering interfacial interactions with the substrate, PS-*b*-PMMA also benefits from a large amount of effort investigating various options for non-preferential and preferential surfaces.[22-28]

Yet in spite of all these benefits, PS-*b*-PMMA has a relatively low Flory-Huggins interaction parameter (χ) which limits the realization of sub-10 nm resolution,[29] and also negatively impacts the interfacial width as well as the roughness of the resulting pattern.[30-31] Because of these limitations, PS-*b*-PMMA faces many challenges in order to keep up with the ever increasing feature sizes demanded by the semiconductor industry. One particularly successful approach to this issue is simply synthesizing materials structurally close to PS-*b*-PMMA and hoping that

minute changes shift χ more than SFE. This has resulted in the identification of both PS-*b*-PLA as well as PS-*b*-PPC as new candidates for DSA.[1, 32] Recently, we have shown a new strategy utilizing A-*b*-(B-*r*-C) architectures to effectively decouple χ from SFE. While at first this approach was limited to a single polymer system.[33] Recently we have shown how this approach can be generalized using high throughput click chemistry to create a family of materials compatible with DSA.

Building upon this work we now demonstrate the creation of a new generation of BCPs based upon a PS-*b*-polyglyicdylmethacrylate (PS-*b*-PGMA) platform for DSA applications. These materials meet the following requirements: 1) High enough Flory-Huggins interaction parameter (χ) to achieve sub-10 nm resolution, 2) form perpendicular orientation *via* thermal annealing, which is compatible with the current semiconductor fabrication processes, and 3) good etch contrast. In comparison to our previous platform which utilized anionic synthesis, these materials are easily synthesized via RAFT which allows for precise tailoring of volume fraction to insure the resulting morphology is lamellar. Furthermore the clickable group is completely reacted to insure material stability. Here, we also present a novel solution to controlling substrate interfacial energy. As a result of the thiol – epoxide click we introduce a moderately grafting-capable moiety (e.g. -secondary hydroxyl) into the BCP backbone. This grafting group allows the BCP to present its own non-preferential interfacial energy analogous to what has been shown in recent top-coat literature. In combination with the precisely controlled equal surface energy enabled by the A-*b*-(B-*r*-C) architecture, we can achieve not only top-coat but also bottom coat free. As the non-preferential surface is formed in a BCP self-brushing process, we can precisely control the degree of brushing to insure chemical pattern registration. This new material platform allows for an

implementation and trial of new chemistries in fewer processing steps than ever before, accelerating the DSA learning process towards high volume manufacturing.

6.3 High throughput approach to a series of high χ BCPs with equal SFE.

Here we demonstrated a high throughput approach for a series of high χ BCPs with equal SFE using poly (styrene-*block*-glycidyl methacrylate) (PS-*b*-PGMA) as a platform and a robust thiol-epoxy "click" reaction. The thiol-epoxy reaction is selected on account of its robustness and tolerance with air, moisture, a wide range of available functionalities, and its energy efficiency (no heating needed for the reaction to proceed). Further benefits are the χ of the product could be enhanced by the increased polarity of the backbone due to the generation of an additional hydroxyl group formed by opening the epoxide. This generated secondary hydroxyl group along with any other graftable group on the thiol moiety also serves an important role by grafting onto the silicon wafer and acting as its own non-preferential bottom brush layer. As for the thiol selection, we selected polar thiols, *i.e.* MEA, TGM, and 2MP, and less-polar thiols, *i.e.* TF and PTMS. The synthetic details are provided in the supporting information. The resulting materials exhibit perpendicular orientation without topcoat *via* thermal annealing. Furthermore, these new BCPs showed higher χ than industrial standard PS-b-PMMA.

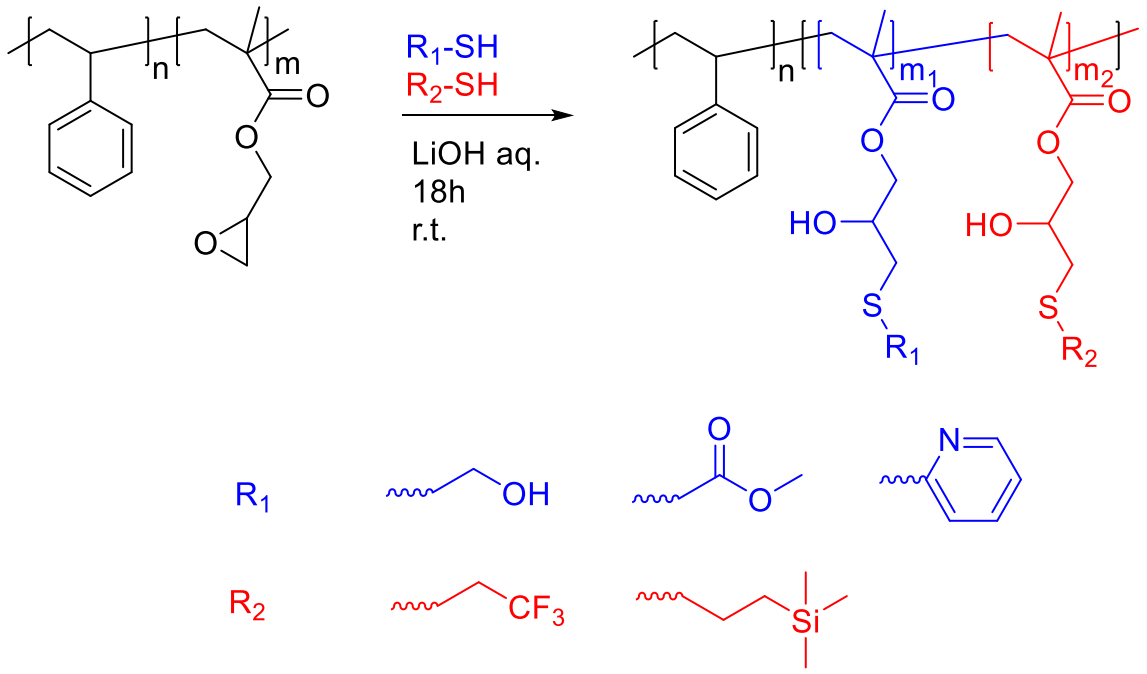

Scheme 1. The synthetic scheme of BCPs used in this work.

Table 6. Summary of BCPs used in this work.

BCP	Thiol R_1	Thiol R_2	n	m_1	m_2	N[a]	T_g °C	T_d °C	L_0 nm	T_{ODT}[b] °C	χ	χN
1	TGM	TF	86	22.1	20.9	231.5	6.4, 64.4	237.7	15.2	n/a*	0.31	71.7
2	2MP	TF	86	15.4	27.6	208.9	39.5, 86.1	200.1	14.3	n/a*	0.21	43.9
3	MEA	TF	86	15.8	27.2	227.1	-1.0, 80.9	225.9	15.8	n/a*	0.42	95.4
4	MEA	PTMS	90	20.2	6.8	178.1	13.3, 78.9	212.1	14.7	n/a*	0.16	28.5
5	MEA	PTMS	30	9.1	3.1	68.6		210.3	8.2	165	0.16	11.0
6	MEA	TF	30	4.3	7.9	69.1	12.4, 60.7	210.7		n/a*	0.42	29.0

[a] N was calculated using a reference volume of 144 $Å^3$. [b] Order-disorder transition temperature. *The T_{ODT} is above its degradation temperature. Density of PGMA= 0.805 g/cm^3.[34] density of PGMA = 1.0 g/cm^3.[35] Density of PS = 1.04 g/cm^3. PHEMA= 1.15 g/cm^3. P2VP density= 1.14 1.04 g/cm^3.

Using a facile thiol-epoxy "click" reaction, we were able to randomly modify the parent polymer PS-*b*-PGMA with different thiols to create a series of high χ BCPs. From bulk SAXS results, the periodicity (L_0) of the resulting BCPs varied depending on the thiol pairs used and the degree of functionalization in the PGMA block. We carried out the SAXS of these materials at different temperatures and found that the order-disorder transition temperatures are above their degradation temperatures. The χ of each material was then calculated using a self-consistent mean

field theory (supporting information). A binary interaction model was used to fit the calculated χ against the degree of functionalization and revealed a good agreement. We further examined the BCP thin films wetting behavior using a "Hole-Island" test (supporting information). The degree of functionalization of BCPs with equal SFE were then identified as illustrated by fingerprints SEM images shown in Figure 38. At equal SFE, these BCPs showed exceptionally high χ values comparing with other reported BCPs. A small feature size L0= 8.2 nm at 150 °C, which is one of the smallest perpendicular lamellar feature sizes without using any topcoat. To compare the SFEs of both blocks, we measured SFEs of modified homo-PGMA using the same thiols. It revealed a linear relationship between SFE and degree of functionalization of homo PGMA. The calculated the degree of functionalization was found very close to calculated value (supporting information). The characteristics of the BCPs with equal SFE were summarized in Table 6.

More surprisingly, we found that all these BCPs thin films exhibited fingerprints instead of "half L_0" topography features, which are typically found with when only one of the two interfacial interactions are balanced.[36-37] This may suggest that not only the free surface interaction but also the substrate interaction is balanced. A possible explanation is that the BCPs can self-grafted onto the silicon surface through hydroxyl group, either generated from the thiol-epoxy reaction or from the thiols used.

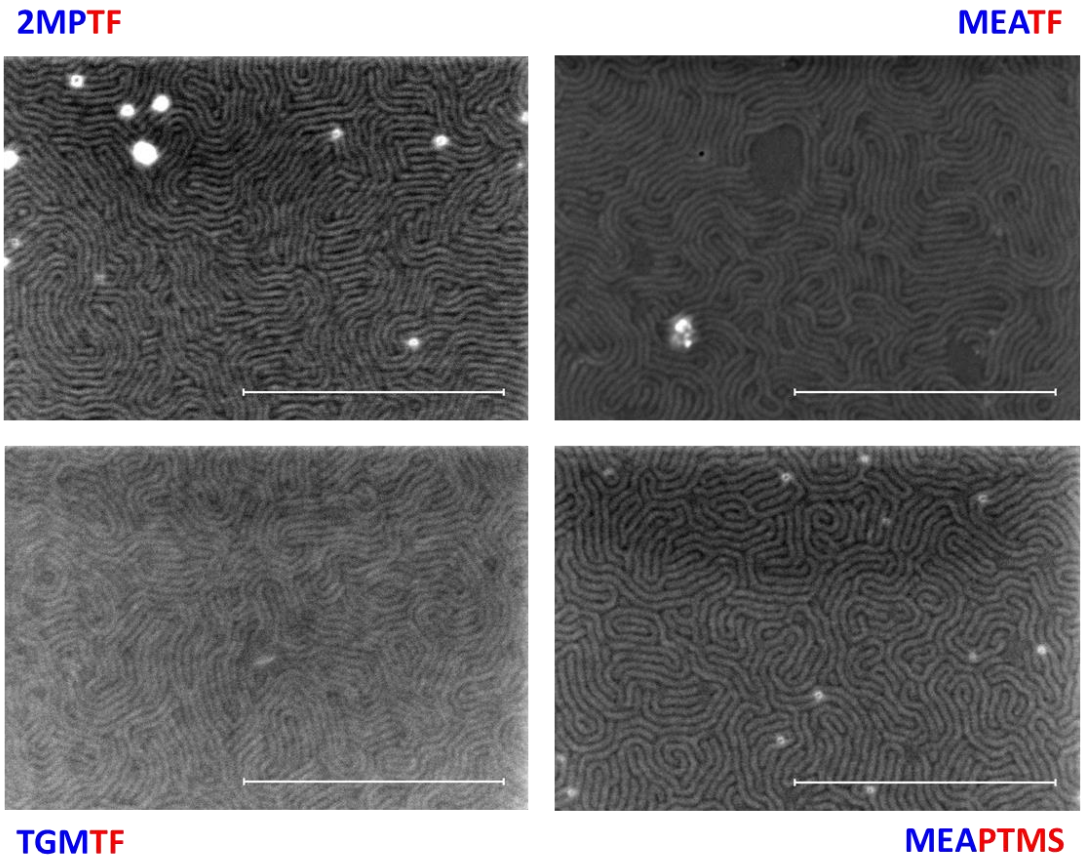

Figure 38. Top-down SEM images of PSPGMA-2MPTF, PSPGMA-MEATF, PSPGMA-TGMTF, and PSPGMA-MEAPTMS. Scale bar is 500 nm.

Table 7. Comparison of φ from calculated (from SFE measurement) and experimental (from I-H tests and SEM) at equal SFE.

BCP		*Calculated*	*Experimental*
1	φ_{TGMTF}	56.8	51.3
2	φ_{2MPTF}	39.3	34.9
3	φ_{MEATF}	19.1	36.8
4	$\varphi_{MEAPTMS}$	--	74.7
5	$\varphi_{4MOTPTF}$	23.9	--

6.4 Self-brushing mechanism enables both the top and bottom interfacial energies equal of BCP thin films and improved LiNe DSA process flow.

To validate the self-grafting of the BCP thin film, we investigated the SFEs of the substrate interface by rinsing the BCP thin films using mixtures of THF/DMF with increasing DMF incorporation. First, a residue thin film was observed after rinsing indicating the presence of a grafting layer. Ellipsometry measurement revealed a remaining film thickness of approximately 8 nm. For comparison this brush thickness is approximately the same as a 10 kg/mol hydroxyl-terminated PS/ PMMA brush grafted onto silicon, which is approximately half the MW of BCPs used. Second, we investigate the SFE of the residue film summarized in Table 8. All the residue thin films showed a very close SFE of 45.26-46.87 mJ/m^2 (OWRK method) or 51.23-52.87 mJ/m^2 (Wu method).

Table 8. Surface free energies of BCP thin films after rinsing.

BCP	SFE calculation model					
	WU			OWRK		
	SFE	Dispersive	Polar	SFE	Dispersive	Polar
1						
2	51.23	39.25	11.98	45.26	38.6	6.66
3						
4	52.87	40.3	12.57	46.87	39.77	7.10

Considering that PS has an SFE of 44.18 mJ/m^2 and PGMA has an SFE of 55.6 mJ/m^2 using OWRK method. The SFE measurements verified that the self-brushing layer is a linear relationship with compositions, which could explain why it is non-preferential to the BCP itself. Particularly from the just the water contact angle (WCA) results, the 2MPTF self-brushing layer had a WCA 72 ° indicating it is not solely PS block exposed to the top surface (PS has a typical WCA of 90 °). It is also unlikely that the PGMA was revealed on top because that requires PS domain attaches on the silicon surface. Therefore, these results indicate that the interface could consist of a both component of PS and modified PGMA. SEM images of the residual brush layer revealed the presence of microphase separation with a domain very close to the thicker film. All this evidence indicates the occurrence of a self-grafting mechanism, although the chain confirmation in the interface between silicon surface and BCP is still unclear.

Because of this surprising balanced substrate interaction and SFE, we implemented BCP thin films into a self-brushing LiNe DSA flow, in which BCP acts as its own non-preferential brush shown in Figure 39a. While normally after trim etching a random copolymer brush previously identified as non-preferentially is backgrafted into the chemical template, before being rinsed clean. Instead the BCP is simply spun onto the prepared guide stripes and annealed, allowing both brush grafting and DSA to occur simultaneously. The time and temperature was carefully selected to insure the self-brushing was occurred on the silicon and not the xPS. The resulting DSA using 2MPTF is shown in Figure 39b, where sub 15 nm full pitch features are obtained after 5x density multiplication with no brush and no topcoat. A general concern with this type of materials is the crosslinking caused by transesterification during annealing.[38-39] We found that the prolonged anneal the thin films results into insoluble residue layer, indicating the presence of crosslinking.

However, the secondary-OH moiety has much slower kinetics in transesterification especially in the absence of catalyzing acid.[38]

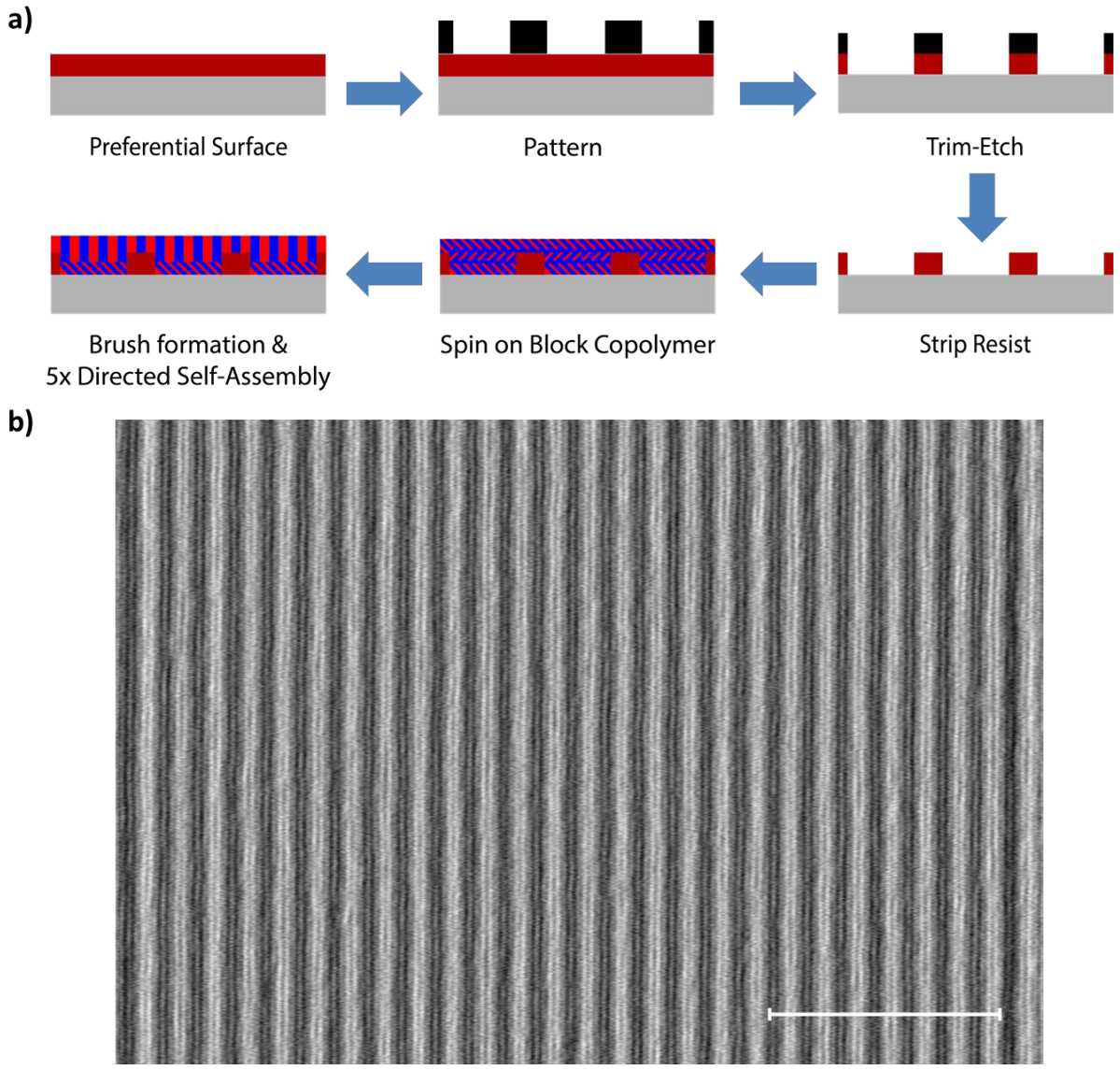

Figure 39. a) Self-brushing DSA flow in which the block copolymer brushes as it assembles forming its own non-preferential substrate. b) 2 micron wide SEM of 5X density multiplication DSA using 2MPTF to achieve 15 nm pitch features. Scale bar 500 nm.

6.5 Enhanced etch contrast through SIS as well SiOx forming etches

Another vital attribute of next-generation BCPs for DSA purposes is the capability for pattern transfer. Here, we first investigated the ability of incorporating sequential infiltration synthesis (SIS) into these new materials. SIS is a process in which some polar moieties, including carbonyls, can coordinate with ALD precursors such as, trimethyl aluminum, allowing for through film alumina structures to be grown.[40] To validate the increased etch resistance of the polar we use an Argon Oxygen based etch developed by TEL on a fingerprint sample which has undergone three cycles of alumina SIS as a fingerprint sample which has not.[41] Figure 40A illustrates the vastly improved etch resistance of MEAPTMS once it has been loaded with alumina. The Alumina domains appear much brighter due to the edge enhancement effect of secondary electron imaging where more signal is received from free standing features. It would also be advantageous for the BCP to be intrinsically etch resistant, although the silicon incorporation in the equal surface energy MEAPTMS is quite low. However; N_2/H_2 based etch gases have previously been shown to give large etch constrast for silicon containing polymers due to the high energy flux around 160 nm wavelength which catalyzes the formation of a protective silicon oxide.[42] Using a similar recipe to that in the literature, a 30 nm thick film of both 2MPTF and MEAPTMS was etched at the same time. For the 2MPTF no residual morphology is seen under SEM; whereas, the lamella morphology is still present in the case of MEAPTMS (Figure 40b). Two methods of selective etching are thus possible for materials on this platform.

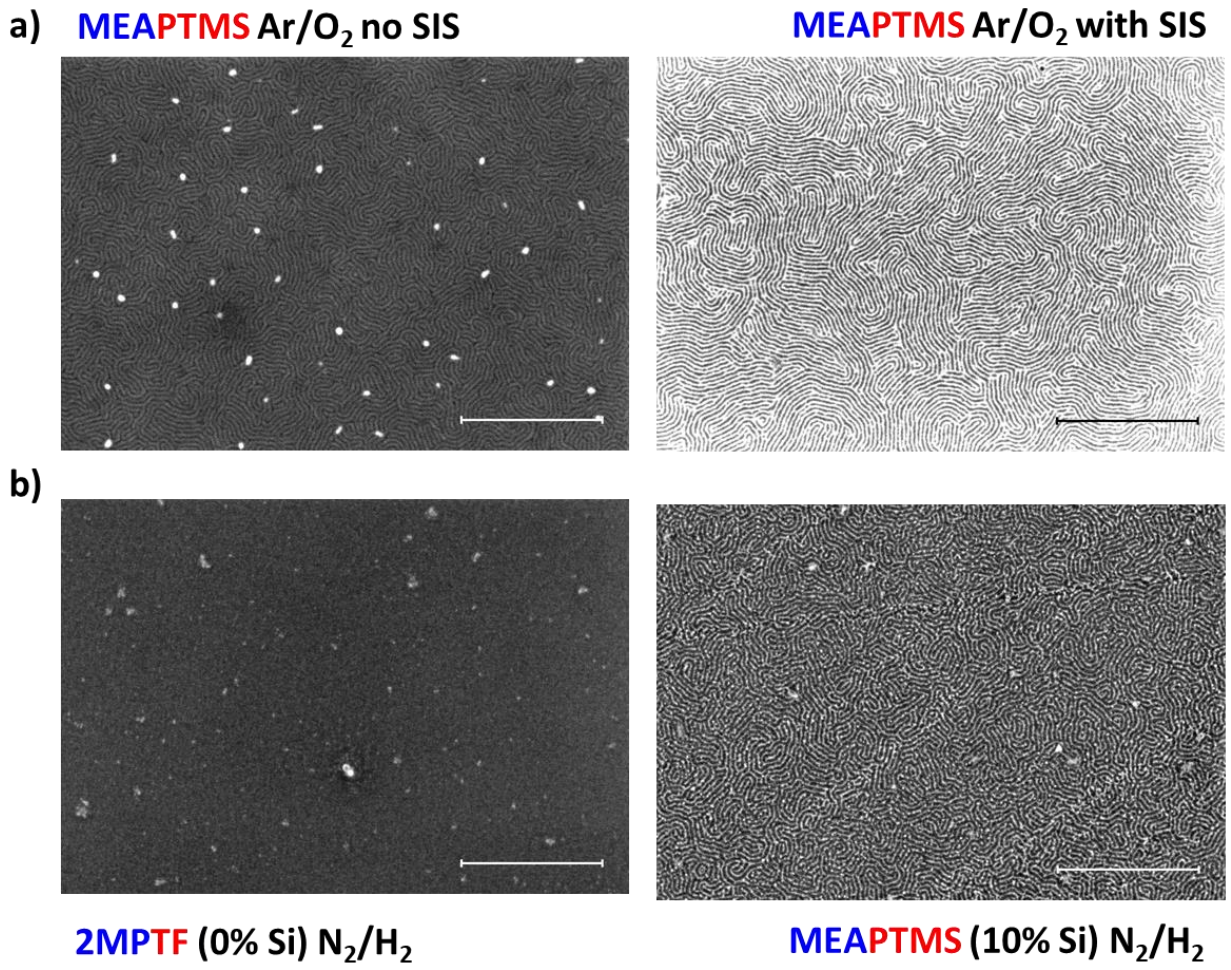

Figure 40. SEM images of two distinct etch strategies both a) SIS followed by an oxygen etch as well as b) natural silicon incorporation etched by nitrogen hydrogen mixtures. Scale bars = 400 nm

6.6 Conclusion

Using PS-*b*-PGMA as a parent platform and the robust thiol epoxy reaction, we were able to achieve a series of high χ BCPs with equal SFE for DSA applications. SFE measurements and top-down SEM images suggests that the BCPs can self-brush onto the silicon wafer balancing the interaction of the substrate interface. Relying on this self-brushing mechanism, we then performed

a self-brushing DSA process and achieved 5x DSA of sub 15 nm full pitch features with thermal annealing. We then demonstrated two distinct methods of etch contrast, including either SIS or the addition of atomic silicon via the thiol epoxy reaction. As a result of this work we expect development and analysis of new DSA materials to rapidly accelerate due to the ease with which new materials can be made.

6.7 Methods

6.7.1 Materials.

Styrene (St, 99%), glycidyl methacrylate (GMA, 99%), 2-cyano-2-propyl benzodithioate (CPDB, 97%), mercaptoethanol (MEA, 99%, Aldrich), methyl thioglycolate (MGM, 95%, Aldrich), 2,2′-azobis(2-methylpropionitrile) (AIBN, 98%), lithium hydroxide, thiols were purchased from commercial sources. LiOH aqueous solution was freshly made before each thiol-epoxy reaction with 20 mg/mL in de-ionized water. St, GMA were removed inhibitor prior to use. AIBN were recrystallized from methanol prior to use. All other chemicals were used as received.

6.7.2 Instrumentation.

Nuclear magnet resonance spectroscopy (NMR) was recorded on a Bruker AVANCE II+ 500. Small-Angle X-ray scattering (SAXS) was measured on a SAXSLAB (XENOCS)'s GANESHA. Differential scanning calorimetry (DSC) was recorded on a TA instruments Discovery DSC 2500. Thermal gravimetric analysis (TGA) was carried out on a TA instruments Discovery TGA. Scanning electron microscopy (SEM) images were captured on a Zeiss Merlin high-resolution field-emission scanning electron microscope using a 1 – 1.5 KeV accelerating voltage at a working distance below 3 mm using the in-lens secondary electron detector, brightness and contrast were adjusted for presentation. Atomic force microscopy (AFM) was performed on a Bruker Nanoscope

IIIa Multimode 5 AFM. Surface free energy measurement was carried out on a KRÜSS drop shape analyzer 100 at room temperature.

6.7.3 Material synthesis

Synthesis of poly (glycidyl methacrylate) (PGMA-CPDB). To a two-neck round bottom flask equipped with a condenser and a magnetic stir bar was added GMA (50.0g, 351.7 mmol), AIBN (0.22g, 1.3mmol), and CPDB (0.89g, 4.0 mmol). freeze-pump-thaw three times, The mixture was stirred at 60 °C for 1h and then quenched by liquid N_2. The resulting polymer was purified by repeatedly precipitated into hexanes three times and dried in vacuum oven.

Synthesis of poly (styrene-*b*-glycidyl methacrylate) (PS-*b*-PGMA-CPDB). To a two-neck round bottom flask equipped with a condenser and a magnetic stir bar was added a solution of styrene, PGMA-CPDB (50.0g, 351.7 mmol), AIBN (0.22g, 1.3mmol) in DMF. The mixture was then performed freeze-pump-thaw three times. The mixture was stirred at 80 °C for 1h and then quenched by immerging into liquid N_2. The resulting polymer was purified by repeatedly precipitated into hexanes three times and dried in vacuum oven.

Typical thiol-epoxy modification on PS-*b*-PGMA-CPDB. To a two-neck round bottom flask equipped with a magnetic stir bar was added a solution of PS-*b*-PGMA (116.0 mg, GMA unit 0.33 mmol), MEA (84 mg, 1.08 mmol, 3.29 eq to GMA unit), TF (22.1 mg, 0.19 mmol, 0.58 eq to GMA unit) in THF (2.5g). The solution was then cooled to 0 °C followed by the addition of LiOH (40 µL, 0.10 eq to GMA unit) aqueous solution. The reaction was then warmed to room temperature and stirred for 18h. The product was obtained as a white powder after repeated precipitation into hexanes 3 times and dried in a vacuum oven overnight.

6.7.4 Flory-Huggins parameter χ calculation.

The χ of each BCP with equal SFE was calculated using a self-consistent mean field theory.

$$d = 1.10aN^{\frac{2}{3}}\chi_{eff}{}^{\frac{1}{6}} \quad (1)$$

$$a_{PSPGMA} = \frac{1}{\sqrt{\frac{f_{PS}}{a_{PS}^2}+\frac{f_{PGMA}}{a_{PGMA}^2}}} \quad (2)$$

$$N=N_{PS}+N_{PGMA}= \frac{\frac{MW_{PS}}{\rho_{PS}}}{144} + \frac{\frac{MW_{PGMA}}{\rho_{PGMA}}}{144} \quad (3)$$

6.7.5 Order-disorder transition temperature

The TODT was determined through tracing the peak intensity of the first order peak present in SAXS, and estimate the temperature which corresponded to the steepest decrease in peak intensity.

6.7.6 Metrology

Film thicknesses were measured using a J.A. Woollam Alpha SE ellipsometer, and fitted using a Si-SiO_x-Cauchy model where the native oxide thickness was preset at 1.5 nm. For films under 10 nm the optical constants were first fit to thick films, and then locked to more accurately capture the film thickness. AFM was conducted on films using a Bruker multimode 5 in tapping mode.

6.7.7 Hole Island test

Solutions of PS-PGMA (0.3 wt % in THF) were spin-coated on the Piranha cleaned Si wafers with film thickness ranging from 1.67 L_0 to 1.76 L_0 ($L_0= 2\pi/q^*$, where q^* is the principle Bragg reflection measured by SAXS). The thin films were then annealed at 150 °C for 1h in vacuum and characterized by AFM and SEM.

6.7.8 Surface free energy measurement

The BCPs solutions in PGMEA or THF were spun coated on piranha cleaned silicon wafer to afford thin films with thickness ~30 nm. In a glove box, the thin films were baked on a hot plate at 150 °C for 1h and then placed on a block of metal to cool to room temperature. SEM images were captured to verify if equal SE has been achieved in both free interface and bottom interface. The thin film samples were then rinsed using THF/DMF (9:1 - 1:9) mixtures with increasing DMF incorporation to remove any unattached materials. The resulting films were then soft baked to remove any residue solvent. SEM and AFM were then carried to examine the surface topography and morphology. The samples were then taken for SFE measurements using two probing liquids: de-ionized water and CH_2I_2. Before each measurement, the film surface was dedusted using dry N_2. The contact angle was measured using the sessile drop method and the drop volume was kept 1 µL. The left and right contact angles of each drop are averaged, and 10 sessile drops were deposited for each sample. The SFE was then calculated using Wu[43] and OWRK method[44-45].

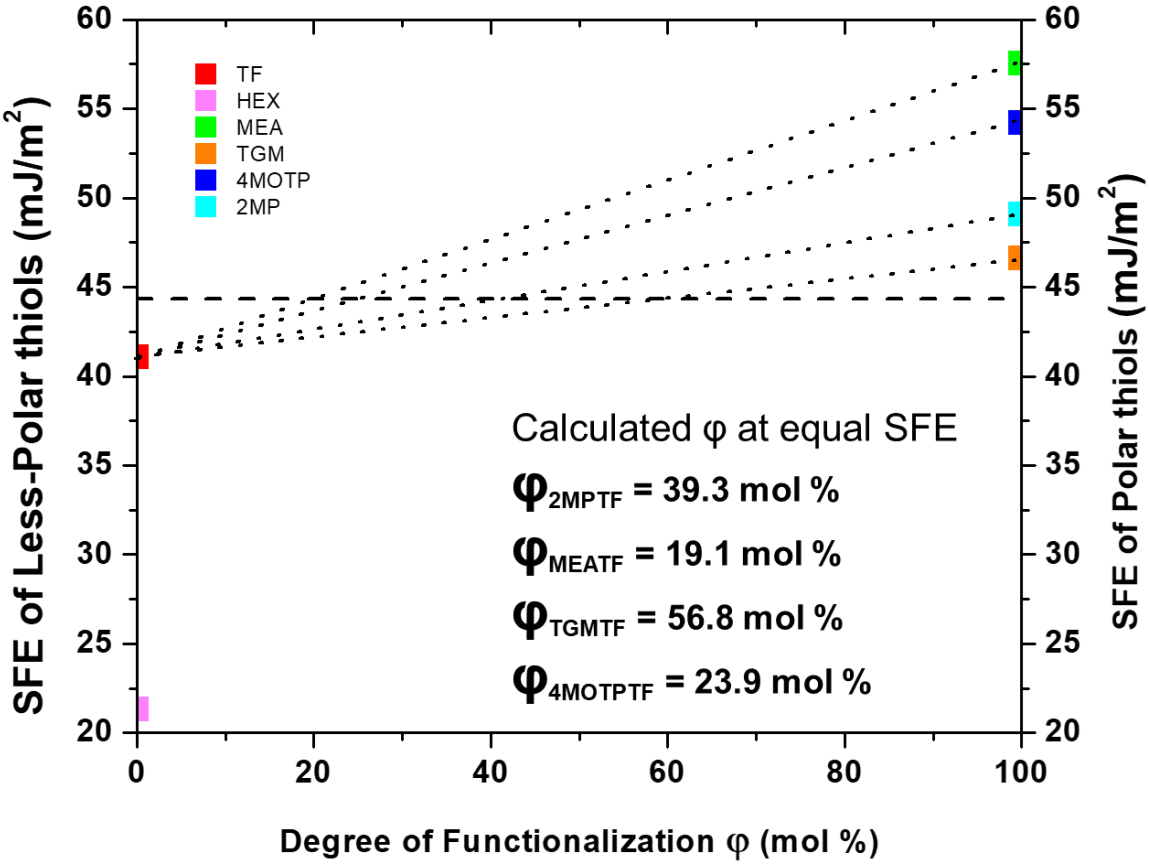

Figure 41. Measured SFE of polar thiols and less-polar thiols modified PGMA.

6.7.9 Thermal properties.

Thermogravimetric analysis (TGA) was carried out in a N_2 atmosphere. The samples were first kept 110 °C for 10 min to remove any attached moisture then followed by a heating ramp to 600 °C at a ramp rate of 10 °C/min. DSC was carried out in N_2 atmosphere. The samples were first thermalized at 130 °C for 10 min and followed by cooling to -80 °C at a rate of 10 °C/min and stabilized for 5 min. The samples were then heated to 130 °C at a ramp rate of 10 °C/min. The glass transition temperature was measured on the second heating cycle.

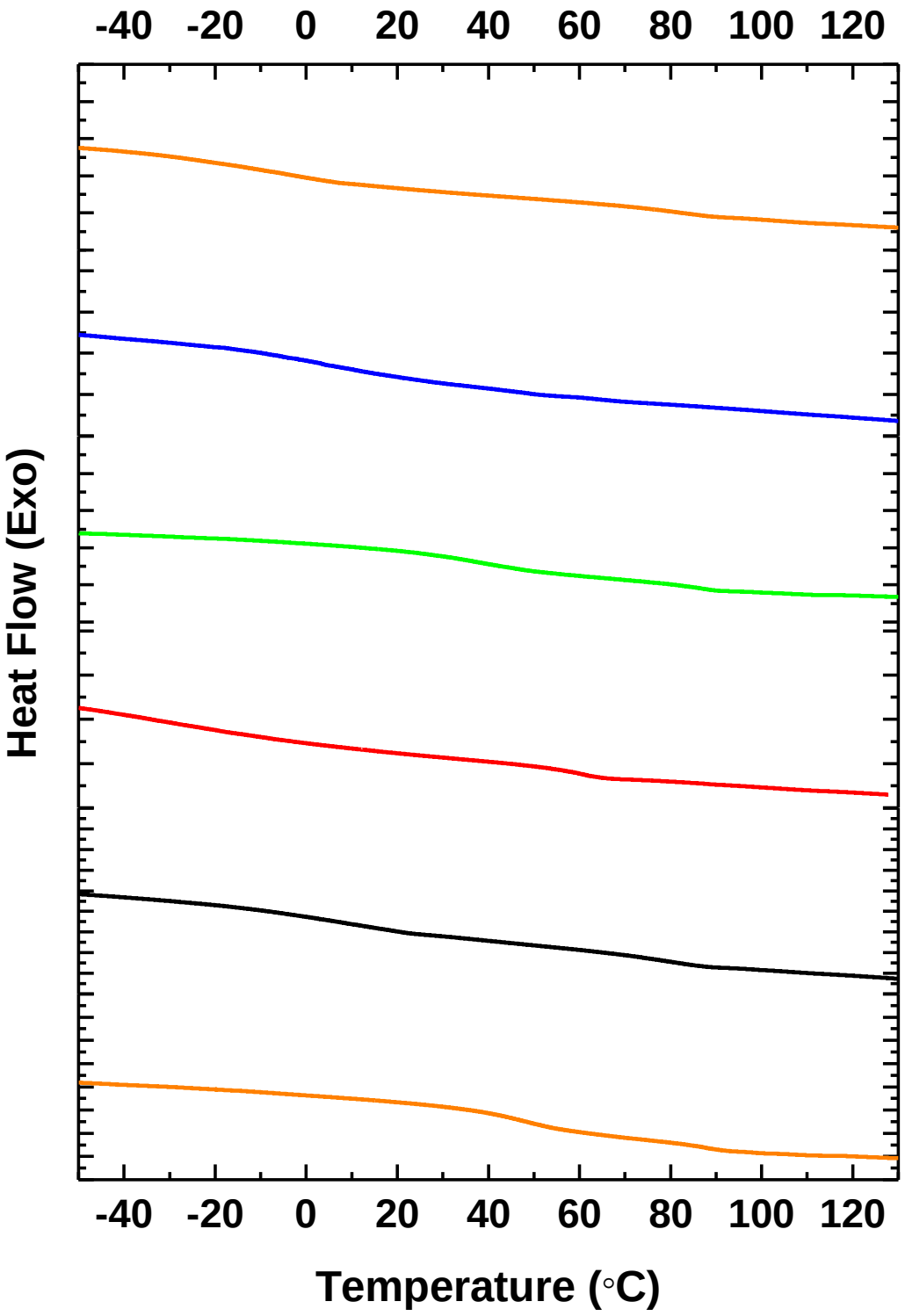

Figure 42. DSC of A-b-(B-r-C) polymers

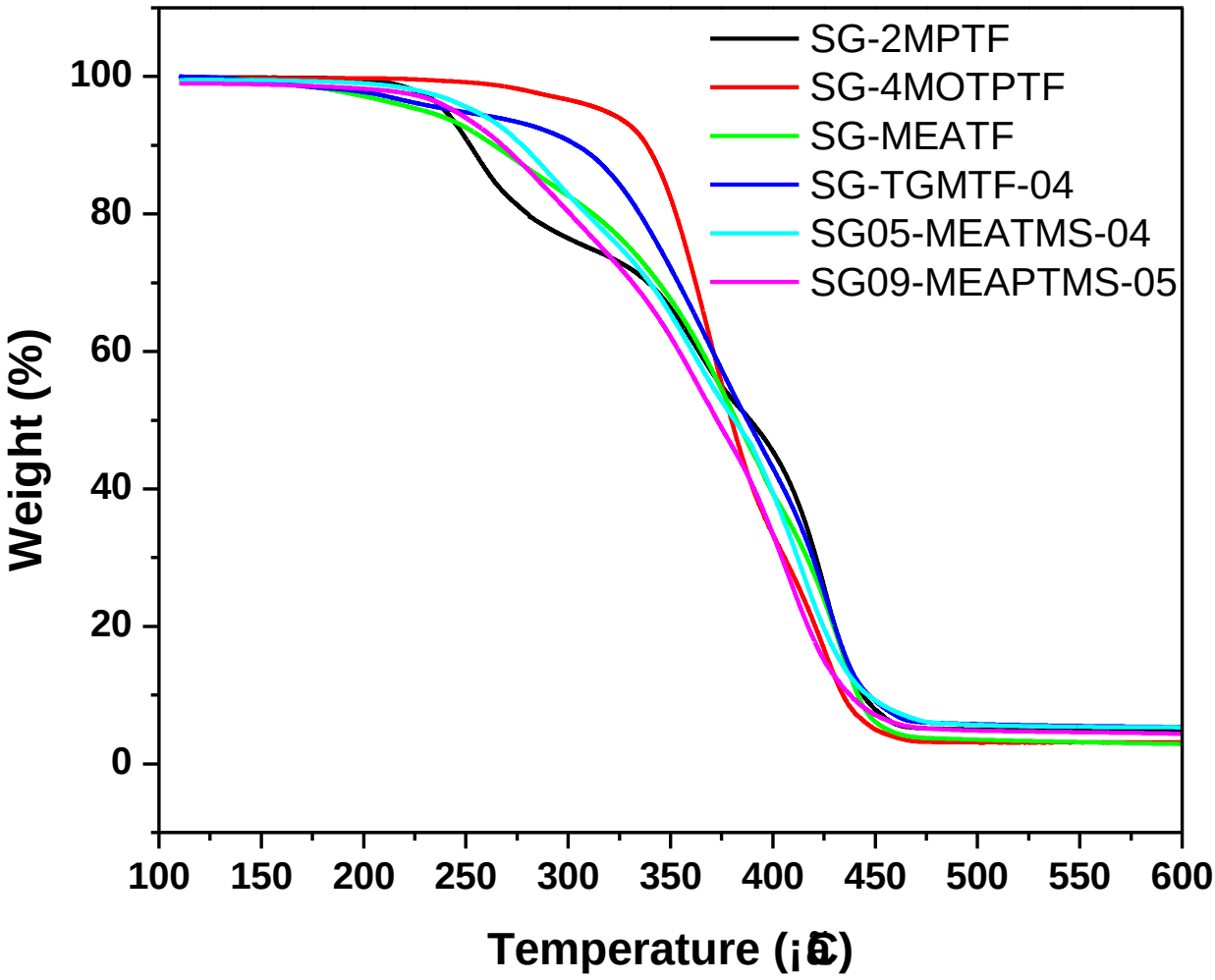

Figure 43. TGA of A-b-(B-r-C) polymers

6.7.10 Self-brushing DSA Process

Prior to DSA, time temperature sweeps were conducted to identify conditions at which the BCP self-brushing would selectively occur only on the silicon wafer. This is critical as self-brushing on the guide stripe would prohibit the chemoepitaxial guiding effect. From these experiments 175°C for 10 minutes was identified as an ideal time and temperature for DSA.

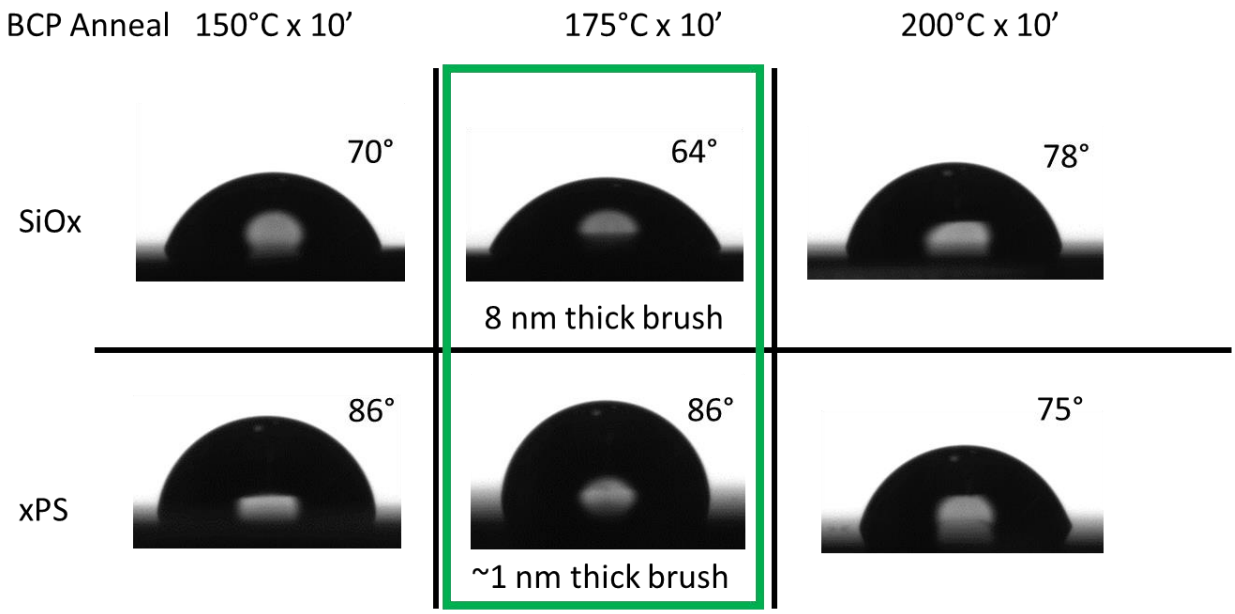

Figure 44. Time Temperature studies of 2MPTF self-brushing on both silicon and xPS showing water contact angle of the residual brush film after rinsing.

In order to conduct the self-brushing DSA process xPS was spuncoat to a thickness of 15 nm and crosslinked onto a clean silicon wafer. The xPS was then patterned on top of using e-beam lithography with CSAR-Neu 7520 from allresist. After patterning the resist was developed using MIF 726 for 1 minute, before a quick water rinse. The pattern was trim etched into the xPS substrate underneath it to achieve approximately 1.5 L_0 wide guide stripes on varying pitches. After stripping any remaining resist, the BCP was spuncoat on top of the xPS pattern to a thickness of 2 L0 and annealed at 175°C for 10 minutes in a nitrogen glovebox.

6.8 Acknowledgements

Part of this work were carried out at the Soft Matter Characterization Facility of the University of Chicago. Surface energy measurements were carried out in KRÜSS Surface Science Laboratory in the University of Chicago. This facility is a joint collaborative venture with KRÜSS GmbH. We acknowledge the MRSEC Shared User Facilities at the University of Chicago (NSF DMR-1420709). This work made use of the Pritzker Nanofabrication Facility of the Institute for Molecular Engineering at the University of Chicago, which receives support from Soft and Hybrid Nanotechnology Experimental (SHyNE) Resource (**NSF ECCS-1542205**), a node of the National Science Foundation's National Nanotechnology Coordinated Infrastructure. The authors thank Intel Corporation and Semiconductor Research Corporation for the support.

6.9 References

1. Yang, G. W.; Wu, G. P.; Chen, X.; Xiong, S.; Arges, C. G.; Ji, S.; Nealey, P. F.; Lu, X. B.; Darensbourg, D. J.; Xu, Z. K., Directed Self-Assembly of Polystyrene-b-poly(propylene carbonate) on Chemical Patterns via Thermal Annealing for Next Generation Lithography. *Nano letters* **2017,** *17* (2), 1233-1239.

2. Kim, H.-C.; Park, S.-M.; Hinsberg, W. D., Block copolymer based nanostructures: materials, processes, and applications to electronics. *Chem. Rev.* **2009,** *110* (1), 146-177.

3. Onses, M. S.; Song, C.; Williamson, L.; Sutanto, E.; Ferreira, P. M.; Alleyne, A. G.; Nealey, P. F.; Ahn, H.; Rogers, J. A., Hierarchical patterns of three-dimensional block-copolymer films formed by electrohydrodynamic jet printing and self-assembly. *Nat. Nanotechnol.* **2013,** *8* (9), 667.

4. Xiong, S.; Chapuis, Y. A.; Wan, L.; Gao, H.; Li, X.; Ruiz, R.; Nealey, P. F., Directed self-assembly of high-chi block copolymer for nano fabrication of bit patterned media via solvent annealing. *Nanotechnology* **2016,** *27* (41), 415601.

5. Xiong, S.; Wan, L.; Ishida, Y.; Chapuis, Y.-A.; Craig, G. S. W.; Ruiz, R.; Nealey, P. F., Directed Self-Assembly of Triblock Copolymer on Chemical Patterns for Sub-10-nm Nanofabrication via Solvent Annealing. *ACS nano* **2016,** *10* (8), 7855-7865.

6. Chapuis, Y.-A.; Ruiz, R.; Wan, L.; Nealey, P. F.; Xiong, S. Solvent annealing of block copolymer films under super-saturated atmospheres. US20150239184A1, 2015.

7. Albert, J. N.; Bogart, T. D.; Lewis, R. L.; Beers, K. L.; Fasolka, M. J.; Hutchison, J. B.; Vogt, B. D.; Epps, T. H., Gradient solvent vapor annealing of block copolymer thin films using a microfluidic mixing device. *Nano letters* **2011,** *11* (3), 1351-7.

8. Suh, H. S.; Kim, D. H.; Moni, P.; Xiong, S.; Ocola, L. E.; Zaluzec, N. J.; Gleason, K. K.; Nealey, P. F., Sub-10-nm patterning via directed self-assembly of block copolymer films with a vapour-phase deposited topcoat. *Nature nanotechnology* **2017,** *12* (6), 575-581.

9. Kim, E.; Kim, W.; Lee, K. H.; Ross, C. A.; Son, J. G., A Top Coat with Solvent Annealing Enables Perpendicular Orientation of Sub-10 nm Microdomains in Si-Containing Block Copolymer Thin Films. *Advanced Functional Materials* **2014,** *24* (44), 6981-6988.

10. Ramirez-Hernandez, A.; Suh, H. S.; Nealey, P. F.; de Pablo, J. J., Control of Directed Self-Assembly in Block Polymers by Polymeric Topcoats. *Macromolecules (Washington, DC, U. S.)* **2014,** *47* (10), 3520-3527.

11. Bates, C. M.; Seshimo, T.; Maher, M. J.; Durand, W. J.; Cushen, J. D.; Dean, L. M.; Blachut, G.; Ellison, C. J.; Willson, C. G., Polarity-Switching Top Coats Enable Orientation of Sub–10-nm Block Copolymer Domains. *Science* **2012,** *338* (6108), 775-779.

12. Cao, Y.; Her, Y. J.; Delgadillo, P. R.; Vandenbroeck, N.; Gronheid, R.; Chan, B. T.; Hashimoto, Y.; Romo, A.; Somervell, M.; Nafus, K.; Nealey, P. F., Using process monitor wafers to understand directed self-assembly defects. *Proc. SPIE* **2013,** *8680* (Alternative Lithographic Technologies V), 86801S/1-86801S/7.

13. Rincon-Delgadillo, P.; Craig, G.; Gronheid, R.; Nealey, P. F., Scale-up of a chemo-epitaxy flow for feature multiplication using directed self-assembly of block-copolymers. *J. Photopolym. Sci. Technol.* **2013,** *26* (6), 831-839.

14. Rincon Delgadillo, P. A.; Gronheid, R.; Thode, C. J.; Wu, H.; Cao, Y.; Somervell, M.; Nafus, K.; Nealey, P. F., All track directed self-assembly of block copolymers: process flow and origin of defects. *Proc. SPIE* **2012,** *8323* (Alternative Lithographic Technologies IV), 83230D/1-83230D/9.

15. Liu, C.-C.; Thode, C. J.; Delgadillo, P. A. R.; Craig, G. S. W.; Nealey, P. F.; Gronheid, R., Towards an all-track 300 mm process for directed self-assembly. *J. Vac. Sci. Technol., B: Nanotechnol. Microelectron.: Mater., Process., Meas., Phenom.* **2011,** *29* (6), 06F203/1-06F203/6.

16. Ren, J.; Zhou, C.; Chen, X.; Dolejsi, M.; Craig, G. S. W.; Rincon Delgadillo, P. A.; Segal-Peretz, T.; Nealey, P. F., Engineering the Kinetics of Directed Self-Assembly of Block Copolymers toward Fast and Defect-Free Assembly. *ACS applied materials & interfaces* **2018,** *10* (27), 23414-23423.

17. Liu, C.-C.; Franke, E.; Mignot, Y.; Xie, R.; Yeung, C. W.; Zhang, J.; Chi, C.; Zhang, C.; Farrell, R.; Lai, K.; Tsai, H.; Felix, N.; Corliss, D., Directed self-assembly of block copolymers for 7 nanometre FinFET technology and beyond. *Nature Electronics* **2018,** *1* (10), 562-569.

18. Liu, C.-c.; Franke, E.; Lie, F. L.; Sieg, S.; Tsai, H.; Lai, K.; Truong, H.; Farrell, R.; Somervell, M.; Sanders, D.; Felix, N.; Guillorn, M.; Burns, S.; Hetzer, D.; Ko, A.; Arnold, J.; Colburn, M., Directed self-assembly patterning for forming fin field effect transistors. *SPIE Newsroom* **2016**.

19. Doise, J.; Bekaert, J.; Chan, B. T.; Hori, M.; Gronheid, R., Via patterning in the 7-nm node using immersion lithography and graphoepitaxy directed self-assembly. *Journal of Micro/Nanolithography, MEMS, and MOEMS* **2017,** *16* (2).

20. Hohle, C. K.; Gronheid, R.; Chi, C.; Liu, C.-C.; Meli, L.; Guo, J.; Parnell, D.; Mignot, Y.; Schmidt, K.; Sanchez, M.; Farrell, R.; Singh, L.; Furukawa, T.; Lai, K.; Xu, Y.; Sanders, D.; Hetzer, D.; Metz, A.; Burns, S.; Felix, N.; Arnold, J.; Corliss, D., Electrical study of DSA shrink process and CD rectification effect at sub-60nm using EUV test vehicle. **2017,** *10146*, 101460Q.

21. Gronheid, R.; Boeckx, C.; Doise, J.; Bekaert, J.; Karageorgos, I.; Ruckaert, J.; Chan, B. T.; Lin, C.; Zou, Y., *EUV patterned templates with grapho-epitaxy DSA at the N5/N7 logic nodes*. SPIE: 2016; Vol. 9776.

22. Han, E.; Stuen, K. O.; La, Y.-H.; Nealey, P. F.; Gopalan, P., Effect of Composition of Substrate-Modifying Random Copolymers on the Orientation of Symmetric and Asymmetric Diblock Copolymer Domains. *Macromolecules (Washington, DC, U. S.)* **2008,** *41* (23), 9090-9097.

23. In, I.; La, Y.-H.; Park, S.-M.; Nealey, P. F.; Gopalan, P. In *Side-chain grafted random copolymer brushes as neutral surfaces controlling the orientation of block copolymer microdomains in thin films*, American Chemical Society: 2006; pp POLY-085.

24. Mansky, P., Controlling Polymer-Surface Interactions with Random Copolymer Brushes. *Science* **1997,** *275* (5305), 1458-1460.

25. Han, E.; Gopalan, P., Cross-linked random copolymer mats as ultrathin nonpreferential layers for block copolymer self-assembly. *Langmuir : the ACS journal of surfaces and colloids* **2010,** *26* (2), 1311-5.

26. Suh, H. S.; Kang, H.; Nealey, P. F.; Char, K., Thickness Dependence of Neutral Parameter Windows for Perpendicularly Oriented Block Copolymer Thin Films. *Macromolecules* **2010,** *43* (10), 4744-4751.

27. Moni, P.; Suh, H. S.; Dolejsi, M.; Kim, D. H.; Mohr, A. C.; Nealey, P. F.; Gleason, K. K., Ultrathin and Conformal Initiated Chemical-Vapor-Deposited Layers of Systematically Varied Surface Energy for Controlling the Directed Self-Assembly of Block CoPolymers. *Langmuir : the ACS journal of surfaces and colloids* **2018,** *34* (15), 4494-4502.

28. Dolejsi, M.; Nealey, P., Utilization of metal–polymer interactions for self-aligned directed self-assembly of device relevant features. *Journal of Micro/Nanolithography, MEMS, and MOEMS* **2018,** *17* (03), 1.

29. Wan, L.; Ruiz, R.; Gao, H.; Patel, K. C.; Albrecht, T. R.; Yin, J.; Kim, J.; Cao, Y.; Lin, G., The Limits of Lamellae-Forming PS-b-PMMA Block Copolymers for Lithography. *ACS nano* **2015,** *9* (7), 7506-14.

30. Matsen, M. W.; Bates, F. S., Unifying Weak- and Strong-Segregation Block Copolymer Theories. *Macromolecules* **1996,** *29* (4), 1091-1098.

31. Sunday, D. F.; Maher, M. J.; Hannon, A. F.; Liman, C. D.; Tein, S.; Blachut, G.; Asano, Y.; Ellison, C. J.; Willson, C. G.; Kline, R. J., Characterizing the Interface Scaling of High chi Block Copolymers near the Order-Disorder Transition. *Macromolecules* **2018,** *51* (1), 173-180.

32. Li, X.; Liu, Y.; Wan, L.; Li, Z.; Suh, H.; Ren, J.; Ocola, L. E.; Hu, W.; Ji, S.; Nealey, P. F., Effect of Stereochemistry on Directed Self-Assembly of Poly(styrene-b-lactide) Films on Chemical Patterns. *ACS Macro Lett.* **2016,** *5* (3), 396-401.

33. Kim, S.; Nealey, P. F.; Bates, F. S., Decoupling Bulk Thermodynamics and Wetting Characteristics of Block Copolymer Thin Films. *ACS Macro Lett.* **2012,** *1* (1), 11-14.

34. Lillethorup, M.; Shimizu, K.; Plumeré, N.; Pedersen, S. U.; Daasbjerg, K., Surface-attached poly (glycidyl methacrylate) as a versatile platform for creating dual-functional polymer brushes. *Macromolecules* **2014,** *47* (15), 5081-5088.

35. Gao, J.; Li, J.; Zhao, S.; Benicewicz, B. C.; Hillborg, H.; Schadler, L. S., Effect of graft density and molecular weight on mechanical properties of rubbery block copolymer grafted SiO2 nanoparticle toughened epoxy. *Polymer* **2013,** *54* (15), 3961-3973.

36. Maher, M. J.; Bates, C. M.; Blachut, G.; Sirard, S.; Self, J. L.; Carlson, M. C.; Dean, L. M.; Cushen, J. D.; Durand, W. J.; Hayes, C. O.; Ellison, C. J.; Willson, C. G., Interfacial Design for Block Copolymer Thin Films. *Chem. Mater.* **2014,** *26* (3), 1471-1479.

37. Kim, S.; Nealey, P. F.; Bates, F. S., Decoupling Bulk Thermodynamics and Wetting Characteristics of Block Copolymer Thin Films. *ACS Macro Lett.* **2012,** *1* (1), 11-14.

38. Connell, L. S.; Jones, J. R.; Weaver, J. V. M., Transesterification of functional methacrylate monomers during alcoholic copper-catalyzed atom transfer radical polymerization: formation of compositional and architectural side products. *Polym. Chem.* **2012,** *3* (10).

39. Otera, J., Transesterification. *Chem. Rev.* **1993,** *93* (4), 1449-1470.

40. Tseng, Y.-C.; Peng, Q.; Ocola, L. E.; Elam, J. W.; Darling, S. B., Enhanced Block Copolymer Lithography Using Sequential Infiltration Synthesis. *The Journal of Physical Chemistry C* **2011,** *115* (36), 17725-17729.

41. Rastogi, V.; Ventzek, P. L. G.; Ranjan, A., Etch considerations for directed self-assembly patterning using capacitively coupled plasma. *Journal of Vacuum Science & Technology A: Vacuum, Surfaces, and Films* **2018,** *36* (3), 031301.

42. Azarnouche, L.; Sirard, S. M.; Durand, W. J.; Blachut, G.; Gurer, E.; Hymes, D. J.; Ellison, C. J.; Willson, C. G.; Graves, D. B., Plasma and photon interactions with organosilicon polymers for directed self-assembly patterning applications. *Journal of Vacuum Science & Technology B, Nanotechnology and Microelectronics: Materials, Processing, Measurement, and Phenomena* **2016,** *34* (6).

43. Wu, S. In *Calculation of interfacial tension in polymer systems*, Journal of Polymer Science Part C: Polymer Symposia, Wiley Online Library: 1971; pp 19-30.

44. Owens, D. K.; Wendt, R., Estimation of the surface free energy of polymers. *J. Appl. Polym. Sci.* **1969,** *13* (8), 1741-1747.

45. Kaelble, D., Dispersion-polar surface tension properties of organic solids. *The Journal of Adhesion* **1970,** *2* (2), 66-81.